National Library of Canada

Acquisitions and Bibliographic Services Branch

395 Wellington Street
Ottawa, Ontario
K1A 0N4

Bibliothèque nationale du Canada

Direction des acquisitions et des services bibliographiques

395, rue Wellington
Ottawa (Ontario)
K1A 0N4

Your file Votre référence

Our file Notre référence

NOTICE

The quality of this microform is heavily dependent upon the quality of the original thesis submitted for microfilming. Every effort has been made to ensure the highest quality of reproduction possible.

If pages are missing, contact the university which granted the degree.

Some pages may have indistinct print especially if the original pages were typed with a poor typewriter ribbon or if the university sent us an inferior photocopy.

Reproduction in full or in part of this microform is governed by the Canadian Copyright Act, R.S.C. 1970, c. C-30, and subsequent amendments.

AVIS

La qualité de cette microforme dépend grandement de la qualité de la thèse soumise au microfilmage. Nous avons tout fait pour assurer une qualité supérieure de reproduction.

S'il manque des pages, veuillez communiquer avec l'université qui a conféré le grade.

La qualité d'impression de certaines pages peut laisser à désirer, surtout si les pages originales ont été dactylographiées à l'aide d'un ruban usé ou si l'université nous a fait parvenir une photocopie de qualité inférieure.

La reproduction, même partielle, de cette microforme est soumise à la Loi canadienne sur le droit d'auteur, SRC 1970, c. C-30, et ses amendements subséquents.

Canada

A Study of Two Electron Defect Systems in Alkali Halide Crystals

by

Zhang Chang Gang

Thesis submitted to the School of Graduate Studies of University of Ottawa in partial fulfilment of the requirements for the degree of PH.D in Physics

Department of Physics
Faculty of Science
University of Ottawa
Ottawa, Canada

© Chang Gang Zhang, Ottawa, Canada, 1993

National Library of Canada

Acquisitions and Bibliographic Services Branch

395 Wellington Street
Ottawa, Ontario
K1A 0N4

Bibliothèque nationale du Canada

Direction des acquisitions et des services bibliographiques

395, rue Wellington
Ottawa (Ontario)
K1A 0N4

Your file Votre référence

Our file Notre référence

The author has granted an irrevocable non-exclusive licence allowing the National Library of Canada to reproduce, loan, distribute or sell copies of his/her thesis by any means and in any form or format, making this thesis available to interested persons.

L'auteur a accordé une licence irrévocable et non exclusive permettant à la Bibliothèque nationale du Canada de reproduire, prêter, distribuer ou vendre des copies de sa thèse de quelque manière et sous quelque forme que ce soit pour mettre des exemplaires de cette thèse à la disposition des personnes intéressées.

The author retains ownership of the copyright in his/her thesis. Neither the thesis nor substantial extracts from it may be printed or otherwise reproduced without his/her permission.

L'auteur conserve la propriété du droit d'auteur qui protège sa thèse. Ni la thèse ni des extraits substantiels de celle-ci ne doivent être imprimés ou autrement reproduits sans son autorisation.

ISBN 0-315-82552-9

Canada

UNIVERSITÉ D'OTTAWA
UNIVERSITY OF OTTAWA

Abstract

The structures of two electron defect systems in alkali halide crystals are studied. The systems which have been studied include: two electrons localized at an anion vacancy (F'-centre); positronium self-trapped at an anion vacancy (Fe+-centre); positron self-trapped at a cation vacancy (F_{anti}-centre); positronium self-trapped at an interstice; and positronium in a Bloch state. An improved version of the extended-ion method which is based on the one electron Hartree-Fock approximation is used to perform these calculations. Its main feature is the exclusive use of floating 1s Gaussian functions as basis. For the multi-electron defect systems, the calculation of matrix elements of two electron interaction terms is a most difficult problem. We developed an effective approach to treat this interaction approximately. The correlation effect of defect electrons is partly accounted for by properly arranged Gaussian basis. The binding energy, thermal dissociation energy, and transition energy between ground state and excited state are calculated for F'-centres. A defect model with negative-U properties was introduced to interprete the deeply bound F'-centre. Calculations of positron binding energies are made for Fe+-centres and F_{anti}-centres. In addition, we evaluate the angular correlation and lifetime of an annihilated electron-positron pair for Fe+-centres, localized positronium and Bloch state positronium. The observed phenomena such as the transition of positronium from Bloch state to localized state, and the crystallographic effect are examined theoretically. The calculated results regarding various properties of crystals are in reasonably good agreement with experiment.

Acknowledgments

I feel privileged to have this opportunity to express my great appreciations to Dr. K. S. Song for all his help, encouragement and support. I enjoyed working with him in such a family-like environment during the course of this research.

I would like to thank Dr. C. H. Leung and Professor L. F. Chen for their constructive discussion and tutoring.

I would like to thank Dr. A. T. Stewart for his raising the issue of positronium states in alkali halide crystals.

I would like to thank professor W. Beall Fowler for his pointing out the possible negative-U effect of F′-centre, as well as his kind reading of the thesis.

I would also like to thank Laura Sears who took time to polish the English writing of this thesis, and all supporting staff of the department for creating such a convenient atmosphere.

Special thanks must go to my wife Sun Hong Bin. Without her constant help, support and commitment, I would not have been able to reach the end of this work.

Last, I would like to thank my home university, Liaoning Normal University, to which I dedicate this work.

Contents

Introduction

This thesis presents a study of the structure of two electron defect systems in alkali halide crystals. The investigated systems are: two electrons localized at an anion vacancy (F'-centre); positronium self-trapped at an anion vacancy (Fe^+-centre); a positron self-trapped at a cation vacancy (F_{anti}-centre); positronium self-trapped at an interstice; and positronium in a Bloch state. The method of the hybrid pseudo-potential which is based on the one electron Hartree-Fock approximation is used to calculate energies, and various other properties.

In our method, the defect electrons are represented by a linear combination of floating 1s Gaussians; the effects of the occupied electron orbitals are treated by the hybrid scheme of an extended-ion model in which the deep core electrons are represented by the first two orders of ion-size parameters and outer shells are treated exactly; the lattice is represented by the Born-Mayer form of pair potentials; and the polarization energy is included through a first order Mott-Littleton treatment. For those multi-electron defect systems, the calculation of matrix elements of the two electron interaction Hamiltonian is a most difficult problem. We developed an effective approach to treat this interaction approximately. Up to the fourth shell, ions surrounding the defect are allowed to move, and the defect structure is determined self-consistently by minimizing the total energy of the system with respect to the positions of the ions. The correlation effect of defect electrons is partly accounted for by a properly arranged Gaussian basis.

The presentation of this thesis corresponds to three chapters.

In chapter one, we present a summary of methods which have been

developed to calculate the defect structure. We start from some basic approximations on which all theories rely. Then different methods in dealing with all aspects of defect structure such as: electronic structure, lattice, and polarization are described. A summary review is presented going from the one-electron approach to recent more advanced ab initio approaches.

In chapter two, we present how the extended-ion approach is adapted to study the two electron defect, F'-centres. First of all, we describe the theoretical structure in detail including the evaluation of various terms in the Hamiltonian, with special emphasis on the newly developed scheme of treating the two electron interaction. Then, the treatment of lattice and energy minimization procedure is followed. Finally, we present our results. For the F'-centre, four alkali halides crystals, NaCl, KCl, NaBr and NaI, are investigated. The calculated binding energies and thermal dissociation energies are in reasonable agreement with experiment. The theoretical calculation of deeply bound systems, as in NaI, also shows a good fit to experiment in terms of transition energy between bound ground state and excited state. Such deeply bound systems were explained by introducing negative-U properties.

In chapter three, applications of our approach to different kinds of two particle defect systems such as Fe^{+}-centres, F_{anti}-centres, positronium self-trapped at an interstice and positronium in a Bloch state are described. An important part of this chapter stresses how the method is extended to treat the Bloch state. The representation of the positron, the evaluations of angular correlations of an annihilated electron-positron pair and lifetime are also described. The calculated results and corresponding discussions are given in the last section of the chapter.

For the Fe^{+}-centre, the calculated positron binding energies and emission

photon angular correlation curves agree with those of observations. This is because the angular correlation depends mainly on the centre of mass motion of defect electrons which follows the Boltzmann distribution. The advantage of using a Gaussian basis provides a better representation of this distribution. The calculated lifetimes are not as good as the above mentioned quantities, mainly because of a wave function which does not possess a cusp on which the lifetime depends sensitively. The basis we use does not have independent control of relative motion with which the lifetime associates.

For the extended defect systems such as positronium self-trapped at an interstice and Bloch state positronium, the approach which we have been using successfully is modified to cope with an extended state. The energy difference between the self-trapped positronium state and a Bloch state positronium is calculated. The experimental observations show that at very low temperature positronium stays mainly in Bloch state, and it turns into a self-trapped state as temperature rises. Our calculations agree qualitatively with such observations. Most excitingly, by taking advantage of the floating Gaussian basis, the experimentally reported crystallographic effect is very well explained by our theoretical model.

Chapter I Summary of Methods in Defect Structure Calculation

1.1 Introduction

To present a study on the structure of two-electron defects in alkali halide crystals, we shall begin by firstly reviewing some concepts, basic approximations, various methods and approaches employed in this area of research. Following this line, we explain the concept of point defects in section 1.2, which is a basic model to treat defects. In section 1.3, the basic approximations are introduced. We shall say that those approximations are the backbones of the whole theoretical structure. We present a few ways in which the lattice is treated in section 1.4. The defect is hosted by the lattice, so the behaviour of the lattice and its response to the existence of the defect are important aspects of this study. In this section, we describe the pair potential, and the shell model. The lattice response to the defect is given in the section on lattice relaxation and polarization. Several methods used in defect electron structure calculations are presented in section 1.5. They include the conventional methods such as effective-mass method, Green's function method, point-ion method and extended-ion method. In addition, the approach used in our study, i.e., the hybrid pseudo-potential approach and its advantages are described in this section as well. In the final section of 1.6, a more advanced approach such as ICECAP is described.

1.2 Point Defects

It is common knowledge that there exist defects in real solids. The aim of

this work is to study certain point defects in alkali halide crystals with more than one electron.

By a point defect we mean one that has no macroscopic size; it is limited to at most a few atomic diameters in all directions. Such single point defects are not supposed to interact with each other. We can think of a single defect as having been created in a crystal that was originally perfect and infinite. We then view the infinite crystal as still approximately perfect: we say that it is weakly perturbed. However, there remains a region that is characteristic of the defect with substantial deviation from the embedding crystal lattice. We therefore view the system as consisting of defect and lattice parts.

1.3 Basic Approximations

When we write down the non-relativistic Hamiltonian for a system of electrons and nuclei, the Hamiltonian is composed of the electron-electron term, the nucleus-nucleus term and the electron-nuclear interaction term. As the exact solution of the Schrodinger equation is intractable, some basic approximations have to be made to simplify the problem. We enumerate in the following the principal ones.

First, an adiabatic approximation is introduced to separate the electronic and nuclear motion, i.e., the electronic Schrodinger equation is solved for fixed nuclear positions, and the electronic eigenvalues contribute to the potential determining the nuclear motion. Lattice dynamic effects are ignored, on the other hand. Thus the electronic Schrodinger equation is solved only for the nuclei at their mean positions.

Second, the Hartree-Fock approximation can further reduce the

complexities of the many-body problem. The fundamental idea is to associate a specific wave function with each electron, such that an approximate wave function for an N-electron system can be constructed by N independent functions of the coordinates and spin of a single particle. The approximate wave function is to be made antisymmetric and possesses other relevant space and spin symmetries. The many-body problem is simplified at the expense of losing inter-particle correlations. Physically, the problem of mutually interacting electrons has been reduced to the problem of independent electrons moving in an effective external potential which is to be determined self-consistently from the electronic charge distribution induced by it.

In applying the Hartree-Fock approximation to defect calculations, it may take different forms depending upon the material under study. For point defects in strongly ionic crystals, it is usually assumed that only the defect-electron wave functions are varied, while the core electrons contribute to the potential in which the defect electrons move and provide a constraint, since the defect electron wave functions must be orthogonal to those of occupied core states. Thus the system Hamiltonian reduces to that of a few electrons, and the calculation turns out to be much less complex. For deep energy defects in covalent crystals, for example, many electrons and atoms are involved. This is because in these materials the band gap is small and it is not possible to distinguish the defect electrons from other electrons. Now what we have is a many electron Hartree-Fock Hamiltonian. The calculation becomes very complex due to the large number of two-electron multi-centre integrals in matrix elements. Depending on the severity of approximations in evaluating matrix elements, the zero differential overlap approximations such as CNDO, INDO, and NDDO[1.1] are introduced to simplify

calculations. At the same time, semi-empirical approaches are also used. In those methods, atomic and other spectroscopic data is employed to simplify some of the matrix elements in the Hartree-Fock equations.

1.4 Lattice Dynamics

1.4.1 Pair Potential

The simplest model to represent the lattice is the continuum approximation in which the infinite lattice is approximated by a classical polarizable continuum. In a more realistic picture, an ionic crystal is regarded as composed of spherical, non-overlapping ions, bearing net charges of integral amount. The electrostatic interactions of those charges give rise to a net binding (Madelung energy).

Born and Mayer developed a classical model to evaluate the lattice energy of a crystal. In this model, the lattice energy of an ionic crystal is described as composed of energy terms arising from interactions between point charges and the overlap repulsive interactions. The Born-Mayer model requires the adoption of a specific functional dependence for the repulsive energy on the distance between the ions, involving strength and hardness parameters to be determined from crystal data. The repulsion between the various ions is approximated as assuming from central two-body forces, because many-body forces involving more than two ions are not usually important for ionic crystals.

In ionic materials, the long-range electrostatic forces are important. They can be included either by calculating the lattice sums out to infinity by the Ewald method[1.2], or by including a further cluster of point charges, outside the quantum-mechanical cluster. If there is a charged defect in ionic materials, the

problem is even more difficult, due to the long-range polarization. At large distances this contribution can be accounted for approximately by the classical method of Mott and Littleton, which associates the polarization produced within each unit cell with that predicted on the basis of macroscopic dielectric theory.

1.4.2 Shell Model

The shell model, developed by Dick & Overhauser[1.3], simulates the ions in a better way and it divides the ion into two point-charges with simple harmonic coupling between them. One is called the core and the other the shell, whence the name of shell model. The core is taken to carry the entire mass of the ion. The displacement of the shell from the core, which produces the ion's polarization, is controlled by Coulomb forces from other ions, and by the shell's coupling to its own core, as well as by its coupling to the shells of other ions via the short-range forces. The latter feature is essential, as it ensures that the ion's polarization represents a proper balance between internal and external forces. The shell model of an ionic lattice is described in terms of several parameters such as shell charge, shell-core coupling constant and shell-shell coupling constant. Determination of these values resorts to optimizing agreement between calculated and experimentally measured crystal properties such as lattice spacing, elastic and dielectric constants, and normal mode vibration frequencies.

1.4.3 Lattice Relaxation and Polarization

A point defect such as a vacancy or an impurity atom in a crystal lattice causes a certain distortion. It becomes necessary to obtain a precise knowledge about the distortion of surrounding lattice points, because many defect properties

such as transition energies, bandwidth and many other parameters are sensitive to the lattice configuration. A number of methods have been developed to calculate the static polarization and distortion near a defect.

The first, due to Eshelby[1.4], treats the defect as a singularity in an elastic continuum. This singular form of displacement gives a non-zero stress at the surface of the solid, and therefore it is incorrect. The additional 'image' displacement is created to ensure that this stress vanishes. It counts the actual displacement as the sum of the displacement in an infinite medium and an 'image' displacement as the perturbing effect of the boundary.

The second, developed by Mott and Littleton[1.5], considers the equilibrium of nearest neighbours in detail and regards the rest of the medium as a polarized continuum, i.e., two parts (Region I and II) of the lattice are treated differently. In Region I, the method assumes that the ions behave as point dipoles; the interaction of each ion in Region I with the defect charge and with the other ions in this region is counted as a function of the displacements and moments of ions in Region I only. The coupling between the displacements in Region I and the total moments in Region II contributes to the forces on the ions in Region I. In Region II, it assumes that the moments can be obtained from the macroscopic polarization induced by the effective charge of the defect. Thus the total energy is reduced to a function of the Region I variables alone. The method is iterative in that the size of Region I is progressively increased until the results are insensitive to the boundary.

The third method is that used by Kanzaki[1.6] and Matsubara[1.7]. The calculation is based entirely on the discrete nature of the crystal lattice and the distortion and polarization are calculated explicitly. The essential feature of this

method is to adopt the normal coordinate expansion for displacements. It is recognized that the lattice defect introduces extra terms in total energy. These depend on the displacements and dipole moments. This total energy of the distorted lattice is expanded in powers of the components of the displacements, and all terms beyond the second degree in the expansion are neglected. The appropriate derivatives of the energy are forces and field. The method solves a set of coupled linear equations of equilibrium for the displacements under these forces. A Fourier transform is applied to separate equations for the different wave-vectors. These decoupled equations can be solved by matrix multiplication. Finally the lattice displacements are obtained after an inverse Fourier transform.

It is seen from this method that the dynamical matrix of the host lattice is a key quantity. In calculating the dynamical matrix, there are two important models: Kellermann's rigid-ion model[1.8] and the shell-model[1.3].

The rigid-ion model ignores the polarization of the lattice ions and treats them as point ions interacting by long-range Coulomb and short-range repulsive forces. The parameters in the dynamical matrix can be expressed in terms of the ionic charge and elastic constant and the equilibrium lattice parameter. In the case of alkali halides, the matrix is (6*6).

The shell-model, which is a great improvement on point polarizable ion models, takes into account the polarization of the ions more satisfactorily. The outer electrons of each ion are treated as a shell which can move relative to the core, giving a dipole moment. The shell mass is assumed negligible. Arbitrary short-range forces connect the shells to their cores and the shells to neighbouring shells. The repulsive interaction is assumed to occur entirely between the shells of the ions and ignores the shell-other-core and core-core interactions. The

parameters in the dynamical matrix can be expressed in terms of those needed for the rigid-ion model together with the shell charges and the shell-core force constants. When the shell model is used to represent ions of alkali halides, the matrix becomes (12*12).

1.5 Electronic Structure of Isolated Defect

In principle, all electron states of a crystal should be determined self-consistently in a defect electron structure calculation, but a rigorous treatment is always not practical. For large gap ionic crystals, it is possible to employ more practical methods which are based on the few-electron approximation under which the electrons are divided into two groups. The first group contains the defect electrons, the electrons associated with the defect whose one-electron wave functions are particularly sensitive to the perturbing potential. The second group of the electrons, the core electrons, includes all the remaining electrons. First, it is assumed that the core electron wave functions are not significantly altered from the perfect crystal form. Second, it is assumed that the response of the core electrons to the presence of the defect can be represented by simple polarization effects and that the polarization can be calculated from the response of the perfect lattice. Thus the matrix elements of the perturbation due to a defect among core states must be appreciably less than the band gap of the perfect crystal. If the matrix elements are larger than this then more electrons must be classified as defect electrons. This approximation simplifies the problem to one in which only the defect-electron wave functions are varied in variational calculations and the core electrons thus contribute to the potential in which the defect electrons move and provide a constraint. It refers to the first group as a defect region which can

be simulated by a molecular cluster of ions whose electronic structure deviates significantly from that of the perfect lattice and therefore a quantum-mechanical treatment is needed to determine the defect electronic structure. In the following we present a few methods which are effective in defect structure calculations.

1.5.1 Effective-Mass Method and Green's Function Method

The effective-mass method is very useful in electronic structure calculations of shallow energy levels. The value comes in part from the ease of applying simple versions of the theory and in part from the fact that the approximations in the method are well defined. It reduces the many-body problem to a one-body problem, and the complexity of the perfect-lattice potential is eliminated, entering only through an effective mass and a dielectric constant. Even many-body effects can be included through these parameters. This method is not adequate for strongly localized defect electron calculations.

Green's function methods provide a convenient technique for solving the one-electron equation for a given potential. The only obvious restriction on the potential is that it is of short range in some convenient basis, usually the Wannier function representation. The Green's function method is actually useful for shallow states with very short-range potentials. Defect like the F-centre in ionic crystals will be badly treated by a Green's function method because the distortion and polarization of the host lattice are sensitive to the defect electron wave function[1.1].

1.5.2 Point-Ion Method

The simplest possible model is to treat the ions neighbouring a defect as

classical point charges[1.9]: the dominant effect binding the defect electrons is the Madelung potential. The results are often in acceptable agreement with experiment in terms of energy and are easily derived. Pseudo-potential arguments indicate that the point-ion approximation is a valid first approximation for colour centres[1.1], but discrepancies are mainly associated with poor wave functions.

1.5.3 Extended-Ion Method

In many cases the point-ion model does give results which are reasonably good. It is inadequate when information on defect effects, such as polarization and relaxation, on the lattice is needed. The ion can not be viewed as a structureless point and its inner structure has to be considered. This can be achieved by representing the lattice as an assembly of ions with appropriate electronic structure, and possibly by incorporating polarization and distortion. There are three aspects in the electronic structure of ions: the short-range screened Coulomb interaction with the defect wave function; exchange interactions; and orthogonalization to the occupied ionic orbitals. The last effect can be incorporated by carrying out an explicit orthogonalization[1.10-12] of the defect wave function to ions or by casting the Hamiltonian in pseudo-potential form[1.13-16]. The difference between a pseudo-potential method and direct orthogonalization is more a formal one than that of structure. It is usually assumed that the occupied core electron states are much more tightly bound than the state associated with the defect. Then two approaches can be introduced to improve the calculations: an extended-ion method and an ion-size method, the latter being an approximation of the former. Both models involve solving the one-electron Hartree-Fock equation of the defect

systems.

a) Ion-size Method

An attractive approach to the extended-ion treatment is the pseudo-potential method in which an extra term is added to the Hamiltonian. The method was originally developed by Gourary & Fein[1.13]. The main idea is based on that the positive kinetic energy associated with the rapid oscillations of the wave function within the core, arising from the requirement of orthogonality, cancels largely the negative potential energy of the electron when it is close to a nucleus and inside the screening core electrons. This substantial cancellation can simplify greatly subsequent parts of the calculation.

A simplified and convenient version of the pseudo-potential involves so-called ion-size parameters, proposed by Bartram et al[1.15]. This assumes that the pseudo wave function varies slowly over the ion cores, that ion-core wave functions on different sites are orthogonal, and that the core wave functions may be approximated by free-ion core functions. Thus the integrations over the core orbitals come up with ion-size parameters which are properties of each individual ion and have no dependence on the wave functions used, provided that this is slow-varying. Unfortunately, in many cases the slow-varying approximation does lead to some difficulties. It provides, however, a simple and convenient way for estimates of ion-size corrections.

b) Extended-ion Model

Extended-ion models avoid the assumption that the pseudo wave function varies slowly over the ion cores; here the detailed electronic structure of the ions is considered. Depending on the degrees of detail included in the electronic structure, complexity increases correspondingly. The estimates of lattice

distortion and electronic polarization can also be made by such models.

The hybrid pseudo-potential approach which has been developed by Song and his co-workers[1.17-18] based on the one electron Hartree-Fock approximation is an example of extended-ion treatments . It has two basic components. One is the exclusive use of floating 1s Gaussian basis functions. By floating basis we mean that the basis can be centred at any appropriate positions in the lattice. The other is the hybrid scheme of representing the effects of the occupied electrons. Only deep core electrons are represented by the first two orders of ion-size parameters, first introduced by Bartram et al[1.15], while the outer s and p shells are calculated explicitly by interpolation, because the diffuse nature of the outer s and p electrons as opposed to the deep core electrons may lead to a breakdown of the slow varying approximation. A set of efficient and accurate interpolation formulae are proposed to represent the Coulomb, exchange and overlap integrals between the outer shells and the excited electron expressed by a linear combination of floating 1s Gaussians. The efficiency of the formulae is attributed to the fact that the basis functions are Gaussians. The linear combination of Gaussians allows us to represent partly the correlation effect through extra degrees of freedom, because the correlation effect has been proved to be very important in those defect systems containing more than two particles. The energy of the distorted lattice is made up of the electrostatic Coulomb energy, the short range repulsive interaction of ion cores, and the polarization energy represented by the Mott and Littleton method.

1.6 Other More Advanced Methods

The ultimate aim of defect structure calculations in solids is to reach the

same level of sophistication as is reached by the quantum chemist in molecular calculations. Because of the number of atoms involved in a defect embedded in a crystal, there are some basic problems to address. A relatively small size(about a dozen atoms) quantum cluster is embedded inside an infinite lattice. Although there are no difficulties in solving the all electron Hartree-Fock equations of the quantum cluster, the problem of the boundary between the quantum cluster and the remainder of the crystal is multiple and complex. This includes the polarization of the region outside the quantum cluster and how to represent the electrons in the outside region. Various attempts have been made. Comprehensive reviews are given in reference[1.19-20].

In this section, we are going to present the most typical method called Ionic Crystal with Electronic Cluster Automatic Program or ICECAP in short. It is a program being developed to carry out a complete cluster-lattice calculation, and is described by Harding et al[1.21]. ICECAP is a computer program which simulates a quantum cluster embedded in an infinite crystal. In this method, the electrons of a small molecular cluster containing the defect are treated quantum-mechanically. The bare nuclei of the cluster and the ions of the remainder of the crystal are described in terms of point charges, point masses, and classical potentials. The total system energy is composed of three parts: 1. the Hartree-Fock total energy for the cluster including Coulomb interactions with the embedding lattice; 2. the interaction energy of the embedding lattice ions (shell and cores) among themselves plus their short-range interaction with the cluster; 3. the Coulomb energy of the cluster nuclei interacting among themselves and with the embedding lattice.

The ICECAP program evaluates the total energy by combining two

programs: a Hartree-Fock cluster program (UHF) which evaluates the above mentioned energy, one, and HADES which evaluates the remaining two parts of the energy. The iterative cycle varies the ionic positions in the cluster to minimize the total energy. This method was successfully applied to defect systems such as the F-centres and hydrogen in MgO, the V_k-centre in LiF, Cu^+ in NaF and the F^+-centre in MgO by Vail et al[1.22-24]. Application of this method to more complex systems like the self-trapped exciton[1.25-26] has encountered technical difficulties due to the lowering of symmetry during lattice distortion.

The method attempts to calculate the eigen-energy spectrum of a given defect as correctly as possible but inevitably starting with a rather simplified model. Such an approach seems to be quite promising and adequate for previously experimentally well studied defects. As a complete ab initio self-consistent approach, it depends very much on computer resources and is of course expensive to operate. It may be a better way to study defect systems by using those simpler, inexpensive methods, until enough knowledge has been accumulated, then more precise determinations could be performed by this calculation.

References 1

1.1 A. M. Stoneham, Theory of Defects in Solids (Oxford University Press, 1975)

1.2 M. P. Tosi, Solid State Physics, Vol.16, ed. by F. Seitz & D. Turnbull(Academic Press, New York and London, 1964) p. 14.

1.3 B. G. Dick & A. W. Overhauser, Phys. Rev. 112 (1958) 90

1.4 J. D. Eshelby, J. Appl. Phys. 25 (1954) 255

1.5 N. F. Mott & M. J. Littleton, Trans. Faraday Soc. 34 (1938) 485

1.6 H. Kanzaki, J. Phys. Chem. Solids 2 (1957) 24

1.7 T. J. Matsubara, J. Phys. Soc. Japan 7 (1952) 270

1.8 E. W. Kellermann, Phil. Trans. A238 (1940) 513

1.9 B. S. Gourary & F. J. Adrian, Phys. Rev. 105 (1957) 1180

1.10 F. Martino, Internat. J. Quantum Chem. 2 (1968) 217, 233

1.11 R. F. Wood & U. Opik, Phys. Rev. 179 (1969) 783

1.12 U. Opik & R. F. Wood, Phys. Rev. 179 (1969) 772

1.13 B. S Gourary & A. E. Fein, J. Appl. Phys. Suppl. 13 (1962) 331

1.14 L. K. Kubler & R. J. Friauf, Phys. Rev. A140 (1965) 1742

1.15 R. H. Bartram, A. M. Stoneham & P. Gash, Phys. Rev. 176 (1968) 1014

1.16 C. H. Wood & S. Wang, Phys. Rev. B7 (1973) 2810, 2827

1.17 L. Emery, C. H. Leung & K. S. Song, J. Phys. C: Solid State Phys. L361, 15(1982)

1.18 K. S. Song, L. Emery, G. Brunet & C. H. Leung, Nucl. Instrum. Methods, B1, 456(1984)

1.19 A. J. Fisher, Reviews of Solid State Science, edited by C N R Rao, World Scientific(Singapore, New Jersey, London, Hong Kong), Vol. 5, Nos. 2&3,

1991, page 107

1.20 J. M. Vail, R. Pandey & A. B. Kunz, Reviews of Solid State Science, edited by C N R Rao, World Scientific(Singapore, New Jersey, London, Hong Kong), Vol. 5, Nos. 2&3, 1991, page 241

1.21 J. H. Harding, A. H. Harker, P. B. Keegstra, R. Pandey, J. M. Vail & C. Woodward, Physica B131 (1985) 151

1.22 J. M. Vail, J. Phys. Chem. Solids 51 (1990) 589

1.23 J. M. Vail, A. H. Harker, J. H. Harding & P. Saul, J. Phys. C: Solid State Phys. 17 (1984) 3401

1.24 R. Pandey & J. M. Vail, J. Phys.: Condens. Matter 1 (1989) 2801

1.25 A. L. Shluger, N. Itoh, V. E. Puchin & E. N. Heifets, P. R. B44, 1499(1991)

1.26 R. C. Baetzold & K. S. Song, J. Phys.: Cond. Matter, 3, 2499(1991)

Chapter Two F'-Centre in Ionic Crystals

2.1 Introduction

The F'-centre is formed where two electrons are trapped at an anion vacancy. For alkali halide crystals, a large amount of experimental results have been obtained in this area of research[2.1-2.3]. Our principal interest is in the energy spectrum of the F'-centre, so we present some observed results first. In the literature, alkali halides were divided into two groups based on their characteristics. Those alkali halides (such as KCl, NaCl,...) with comparable cation and anion size were categorized as group I. In the group I materials, the main F' band lies at considerably lower energies than the F band. Also, a back-tunnelling into the ground state of the original F centre occurs subsequently, such that the F' state in the vicinity of an F centre works only as a short-lived intermediate state in the non-radiative deexcitation of the excited F centre. The observation shows that the band shape is rather broad with about 2.0eV half-width. The observed F' band of NaCl, for example[2.4], has an absorption peak at 2.4eV, and a band edge between 1.1eV and 1.7eV, depending on the different experiments. The optical binding energies in several other shallow bound alkali halides are about 1.0eV[2.1-2.3]; no bound excited states are observed. On the other hand, the crystals with small cation to anion ratios, like NaI, fall into group II. In group II materials, the back-tunnelling is not possible due to the very low-lying F' state, so that the F' centre produced by low temperature tunnelling from the relaxed excited F centre state to the F' state is no longer a short-lived intermediate but a totally stable state. Both bound ground and excited states are found in group II materials. The experiments on NaI show that the optical absorption peak

(corresponding to the transition from the excited triplet state to the conduction band) occurs at 1.45 eV, and the edge appears at about 1.0eV. Moreover, the absorption energy from the ground state to the excited singlet state is 2.4 eV[2.5].

Different methods have been developed in theoretical studies of the F'-centre. They include the continuum approach by Lynch & Robinson[2.4], the semicontinuum method by Pincherle[2.6], the polaron approach by Arora & Wang[2.7], point ion models by Raveche[2.8], and so on. Semicontinuum and continuum models, either with or without a central square well potential tc supplement the coulomb potential of the anion vacancy, lead to results which do not seem encouraging. In the polaron approach, the electronic and ionic polarizations are accounted for as exchange effects of excitons and phonons, respectively, between the two trapped electrons. The hydrogenic 1s trial function was used to get the ground state energy. Unfortunately, the results were in poor agreement with the experimental F' optical binding energies[2.9].

Generally, the point ion models yield better results. Based on this model, La and Bartram[2.10] start from a square well model and treat the difference between this and the point ion potential as a perturbation and utilize the Krumhansl-Schwartz approximation to calculate polarization effects. Krumhansl and Schwartz[2.11] developed the semicontinuum method to treat F-centre polarization and in their model, the anion vacancy is approximated by a spherical cavity of radius R in a dielectric continuum characterized by k, the static dielectric constant, and k_0, the square of the index of refraction; outside the cavity, the anion vacancy was taken as a point charge. Calculations of many alkali halides are favourable (in terms of comparison to absorption peaks) except for KCl[2.10]. Similar to this work, Strozier and Dick[2.12] considered also the leading corrections

to the potential and the orthogonality constraint from the finite extent of the ions. Polarization and distortion were treated in a continuum model. Only KCl was studied, the results agreeing fairly well with those of the experiment.

The above calculations differ so much in detail, each stressing a different feature, that a full comparison is of little value. All theories give a single bound state. The photoionization thresholds are in the right general range.

Those models, employing crude approximations to the lattice, fail to predict accurately various properties of the F'-centre. Therefore, we are motivated to study the F'-centre in ionic crystals by another approach.

In our approach, the defect electrons are represented by a linear combination of floating 1s Gaussian wave functions orthogonalized to the core orbitals of surrounding ions. All terms which are contained in the one-electron Hartree-Fock equations are treated according to a method developed earlier for single electron defects. Originally, this method was developed by Leung and Song[2.13] to study F-centres. Afterwards, it was modified and applied to investigate many single electron defects by Song and his co-workers[2.14,2.15,2.16]. In the present study with more than one electron, a method is developed to treat the two-particle interaction in the same way as for the single particle system. Among terms in the two-particle interaction, only those which are important are retained and represented by an interpolation scheme. Pair potentials of the Born-Mayer form are employed to represent the lattice; the polarization effect is counted by dividing the lattice into a discrete part and a continuous part and the contributions from both parts are summed together. The electron wave functions and the lattice relaxation are determined in a self-consistent way.

Four alkali halides, NaCl, KCl, NaBr, NaI, are studied in the present work.

These four crystals represent both group I and II described above. The calculated optical binding energies for NaCl and KCl, and transition energies for NaI are in good agreement with the observed ones. We introduced negative-U propertise to explain a deeply bound state in NaI, and also estimated the value of negative-U by our model. Our calculations provide detailed information about how the lattice relaxes in ground states and excited states. The floating Gaussian basis we employed allows a certain degree of freedom of electron-electron correlation. For example, the same method can be applied to the study of positron centres with some modifications. This work is to be presented in the next part of this thesis.

In the following parts, we first present our method of calculation in detail in section 2.2. All interesting results are reported in section 2.3. Finally some further discussions are given in section 2.4.

2.2 Method of Calculation

2.2.1 Lattice Coulomb Energy

The electrostatic Coulomb energy is calculated by considering an infinite lattice of point charges. The lattice Coulomb energy is the sum of all Madelung electrostatic energies of individual ions, making sure a given pair of point charges is not counted twice. For ions which remain at their perfect lattice sites, the potential is simply the Madelung potential with corrected contributions from those ions which have been displaced. For ions that have been displaced from their perfect lattice sites, the Madelung potential expanded in cubic harmonics[2.17] is employed. The idea is to replace the normal slowly converging Coulomb potential by a rapidly convergent sum over cubic harmonics:

$$V(r) = \sum_i \frac{q_i}{|r - R_i|} \quad \rightarrow \quad V(r) = \sum_{l=0}^{\infty} \frac{e}{d} b_l Y_l(r) \left(\frac{r}{d}\right)^l \tag{2.1}$$

where R_i and q_i are lattice sites and charges, d is the n-n cation-anion distance, b_l's are the coefficients specific to a lattice structure, $Y_l(r)$ are cubic harmonics of order l. This potential can be interpolated in any direction by using one set of coefficients and therefore it can be calculated at any point within the unit cell. Since the interpolation formula assumes all other ions are at their perfect lattice sites, the interpolated potential is then corrected for the displacement of the other ions that have been moved. The energy is then calculated and added to the total. For the FCC structure these coefficients have been determined up to the tenth order previously[2.17] and those we need are shown in Table 2.1.

2.2.2 Repulsive Energy

The short range repulsion of ion cores is expressed in the Born-Mayer form[2.18]

$$V_{ij} = A_{ij} \exp\left(-\frac{r}{\rho_{ij}}\right) \tag{2.2}$$

where r is the separation of ions i and j, and A_{ij} and ρ_{ij} are constants characteristic of each pair. The values of the coefficients were calculated by the method of Reitz, Seitz and Genberg[2.18] from the elastic constant, the lattice constant, and the Madelung constant of the crystal. For the alkali halide crystals studied in this work, they are given in Table 2.2.

Since the distances between positive ions and negative ions are much larger than the cation-anion distance, and the ionic radius of the cations is smaller than that of the anions, both cation-cation and anion-anion interactions have been neglected.

Table 2.1

Madelung potential interpolation coefficients for the FCC structure (dimensionless).

Coefficient	Cation Site	Anion Site
b_0	-1.747565	1.747565
b_3	0.00000	0.00000
b_4	-1.789291	1.789291
b_6	-0.247375	0.247375
b_7	0.00000	0.00000
b_8	-0.7735539	0.735539
b_{10}	-0.126339	0.126339

Table 2.2

Repulsive Constants ρ_{+-} (in unit of Bohr radius), A_{+-} (in unit of Hartree), and lattice constants r_0 (a.u.) at room temperature and 0K.

Crystal	ρ_{+-}	A_{+-}	r_0	temperature
NaCl	0.6066	40.1392	5.330	(300K)
NaCl	0.5700	63.4122	5.287	(0K)
KCl	0.6120	83.2650	5.950	(300K)
KCl	0.5694	150.846	5.900	(0K)
NaF	0.5480	24.5030	4.379	(300K)
NaF	0.5139	37.7410	4.354	(0K)
NaBr	0.6198	50.8510	5.648	(300K)
NaI	0.6520	60.3930	6.117	(300K)

2.2.3 Electronic Energy

For the defect system of an F'-centre, we start from the Schrodinger equation

$$H\psi = E\psi \tag{2.3}$$

$$H = H_1 + H_2 + H_{12} \tag{2.4}$$

where H_{12} is the coulomb interaction between the two electrons and H_1 and H_2 are single electron Hartree-Fock Hamiltonians of the form

$$H_i = -\frac{1}{2}\nabla_i^2 + V_{pi}(r_i) + V_{sc}(r_i) + V_{ex}(r_i) \qquad (\text{in a.u.}) \tag{2.5}$$

where the point ion potential V_{pi}, screened Coulomb potential V_{sc}, and exchange potential V_{ex} are:

$$V_{pi}(r) = -\sum_{\gamma}\frac{\tilde{Z}_\gamma}{|r - R_\gamma|} \tag{2.6}$$

$$V_{sc}(r) = -\sum_{\gamma}\frac{Z_\gamma - \tilde{Z}_\gamma}{|r - R_\gamma|} + 2\int \sum_{\lambda}^{n_\lambda}\frac{|\chi_{\gamma\lambda}(r_2)|^2}{|r - r_2|}dr_2 \tag{2.7}$$

$$V_{ex}(r_1) = -\sum_{\gamma\lambda}\int \frac{\chi_{\gamma\lambda}(r_1)\chi^*_{\gamma\lambda}(r_2)P_{12}}{r_{12}}dr_2 \tag{2.8}$$

and $\mathbf{r}$ is the defect electron position vector, R_γ is the position of the γth lattice site, $\chi_{\gamma\lambda}$ is the λth (doubly) occupied atomic core orbital on the γth atom, Z_γ is the nuclear charge, $\tilde{Z}_\gamma$ is the total charge of the ion or atom. The summation in γ includes all the atoms present in the problem.

We assume the F' electron wavefunction is a linear combination of products of two individual electron wavefunctions

$$\psi(r_1, r_2) = \sum_i C_i \phi_i(r_1, \alpha_{1i}, R_{1i})\,\phi_i(r_2, \alpha_{2i}, R_{2i}) \tag{2.9}$$

Here we do not write the electron spin coordinates explicitly. We show that the space symmetry of the wave function takes care of spin automatically. For example, the wave function is a linear combination of 4 basis: $\phi_m(r_1)\phi_m(r_2)$, $\phi_m(r_1)\phi_{-m}(r_2)$, $\phi_{-m}(r_1)\phi_m(r_2)$, $\phi_{-m}(r_1)\phi_{-m}(r_2)$, where the basis function is localized either at m or -m, they form the following singlet states:

$$\phi_m(r_1)\phi_m(r_2)(\alpha\beta - \beta\alpha) \tag{2.10}$$

$$\phi_{-m}(r_1)\phi_{-m}(r_2)(\alpha\beta - \beta\alpha) \tag{2.11}$$

$$[\,\phi_m(r_1)\phi_{-m}(r_2) + \phi_{-m}(r_1)\phi_m(r_2)\,](\alpha\beta - \beta\alpha) \tag{2.12}$$

and the triplet state:

$$[\,\phi_m(r_1)\phi_{-m}(r_2) - \phi_{-m}(r_1)\phi_m(r_2)\,](\alpha\alpha). \tag{2.13}$$

Note that the two remaining components of the triplet state given by Eg.(2.13) share the same space part. In addition, among the above three singlet states, we are interested only in the state which gives the lowest energy, i.e., Eg.(2.12), the other two are associated with different orbital states. Since the Hamiltonian is symmetric, its eigenfunction (just the orbital part) must either be symmetric or antisymmetric (w.r.t. interchange of two electrons). By using the above basis functions, the eigenfunctions are either symmetric or antisymmetric, which corresponds to singlet or triplet states respectively.

In eq.(2.9), the single particle wave function is written as

$$|\phi_i(r)\rangle = |G_i(r)\rangle - \sum_{\gamma\lambda} |\chi_{\gamma\lambda}\rangle\langle\chi_{\gamma\lambda}|G_i(r)\rangle \tag{2.14}$$

which is a one-electron pseudo-wavefunction $G_i(\mathbf{r})$ orthogonalized to the core orbitals $\chi_{\gamma\lambda}$. In (2.14), $G_i(r) = N_i \exp[-\alpha_i(r - a_i)^2]$ represents the 1s floating Gaussian. We take orthogonalized floating Gaussians as basis functions, because first of all, various terms of eq.(2.5) can be evaluated analytically, and secondly, in placing them judiciously on or around the defect centre we can treat as many different

symmetries of excited states as we want. Similarly, we can construct the two electron pseudo-wavefunctions:

$$|\phi_i(r_1)\phi_i(r_2)\rangle = |G_i(r_1)G_i(r_2)\rangle - \sum_{\gamma\lambda} |\chi_{\gamma\lambda} G_i(r_2)\rangle\langle \chi_{\gamma\lambda}|G_i(r_1)\rangle -$$

$$\sum_{\gamma\lambda} |\chi_{\gamma\lambda} G_i(r_1)\rangle\langle \chi_{\gamma\lambda}|G_i(r_2)\rangle + \sum_{\gamma\lambda}\sum_{\eta\kappa} |\chi_{\gamma\lambda}\chi_{\eta\kappa}\rangle\langle G_i(r_1)|\chi_{\gamma\lambda}\rangle\langle\chi_{\eta\kappa}|G_i(r_2)\rangle \quad (2.15)$$

The problem now is to solve the secular equation for the state ψ and its energy E

$$|H_{ij} - E S_{ij}| = 0 \quad (2.16)$$

with

$$H_{ij} = \langle\phi_i(r_1)|H_1|\phi_j(r_1)\rangle\langle\phi_i(r_2)|\phi_j(r_2)\rangle +$$

$$\langle\phi_i(r_1)|\phi_j(r_1)\rangle\langle\phi_i(r_2)|H_2|\phi_j(r_2)\rangle + \langle\phi_i(r_1)\phi_i(r_2)|H_{12}|\phi_j(r_1)\phi_j(r_2)\rangle \quad (2.17)$$

$$S_{ij} = \langle\phi_i(r_1)\phi_i(r_2)|\phi_j(r_1)\phi_j(r_2)\rangle \quad (2.18)$$

In (2.17), the first two terms on the right are the multiplication of one electron Hamiltonian matrix elements $(H_1)_{ij}$, $(H_2)_{ij}$ and overlap matrix elements $(S_2)_{ij}$, $(S_1)_{ij}$. Their calculation is not difficult.

i) Single Particle Term

First, we work on $(H_1)_{ij}$ and $(S_1)_{ij}$. Substituting (2.14) in them gives

$$(H_1)_{ij} = \langle G_i(r_1)|H_1|G_j(r_1)\rangle - \sum_{\gamma\lambda}\langle G_i(r_1)|\chi_{\gamma\lambda}\rangle\langle\chi_{\gamma\lambda}|H_1|G_j(r_1)\rangle$$

$$-\sum_{\gamma\lambda}\langle\chi_{\gamma\lambda})|G_j(r_1)\rangle\langle G_i(r_1)|H_1|\chi_{\gamma\lambda}\rangle + \sum_{\mu\eta}\sum_{\gamma\lambda}\langle G_i(r_1)|\chi_{\gamma\lambda}\rangle\langle\chi_{\mu\eta}|G_j(r_1)\rangle\langle\chi_{\gamma\lambda}|H_1|\chi_{\mu\eta}\rangle \quad (2.19)$$

$$(S_1)_{ij} = \langle G_i(r_1)|G_j(r_1)\rangle - 2\sum_{\gamma\lambda}\langle G_i(r_1)|\chi_{\gamma\lambda}\rangle\langle\chi_{\gamma\lambda}|G_j(r_1)\rangle$$

$$+\sum_{\mu\eta}\sum_{\gamma\lambda}\langle G_i(r_1)|\chi_{\gamma\lambda}\rangle\langle\chi_{\mu\eta}|G_j(r_1)\rangle\langle\chi_{\gamma\lambda}|\chi_{\mu\eta}\rangle \quad (2.20)$$

Note the H_1 in $\langle\chi_{\gamma\lambda}|H_1|\chi_{\mu\eta}\rangle$ and in $\langle\chi_{\gamma\lambda}|H_1|G_j(r_1)\rangle$ can be rewritten as

$$\varepsilon_{\gamma\lambda}\langle\chi_{\gamma\lambda}|\chi_{\mu\eta}\rangle \quad \text{and} \quad \varepsilon_{\gamma\lambda}\langle\chi_{i\lambda}|G_j(r_1)\rangle.$$

$\varepsilon_{\gamma\lambda}$ is the energy of the λth core orbital on the γth atom. It is the free atomic core energy, $\varepsilon^0_{\gamma\lambda}$ from the Clementi wave function table[2.19], shifted by the potential produced by the other ions in the lattice, $\Delta\varepsilon_\gamma$, whose calculation has been done in 2.2.1.

$$\varepsilon_{\gamma\lambda} = \varepsilon^0_{\gamma\lambda} + \Delta\varepsilon_\gamma \tag{2.21}$$

One knows that the overlap between core orbitals is small, and assumes the following relation is approximately true

$$\langle\chi_{\gamma\lambda}|\chi_{\mu\eta}\rangle = \delta_{\gamma\mu}\delta_{\lambda\eta} \tag{2.22}$$

The matrix elements (2.19) and (2.20) transform to

$$(H_1)_{ij} = \langle G_i(r_1)|T_1|G_j(r_1)\rangle + \langle G_i(r_1)|V_{pi}(r_1)|G_j(r_1)\rangle + \langle G_i(r_1)|V_{sc}(r_1)+V_{ex}(r_1)|G_j(r_1)\rangle - \sum_{\gamma\lambda}\varepsilon_{\gamma\lambda}\langle G_i(r_1)|\chi_{\gamma\lambda}\rangle\langle\chi_{\gamma\lambda}|G_j(r_1)\rangle \tag{2.23}$$

$$(S_1)_{ij} = \langle G_i(r_1)|G_j(r_1)\rangle - \sum_{\gamma\lambda}\langle G_i(r_1)|\chi_{\gamma\lambda}\rangle\langle\chi_{\gamma\lambda}|G_j(r_1)\rangle \tag{2.24}$$

On the right hand side of the above equations, the last two terms represent the effect of ion cores contributed by all the atoms present. In our calculation we use atomic orbitals obtained from a self-consistent field(SCF) calculation to represent the core wavefunctions. An anion, surrounded by cations in the lattice, is sitting at a potential well which has the effect of compacting the wavefunction slightly. Cations, on the other hand, are at a potential barrier which expands the wavefunction. This effect is more pronounced for anions than cations. Thus for cations, we used the atomic SCF orbitals of Clementi and Roetti[2.19]. However, for anions, the orbitals were recalculated using the SCF program in the presence of a square potential well.

The evaluation of kinetic energy, point-ion term and the Gaussian overlap

is straightforward. The derivation of these expressions is given in Appendix 2.1. The calculation of the effect of ion cores is complicated. Bartram et al..[2.20] developed a theory to treat the ion-size correction in which the pseudo-wavefunction was assumed to vary slowly over the region of an atomic core. We apply the same approximation to our Gaussians. When the Gaussian is expanded as a multipolar series about the site a_i, its first derivative can be taken as a constant due to this approximation. For instance, in eq.(2.24), because of the expansion of Gaussians in the ion-size term, the angular part of the integral can be readily evaluated, and the radial part can be further expanded in a Taylor's series about the same site. After some manipulation, the two lowest order ion-size terms can be expressed as(derivation is given in Appendix 2.2)

$$\sum_{\lambda} \langle G_i(r_1) | \chi_\lambda \rangle \langle \chi_\lambda | G_j(r_1) \rangle \approx \frac{1}{4} F_{i0}(0, a_i) F_{j0}(0, a_j) B + \frac{1}{8} \left(F_{i0}(0, a_i) F_{j0}^{(2)}(0, a_j) + F_{i0}^{(2)}(0, a_i) F_{j0}(0, a_j) \right) K' + \frac{9}{4} F_{i1}^{(1)}(0, a_i) F_{j1}^{(1)}(0, a_j) \frac{a_i \cdot a_j}{|a_i||a_j|} K \qquad (2.25)$$

where

$$B = \sum_{s\text{-core}} \left(\int \chi_\lambda dr \right)^2 \qquad (2.26)$$

$$K' = \sum_{s\text{-core}} \left(\int \chi_\lambda dr \right) \left(\int \chi_\lambda r^2 dr \right) \qquad (2.27)$$

$$K = \sum_{p\text{-core}} \left(\int \chi_\lambda r \cos\vartheta \, dr \right)^2 \qquad (2.28)$$

are ion-size parameters which have different values for different types of ions and $F_i^{(n)}$ are the expansion terms of G_i.

A similar treatment can be applied to the V_{sc} and V_{ex} term and in the same

order as above, we get

$$(V_{sc} + V_{ex})_{ij} = \frac{1}{4} F_{i0}(0, a_i) F_{j0}(0, a_j) A_0$$
$$+ \frac{1}{8}\left(F_{i0}(0, a_i) F_{j0}^{(2)}(0, a_j) + F_{i0}^{(2)}(0, a_i) F_{j0}(0, a_j)\right) J_0'$$
$$+ \frac{9}{4} F_{i1}^{(1)}(0, a_i) F_{j1}^{(1)}(0, a_j) \frac{a_i \cdot a_j}{|a_i||a_j|} J_0 \qquad (2.29)$$

where

$$A_0 = \int (V_{sc} + V_{ex})\, dr \qquad (2.30)$$

$$J_0' = \int (V_{sc} + V_{ex})\, r^2 dr \qquad (2.31)$$

$$J_0 = \int r \cos\vartheta\, (V_{sc} + V_{ex})\, r' \cos\vartheta'\, dr \qquad (2.32)$$

Here the difference between the Coulomb and exchange interaction should be emphasized. $V_{sc}(\mathbf{r})$ has an expression (2.7) in which the core charge distributes locally. We can introduce a charge density function to represent cores. The evaluation of the Coulomb interaction is easy because it is a local function. On the other hand, the exchange interaction is quite complicated because of its non-local character. We are not going into detail regarding this procedure and, therefore, only give an outline. As it is shown in (2.8), the exchange term can be generally written as

$$\sum_{\gamma\lambda} \int \phi^*(r_1) \frac{\chi_{\gamma\lambda}^*(r_1)\chi_{\gamma\lambda}(r_2)}{r_{12}} \phi^*(r_2)\, dr_1\, dr_2 \qquad (2.32a)$$

First, we need to expand the operator $1/r_{12}$ in spherical harmonics, then use the slow varying approximation to expand the wave function at the γth ion site

$$\phi(r) = \phi(r_\gamma) + \phi'(r_\gamma) \frac{(r - r_\gamma) \cdot r_\gamma}{|r_\gamma|} \qquad (2.32b)$$

where ϕ' is the radial derivative of ϕ (which is assumed to have spherical

symmetry). Through tedious algebra, the integration over spherical coordinates can be carried out and reduced to those $F^{(n)}$ functions in (2.29). The radial part takes the form (2.32) which is actually a two particle integration if we write V_{ex} in full form. This is why the two $r_{\cos\vartheta}$ (r and ϑ are the radial and azimuthal coordinates measured from the γth site along a line joining the site with the centre) are kept in eg.(2.32) because they belong to the expansion of different particle wave functions. Following Zwicker's[2.21] work which was later improved by Song et al..[2.14], the contribution of short range potential and the overlap terms are combined to define the ion-size parameters:

$$A = A_0 - \sum_{s\text{-core}} \varepsilon_\lambda^\ell B_\lambda \tag{2.33}$$

$$J' = J_0' - \sum_{s\text{-core}} \varepsilon_\lambda^\ell K_\lambda' \tag{2.34}$$

$$J = J_0 - \sum_{p\text{-core}} \varepsilon_\lambda^\ell K_\lambda \tag{2.35}$$

Here B_λ, K_λ' and K_λ are individual terms in the summation of eqs.(2.26), (2.27) and (2.28). The total ion-size correction of matrix elements $(H_1)_{ij}$ and $(S_1)_{ij}$ can now be written as

$$\langle G_i(r_1) | V_{sc}(r_1) + V_{ex}(r_1) | G_j(r_1)\rangle - \sum_{\gamma\lambda} \varepsilon_{\gamma\lambda} \langle G_i(r_1) | \chi_{\gamma\lambda}\rangle\langle \chi_{\gamma\lambda} | G_j(r_1)\rangle$$
$$= \sum_\gamma (f_1 A_\gamma + f_2 J_\gamma' + f_3 J_\gamma) - \sum_\gamma \Delta\varepsilon_\gamma (f_1 B_\gamma + f_2 K_\gamma' + f_3 K_\gamma) \tag{2.36}$$

$$\sum_{\gamma\lambda} \langle G_i(r_1) | \chi_{\gamma\lambda}\rangle\langle \chi_{\gamma\lambda} | G_j(r_1)\rangle = \sum_\gamma (f_1 B_\gamma + f_2 K_\gamma' + f_3 K_\gamma) \tag{2.37}$$

Here A and B are the lowest order terms formulated by Bartram et al., and J and K are the ones introduced by Zwicker. J' and K' are parameters of the same order as J and K, but they were neglected in Zwicker's paper. f_1, f_2 and f_3 are functions depending solely on the Gaussians and the vector joining them to the ion site. They are also given in Appendix 2.2.

It is found that when all core orbitals are included in the ion-size parameters, those higher order terms would have slow convergence. Yet when we exclude the outer s and p (OSP) electrons from the sums of eqs.(2.36) and (2.37), convergence turns out to be much faster. The reason is that the diffuse OSP electrons may result in the break-down of the slow varying approximation[2.14].

In our method, we use the first two orders of the ion-size parameters for deep core electrons only, while the OSP shells are calculated explicitly by interpolation. The ion-size parameters used in our calculation are given in Table 2.3.

The OSP interpolation scheme is performed in the following way. The screened Coulomb potential produced by the outermost shell is represented by a single term of the form:

$$V_{sc\gamma}(r) \rightarrow \frac{A_{sc\gamma}\exp\left[-\beta_{sc\gamma}(r-R_\gamma)^2\right]}{|r-R_\gamma|} \tag{2.38}$$

and fits to an interpolation formula

$$\langle G_i(r_1)|V_{sc\gamma}|G_j(r_1)\rangle = \int G_i(r_1)\frac{A_{sc\gamma}\exp\left[-\beta_{sc\gamma}(r_1-R_\gamma)^2\right]}{|r_1-R_\gamma|}G_j(r_1)\,dr_1 \tag{2.39}$$

For ion γ, the interpolation parameters $A_{sc,\gamma}$ and $\beta_{sc,\gamma}$ are determined in this way: the OSP orbitals in their Slater form are fitted to fifteen Gaussians; the contribution of OSP orbitals to the screened Coulomb interaction is calculated exactly for a range of the Gaussians' α_i and R_i, so that the interpolation formula will be applicable to all ions of the same type as ion γ. Then $A_{sc,\gamma}$ and $\beta_{sc,\gamma}$ are determined through a least squares fit. This procedure yields quite satisfactory fits, with RMS deviations not worse than 10^{-4}(in Hartree unit) in all cases. Those fitted parameters are given in Table 2.4.

Table 2.3

Deep core ion-size parameters for several ions (a.u.).

Ion	A	B	J	K	J′	K′
Na^+	6.8780	0.186	-0.0036	0.0000	0.2780	0.007
K^+	26.990	2.080	2.2300	0.2300	4.6800	0.370
Cl^-	26.205	3.143	3.591	0.5870	5.737	0.679
Br^-	33.911	5.018	8.0295	1.7059	8.7547	1.3396
I^-	55.145	11.173	24.0502	6.8634	26.465	5.261

We interpolate the exchange interaction in very much the same way. The exact form of the exchange potential is:

$$\langle G_i(r_1) \mid V_{ex\gamma} \mid G_j(r_1) \rangle = \sum_{\lambda}^{osp} \int G_i(r_2) \frac{\chi_{\gamma\lambda}(r_1)\, \chi_{\gamma\lambda}(r_2)}{|r_1 - r_2|} G_j(r_1)\, dr_1\, dr_2 \qquad (2.40)$$

and we fit this to an expression of the form:

$$\langle G_i(r_1) \mid V_{ex\gamma} \mid G_j(r_1) \rangle = \int G_i(r_1)\; A_{ex\gamma} \exp\left[- \beta_{ex\gamma} (r_1 - R_\gamma)^2 \right] G_j(r_1)\, dr_1 \qquad (2.41)$$

For such a short range interaction, the quality of the fit is slightly worse than the screened Coulomb interaction. The RMS deviation in all cases is better than 10^{-3}. The values of A_{ex} and β_{ex} are listed in Table 2.4.

The overlap integrals are terms of the form

$$ss\sigma = \int G_i(r_1)\, \chi_s(r_1)\, dr_1 \quad \text{and} \quad sp\sigma = \int G_i(r_1)\, \chi_{pz}(r_1)\, dr_1 \qquad (2.42)$$

We fit the overlap of a single Gaussian with the outer S and P states separately. Only the $sp\sigma$ integral needs to be calculated because the $sp\pi$ integral is 0 by symmetry. Any general sp overlap may be decomposed into its σ and π components and only $sp\sigma$ will be non zero.

It is found that an interpolation formula using one Gaussian to represent $ss\sigma$ and $sp\sigma$ is inadequate compared to the accuracy of the screened Coulomb and exchange terms. However, two Gaussians with their exponents related by a simple ratio give fits of sufficient accuracy. Therefore we use two Gaussians to represent the overlap with the outer s core states:

$$ss\sigma \rightarrow \langle G_i \mid \chi_s \rangle = N \int G_i \left[N_1 \exp(-\beta_{sov1} r^2) + A_{sov1} N_2 \exp(-\beta_{sov1} r^2 / \rho_s) \right] dr \qquad (2.43)$$

Here ρ_s is the ratio of the exponents of two fitted Gaussians, which is a parameter

Table 2.4

Short range potential interpolation parameters for several ions (a.u.).

Ion	β_{sc}	A_{sc}	β_{ex}	A_{ex}
Na^+	1.9490	-4.1241	1.0096	-4.1764
K^+	0.8800	-5.3445	0.3872	-2.3839
Cl^-	0.3824	-4.2711	0.2589	-2.5163
Br^-	0.3062	-4.5465	0.1933	-2.0249
I^-	0.2592	-5.2152	0.1221	-1.1958

that is adjusted to give the best least squares fit. Usually ρ_s=4 gives the best fit. A_{sovl} and β_{sovl} are parameters determined by the least squares fitting procedure. N_1, N_2 and N are normalization factors determined by the other parameters of the equation.

Similarly, the overlap with the outer p shell is fitted to a function of the form:

$$sp\sigma \rightarrow \langle G_i | \chi_{pz} \rangle = N' \int G_i \left[N_1' \exp(-\beta_{povl} r^2) + A_{povl} N_2' \exp(-\beta_{povl} r^2/\rho_p) \right] z \, dr \qquad (2.44)$$

Here, all the parameters are determined in the same way as for the s shell overlap. The accuracy of the s overlap is better than 10^{-4} in RMS deviation in all cases, while for the p shell overlap the fit is slightly worse with the RMS deviation generally being one order of magnitude lower. The values of the overlap parameters are listed in Table 2.5.

ii) Two Particle Term

The interaction term involves two particle integration. It is specific for a two particle defect system like the F'-centre. We have to develop a way to treat this term in a similar fashion as the one-electron forms. Thus we are able to deal with the two electron defect systems. Substitution of the wave function (2.15) into the last term of (2.17), after a little tedious work, gives 16 terms in total, expressions of which are given in Appendix 2.3. Those terms can be classified into 5 categories: 0 χ, 1χ, 2χ, 3χ, and 4χ terms. Here, an nχ term (n=0-4) represents a term consisting of an integral involving n core orbitals, multiplied by n overlaps of the form $\langle G_i | \chi_\gamma \rangle$. Among six 2$\chi$ terms, we further classify them into 2χ Coulomb-like terms and 2χ exchange-like terms according to whether the two core orbitals in the integral have the same or different electronic coordinates.

Table 2.5

Overlap interpolation parameters for several ions (a.u.).

Ion	β_{sovl}	β_{povl}	ρ_s	ρ_p	A_{sovl}	A_{povl}	E_s	E_p
Na^+	1.250	1.250	4	6	0.1597	0.0667	-3.076	-1.797
K^+	0.600	1.300	4	5	0.2115	0.8480	-1.9644	-1.1711
Cl^-	0.500	0.375	4	4	0.557	0.3640	-0.699	-0.117
Br^-	1.100	0.350	8	5	1.403	0.4463	-0.679	-0.1332
I^-	1.060	0.310	10	4	1.573	0.8334	-0.551	-0.125

There is only one 0χ term, which involves four Gaussians, and this represents the dominant contribution to $(H_{12})_{ij}$. The calculation of such a term is straightforward and it is given in Appendix 2.4. All the other terms involve overlaps between the Gaussians and the core states. For localized defects, such as the F´-centre, the overlap with the deep core orbitals is much smaller than that with the outer-most s and p valence orbitals. It is thus a good approximation to neglect all the deep core orbitals in all the $n\chi$ terms($n \neq 0$).

Initially, all these terms are evaluated accurately from analytic expressions of these integrals after the OSP valence orbitals are represented by a sufficiently large number (15) of Gaussians which are interpolated from Slater orbitals as we did earlier for OSP orbitals. The results of this tedious calculation show that we need to consider only the 1χ and 2χ Coulomb-like terms, because the remaining 2χ exchange-like, 3χ and 4χ terms are at least two orders of magnitude smaller in comparison. Here we list the estimated order of magnitude of those terms for reference: $1\chi \sim 0.7*10^{-1}$, 2χ(Coulomb)$\sim 0.4*10^{-2}$, 2χ(exchange)$\sim 0.2*10^{-4}$, $3\chi \sim 0.8*10^{-5}$, $4\chi \sim 0.8*10^{-5}$.

In order to further reduce the computation time, we have attempted to represent the OSP valence orbitals by single Gaussians:

$$\chi_{s\gamma} \rightarrow A_s \exp[-\beta_s(r - R_\gamma)^2] \tag{2.45}$$

$$\chi_{p\gamma} \rightarrow A_p(z - Z_\gamma)\exp[-\beta_p(r - R_\gamma)^2] \tag{2.46}$$

where the parameters A´s and β´s are adjusted so as to fit the exact values of the 1χ and 2χ Coulomb-like terms. The fitting was performed by the least squares method over a range of distance between the ion core χ and the floating Gaussian G (0 - 15 a.u.) and a range of Gaussian exponents of G (0.02 - 0.12 a.u.). It is quite interesting that the fitting is generally very satisfactory, with a RMS deviation of

about 10^{-4} in all cases. Taking a closer look, we find the factor A's are around 1 and for the same ion, the β's are rather close to a common value. This implies that common parameters may be found. In other words, the core orbital can be represented by fitted single Gaussians no matter where it may appear. In fact, we know the interpolation program keeps searching until the best fit is reached. Besides the best fit, there are a couple of local minimums which provide us with some degrees of freedom in choosing fitted Gaussian parameters. So a single Gaussian with common parameters can be found to represent the s core of the same ion at the expense of sacrificing a little RMS. Now we have two single Gaussians, one for the cation and the other for the anion. The fitting is still good enough with RMS deviations better than 10^{-3}.

The p cores are more complicated due to different geometries and configurations. There are three basic terms $_1\chi(p_x)$, $_2\chi(p_xp_x)$ and $_2\chi(p_xs)$ which need to be fitted. All the remaining terms could be taken care of by direction cosines. The fitting procedure is the same as that of the s cores. The parameters also suggest that the same idea as used in the s cores could be applied. Thus a single Gaussian could be chosen to represent the p core without caring which type of term it is in. The fitting is not worse than that of the s core. Now all the parameters chosen in such a way, for both s and p cores, are exhibited in the following Table 2.6.

With these parameters, the interaction Hamiltonian matrix element calculation becomes much more simple, because all terms involve Gaussians only. The core orbitals in overlap integrals have been fitted earlier in the single particle term. We simply use the fitted parameters of $_{ss\sigma}$ and $_{sp\sigma}$ to carry out overlap integrations and then multiply them by the corresponding interaction

integrals. What we need to do next is to work out all configurations and geometries, then replace core orbitals with corresponding fitted Gaussians and perform the calculation. Due to summation on the atomic site, for the terms with more than two cores, we have to consider the situation where cores could be either at the same site like $\langle \chi(r_\lambda) G_i(r_2) | H_{12} | \chi(r_\lambda) G_j(r_2) \rangle$(called on-centre cores) for example, or different site (off-centre cores like $\langle \chi(r_\lambda) G_i(r_2) | H_{12} | \chi(r_\mu) G_j(r_2) \rangle$ $\lambda \neq \mu$, for instance). Certainly our interpolation is performed only for on-centre cores and the similar fitting for off-centre cores shall not be a problem in principle. As a matter of fact, the off-centre cores appear only in the 2χ Coulomb-like term. Estimation based on exact calculation can be used to compare the on-centre and off-centre cores. It is found that the values of those integrals involving off-centre cores are about one-fourth of those involving on-centre cores. This is because the compact character of core orbitals makes the overlap between the core orbitals at different sites very small. Supposing that we could still use those single Gaussians fitted for on-centre cores to perform the off-centre core calculation, we found that such calculated values were about two-thirds of the exact ones. The points here are: first, the contributions of off-centre cores themselves are small, and second, our calculation using Gaussians for on-centre cores is not too bad. Therefore, a crude approximation is made here for off-centre cores employing single Gaussians fitted for on-centre cores. This may have a minor influence on our results. Up until now, the total Hamiltonian matrix element can be worked out without any further problem; the total overlap matrix element can be simply obtained by the same procedure with the Hamiltonian dropped. Hence, the electronic energy of the F'-centre can be easily found through solving the secular equation (2.16). It yields eigenvalues and eigenvectors simultaneously.

Table 2.6

Interaction term interpolation parameters for several ions (a.u.).

Ion	β_s	A_s	β_p	A_p
Na^+	0.93	1.00	0.97	1.00
K^+	0.408	1.00	0.437	1.00
Cl^-	0.28	1.00	0.23	1.00
Br^-	0.22	1.00	0.203	1.00
I^-	0.17	1.00	0.145	1.00

2.2.4 Polarization Energy

Due to the net charge of the defect system, the lattice polarization effect is quite strong. Because of the existence of the long range coulomb interaction, our cluster model with limited a number of ions(619) may not be enough. Therefore we develop a method in which the lattice is divided into two regions. The polarization effects are treated differently in these two regions. Region I contains those ions close to the vacancy, and region II represents the rest of ions up to infinity. The polarization energies of region I ions are calculated by the Mott-Littleton method of lowest order[2.22] in which the ions are assumed to behave like point dipoles with polarizability equal to the free atomic polarizability[2.22] and the polarization energy is proportional to the local field. Another approximation is that all dipole vectors and electric field vectors are constrained to be radial. This is reasonable because the electron charge cloud and the atomic displacements are of nearly radial symmetry. Thus the polarization energy can be expressed as

$$E_{pol}^{I} = -\frac{1}{2}\sum_{\gamma}\alpha_{\gamma}E_{loc}^{2}(R_{\gamma}) \qquad (2.47)$$

where E_{loc} is the local electric field produced by all other ions and the defect system in the neighbourhood of an ion at R_γ, and α_γ is the free atomic polarizability of ion γ. This is valid when the overlap between neighbouring atoms is small. For those systems we are considering, large displacements rarely occur, therefore such an approximation should be reasonably good. As a matter of fact, as will be seen in the discussion of lattice distortion, the first and the third shell ions around the defect move inward, while the second and the fourth shell ions go outward, thus the relative distance of neighbouring atoms changes very little. The above expression of polarization energy was developed by Druger and Knox[2.23] which includes the contributions of the induced dipole moment in the field. In our work,

we neglect the effect of induced dipoles, but we still have adopted this expression as an approximation.

There are two main contributions to the local electric field at any ion site: one is the electric field due to lattice distortion and the other is the electric field produced by defect electrons. First we determine the lattice potential V generated by lattice distortion, then we calculate the gradient of the potential numerically in the immediate neighbourhood of the ion in question by linear interpolation.

$$E_{LD} = -\nabla V \tag{2.48}$$

Here the calculation of the potential follows the method described in 2.2.1.

Second we use the eigenfunctions from the electronic energy calculation to get the field created by defect charges. The charge density of the F'-centre is

$$\rho(r) = -\int |\psi(r_1, r_2)|^2 \left[\delta(r - r_1) + \delta(r - r_2)\right] dr_1 dr_2 + \delta(r) \tag{2.49}$$

in which $\delta(r)$ represents the positive effective charge of the vacancy. In this part of the calculation, we neglect the orthogonality constraint to the wavefunctions, so the wavefunctions have to be renormalized. Then the field can be determined by Gauss's Law

$$E_{DF}(R_\gamma) = -\sum_{ij} Q^*_{ij}(R_\gamma) \frac{R_{ij} - R_\gamma}{|R_{ij} - R_\gamma|^3} \tag{2.50}$$

where $R_{ij} = \frac{\alpha_i a_i + \alpha_j a_j}{\alpha_i + \alpha_j}$ is the reduced position of the contracted Gaussians and $Q^*_{ij}(R_\gamma)$ is defined as the effect charge enclosed in a Gaussian sphere. Adding this field to the one obtained from lattice distortion and summing over all ions in region I, we get the polarization energy in this region:

$$E^I_{pol} = -\frac{1}{2} \sum_\gamma \alpha_\gamma \left[E_{LD}(R_\gamma) + E_{DF}(R_\gamma)\right]^2 \tag{2.51}$$

The outer region II is treated as a dielectric continuum following the

method developed by Hardy and Lidiard[2.18]. The method is derived to discuss the polarization and displacements caused by charged point defects in ionic crystals. Similarly the ions are assumed to be point dipoles. These dipoles are generated by the electric field acting on the ions, electric dipoles, and also by the relative movement of anions and cations which lead to deformation dipoles. Thus the dipole moment of a unit cell can be written as a sum of the dipole moment of the anion and cation, and the deformation dipole moment. These dipole moments are given by

$$\vec{\mu}_{+,-} = \left(\frac{Z\,e\,r}{r^3}\right)\frac{v_a}{4\pi}\left(1-\frac{1}{\varepsilon_0}\right)\frac{\alpha_{+,-}}{\alpha_+ + \alpha_- + \dfrac{2(e^*)^2}{p}} \tag{2.52}$$

$$\vec{\mu}_d = \left(\frac{Z\,e\,r}{r^3}\right)\frac{v_a}{4\pi}\left(1-\frac{1}{\varepsilon_0}\right)\frac{\dfrac{2e^*(e^*-e)}{p}}{\alpha_+ + \alpha_- + \dfrac{2e^{*2}}{p}} \tag{2.53}$$

where Ze is the effective charge in the defect, v_a the unit cell volume, ε_0 the static dielectric constant, α_+, α_- the polarizabilities of anions and cations, e^* the Szigeti effective charge[2.24], and p the force constant which can be determined by the n-n distance r_0 and the n-n part of the compressibility through the relation $\kappa_{nn}=12r_0/p$. The moments so obtained are then generally assumed to be correct for all ions except those in the immediate vicinity of the defect. Even though there is still a question how close to the defect do the moments remain valid, we can choose the region I large enough to make it safe to do so. We are dealing with crystals with cubic symmetry, so the dielectric constants are scalars. The electric field in this region is

$$E^{II} = \frac{D}{\varepsilon_\infty} = \frac{Zer}{r^3 \varepsilon_\infty} \tag{2.54}$$

where ε_∞ is the high frequency dielectric constant. Finally the corresponding energy is

$$E^{II}_{pol} = \frac{1}{2}\int_{\Omega}^{\infty} E^{II} \cdot \left[\vec{\mu}_+ + \vec{\mu}_- + \vec{\mu}_d \right] \frac{dr}{v_a} \tag{2.55}$$

Here Ω=nva/2 is the volume of the region I to be determined by assuming the region I is a sphere of radius r and contains n ions. All constants appearing in the equations are listed in Table 2.7.

In principle the larger the region I is, the more accurate the result can be. In our cluster model, there is a sub-cluster which contains those ions allowed to move. It is natural to take this sub-cluster as region I so that its size can be adjusted at will. With the increase of region I, the boundary effect becomes small, but the calculation turns expensive. Fortunately, it is found that there is a good convergence of energy as the region I expands shell by shell when it exceeds the third shell. So we make the decision to take ions in the first four shells as region I so that better accuracy can be kept. Now the total polarization energy is simply the sum of two parts:

$$E_{pol} = E^{I}_{pol} + E^{II}_{pol} \tag{2.56}$$

where I and II represent discrete region I and continuous region II, respectively.

Table 2.7

Constants for the polarization energy calculation of the continuum.

	NaCl	KCl	NaBr	NaI	
κ_{nn} (cm^2/dyne)	$4.26 * 10^{-12}$	$5.63*10^{-12}$	$5.08 * 10^{-12}$	$7.07 * 10^{-12}$	(2.25)
r_0 (cm)	$2.820 *10^{-8}$	3.1467	$2.987 *10^{-8}$	$3.237 *10^{-8}$	(2.26)
p (dyne / cm)	$8.236 *10^{4}$	$6.707*10^{4}$	$7.04 *10^{4}$	$5.48 *10^{4}$	
α_+ (cm^3)	$0.28 *10^{-24}$	$1.149*10^{24}$	$0.28 *10^{-24}$	$0.28 *10^{-24}$	(2.25)
α_- (cm^3)	$2.92 *10^{-24}$	$2.92*10^{-24}$	$4.12 *10^{-24}$	$6.41 *10^{-24}$	(2.25)
s	0.74 0.80	0.69	0.71	(2.25)	
ε_0	5.62	4.68	5.99	6.60	(2.25)
ε_∞	2.25	2.13	2.62	2.91	(2.25)

2.2.5 Minimization Method

Up to now, we have solved the problem of energy calculation, but there remains a question of finding the minimum energy configuration of the multidimensional space of the crystal. So a minimization procedure is developed to solve this problem[2.27]. We minimize the total energy with respect to individual ion position:

$$E_t = E_{coul} + E_{rep} + E_{elec} + E_{pol}^{I} \qquad (2.57)$$

where the various constituent energies have been described in the previous sections.

We treat three degrees of freedom at one time by optimizing the positions of each ion individually. The same process is carried out in sequence over all ions allowed to move. We then repeat the whole procedure and iterate until we reach the energy convergence to some pre-determined value. For the present work in which ions in region I are allowed to move, the convergence is usually obtained after about ten iterations.

The energy gradient is evaluated by an interpolation scheme which was developed by Brunet, Leung & Song[2.27]. First, we interpolate the energy surface to first order of ion displacement:

$$E = a_0 + a_1x + a_2y + a_3z \qquad (2.58)$$

This requires the energy to be sampled at four points. In practice we need only calculate the energy at three points since one point can be the energy before the ion is moved, which is obtained from the minimization of the previous cycle. For the other three sampling points we choose three mutually perpendicular directions to avoid problems with linear dependence, when we solve the set of 4 simultaneous equations for the coefficients of eq.(2.58). We can now calculate the

direction and magnitude of the gradient of the energy surface in these three dimensions. As with the polarization energy, we must choose sampling points which are close together by the definition of the derivative, and yet not so close as to lose accuracy in the numerical treatment.

Then to calculate the minimum energy position of the ion, we interpolate to second order along a line in the direction of $-\nabla E$:

$$E = a + \delta b + c\delta^2 \qquad (2.59)$$

where δ is the displacement of the ion in this direction.

Here we need to evaluate the energy at only one more point since we already know a and b (a is the energy at $\delta=0$ while $b = |\nabla E|$ at $\delta=0$). Then it is straightforward to determine the position of minimum energy, δ_m:

$$\frac{dE}{d\delta} = 0 \quad \text{at} \quad \delta_m \quad \rightarrow \quad \delta_m = \frac{b}{2c} \qquad (2.60)$$

The ion is then moved a distance δ_m in the $-\nabla E$ direction. We reevaluate the energy with the ion at this position and compare it with the other energies that have been calculated in the course of the minimization, and the ion is placed at the position that gives the lowest energy.

We can determine how good the interpolation is by evaluating eq.(2.59) with $\delta=\delta_m$. It was found that such a quadratic interpolation is quite accurate.

2.2.6 Choice of Basis

There are some obvious features in our choice of basis. First, both the position and decay factor of the floating Gaussians have to be optimized. Second, depending on the symmetry of the state of interest, the basis can be combined in certain ways to simulate different orbitals. For instance, a p-like state can be easily formed by a pair of Gaussians

$$\psi_P \rightarrow [\, G(\alpha_i, r-R) - G(\alpha_i, r+R) \,] \qquad (2.62)$$

The use of a Gaussian basis also makes all interpolation formulae become very simple.

There are several other more subtle advantages in our approach associated with the floating Gaussian basis. Since the Hamiltonian H is symmetric w.r.t., the interchange (P_{12}) of $\mathbf{r}_1$ and $\mathbf{r}_2$, the eigenfunction of H must be either (space) symmetric or (space) antisymmetric w.r.t. P_{12}. These correspond to spin singlet and spin triplet states, respectively. In our method, the basis set $\{\phi_i(r_1)\phi_i(r_2)\}$ must be chosen to include the basis $P_{12}\{\phi_i(r_1)\phi_i(r_2)\}$. Then diagonalization of H would yield directly symmetric (singlet) states and antisymmetric (triplet) states. In addition, the form of our two-electron wave function, being a combination of product Gaussian functions, shows that the present method is quite distinct from the usual H-F approximation, and that electron correlation is partly contained. For example, one combination of such basis arranged as follows:

$$G(\alpha_i, r_1 - A)G(\alpha_i, r_2 + A) + G(\alpha_i, r_2 + A)G(\alpha_i, r_1 - A) \rightarrow$$

$$\exp\left[-\alpha_i (r_1^2 + r_2^2 + 2A^2)\right] \cosh(2\alpha_i A \cdot r_{12}) \qquad (2.61)$$

takes the correlation effect into account in a special form as it is seen that $\mathbf{r}_{12}$ appears in the right hand side. We refer to this type of basis as an off-centre basis. It may be true that the correlation is not fully counted by these sorts of basis, because $\mathbf{r}_{12}$ appears in the form of a projection in some direction instead of $\mathbf{r}_{12}$ itself explicitly. However, we can add more off-centre basis to increase the weight of correlation.

2.2.7 Lattice Relaxation and Basis Optimization

For simplicity, we shall indicate only the Gaussian part of the F'-centre wave function. The ground state of F' electrons is expected to be in the 1s1s state where both electrons reside in the lowest 1s state, so first we consider this state. The wave function is taken as:

$$\psi_g(r_1, r_2) = G(\alpha_i, r_1 - 0)\, G(\alpha_i, r_2 - 0) \tag{2.63}$$

where α_i is determined by minimization of the electronic energy with the lattice held in its perfect configuration. This type of basis is called an on-centre basis due to its being placed at the centre of the vacancy site. Obviously it is an s-like basis. We use this basis to determine the lattice distortion through minimization of the total energy of the system. Ions in region I are allowed to relax explicitly. Generally, it is sufficient to include the four neighbouring shells to the vacancy as region I for good convergence. The results of the nearest neighbour cation displacements are given in Table 2.8. Experimental data are not available. To our best knowledge, so far there has been no clear figure about lattice relaxation in F'-centers. Our calculated values are generally much larger than those obtained by Berezin[2.28]. This may be due to the fact that in Berezin's work, only six nearest cations were allowed to move. It is found that the first shell cations move inward 12% (NaCl), 14% (KCl), 16% (NaBr) and 16% (NaI) in term of the nearest neighbour distance a, but the O_h symmetry of the defect is kept unchanged. It also shows a general trend that the first shell ions of those crystals having larger nearest neighbour distance shrink more. The second shell ions then experience non-negligible outward distortion. In terms of a, these are 5.6%, 2.6%, 5.7%, and 1.4% for NaCl, KCl, NaBr and NaI respectively. The displacements of the third and fourth shell ions are generally small.

Excited states can be treated in a similar way. We are interested in the

lowest excited state which may be either $(1s2s)^{S=1}$ or $(1s2p)^{S=1}$ (superindex 3 will be used to represent a tripelt state). Using a Gaussian basis approach, we have difficulty to simulate 2s state accurately. In this work we choose $(1s2p)^3$ to be the excited state to study. We represent a p-like wave function by a pair of Gaussians like eq.(2.58), and $(1s2p)^3$ can be constructed as:

$$\psi(r_1, r_2) = G(\alpha, x_1)[G(\alpha, r_2 - (-x, 0, 0)) - G(\alpha, r_2 - (x, 0, 0))] - [G(\alpha, r_1 - (-x, 0, 0)) - G(\alpha, r_1 - (x, 0, 0))] G(\alpha, x_2) \quad (2.64)$$

As in the ground state, α and x are treated as variational parameters, and the distortion field is determined using the optimized parameters. The results are also given in Table 2.8. It is interesting to note that for the excited state the ions on the [1,0,0] axis have very small distortions, but those on the [0,1,0] and [0,0,1] axes move inward by a large amount for the excited state, and symmetry is lowered to D_{4h} point group.

Because of the excessive computing time involved, we have not refined our calculation for the lattice distortion by using a larger basis set for electron wave function. We have however used the above determined lattice configuration to improve the electron wave function. The system total energy can be further minimized by enlarging the basis set for both ground state and excited state. It is known from the Hydrogen molecule that the electron correlation is not a negligible contribution. In the lattice it is supposed to be even stronger. To count this effect, off-centre bases are introduced along each principal axis, and thereby the configuration interaction lowers the energy a considerable amount (0.7 eV). The convergent energy is obtained by using the basis set consisting of 5 on-centre bases (with optimized α_i : 0.03 - 0.07 in a.u.) and 6 off-centre bases (with α_i : 0.05 in a.u.; x,y,z : 0.1 in unit of a) placed symmetrically along each axis.

Table 2.8

The coordinates of ion displacement in both ground state(G.S.) and excited state(E.S.) in a.u..

	NaCl			NaBr			NaI			KCl			
	δ X	δY	δZ	δX	δY	δZ	δX	δY	δZ	δX	δY	δZ	
G.S.	0.63	0.0	0.0	0.94	0.0	0.0	1.44	0.0	0.0	0.86	0.0	0.0	(-1 0 0)
E. S.	- 0.09	0.0	0.0	0.00	0.0	0.0	0.35	0.0	0.0				(-1 0 0)
	0.00	0.0	0.80	0.00	0.0	1.14	0.00	0.0	1.67				(0 0-1)

In fact, the exact ground state of the F'-centre can not be a pure s state since it must contain cubic harmonic contributions to allow the electrons to avoid the ion cores. Our ground state basis set containing both on-centre and off-centre bases is not a pure s state. In dealing with two bound electron systems like H_2, and F'-centres, one always tries to introduce the correlation terms into the variational trial wavefunction so that the configuration interaction would improve the result (2.10). Fortunately our method does include this contribution. That's why we feel more confident of our results.

The excited state energy can also be calculated by the same technique. The lattice configuration for excited state has been determined earlier, however, a large p-like basis set would improve the energy. It is found that one with combinations of three p-like Gaussians (α_i : 0.04, 0.05, 0.06 in a.u.; $\pm x$: 0.05, 0.04, 0.02 in unit a) gives the best energy. We would remark that in actual calculations, it is more convenient to use distinct pairs of Gaussians as basis functions. Diagonalization of the Hamiltonian would in general yield singlet and triplet states of various symmetry, and the advantage of using Gaussian basis functions is shown clearly.

2.3 Results

2.3.1 Optical Binding Energy & Thermal Dissociation Energy

An aspect that is frequently investigated, both experimentally and theoretically, is the optical binding energy of F' electrons. Usually, what is experimentally observed is the F' absorption spectrum or the F' band. Crystals in the freshly-quenched state are believed to contain atomically-dispersed F centres

almost exclusively. On illuminating such a crystal with light that falls spectrally within the F band range at a temperature above liquid nitrogen temperature, a new band labelled F' appears at the expense of the F band. The F' band is very wide (halfwidth about 2 eV), the larger portion of it usually extending on the long wavelength side of the F band. A notable exception seems to be NaI (and possibly NaBr too), where the F' band lies chiefly on the high-energy side of the F band(2.30). As the temperature gets higher, the F' becomes increasingly unstable thermally. In many alkali halides, the F' band occurs just as a transient band at room temperature. The F'-centre is also optically unstable: light in the F' band range bleaches that band at arbitrarily low temperatures, the F band recovering in the process. The F' band shape is believed to be temperature-insensitive. Although this conclusion is mainly based on low-temperature measurements (within the F' thermal-stability range), it has also been confirmed at room temperature in absorption experiments(2.31). The temperature insensitivity and the optical bleach ability of the F' band at low temperature, as well as its large halfwidth, suggest strongly that the band corresponds to optical transitions from a bound state to the conduction band. Accordingly, the F' band shape reflects in some way the energy distribution of the density of states in the conduction band. Some observed transition energies at the band edge are shown in Table 2.9.

Theoretically, Strozier & Dick(2.12) calculated the first order optically excited transition from a discrete state to a continuum of final states, and they estimated the shape of the F' band. Also, the F' bands for a few alkali halides were calculated by Lynch & Robinson(2.4) using a semicontinuum approach. Unfortunately we have difficulty in calculating the F' band shape by our method. Instead we can calculate the photoionization edge which is defined as the

difference between the energies of the final state, i.e., F-centre plus a photoelectron at the bottom of the conduction band, and the F' ground state[2.9,2.10]:

$$E_{opt}(F') = E_g(F') - E_g(F^*) + \chi \qquad (2.65)$$

where * denotes the lattice distortion appropriate to the F'-center and χ is electron affinity which is the energy spent to bring the electron from vacuum to the bottom of conduction band. In principle, this quantity can be measured by means of experiment. But so far there are only a few data available due to practical difficulty. We give values of this observable in Table 2.9.

The thermal dissociation energy of the F'-centre has been measured by many researchers. Valuable data have been collected by studying the thermally-stimulated current, thermoluminescence, thermal bleaching of the optical absorption bands, and photostimulated thermo-luminescence. A series of current and glow peaks observed as the samples were slowly warmed up to room temperature have been assigned to various color centers either by monitoring at pre-selected wavelengths within the absorption spectrum during warm up, or by studying the entire spectrum after rapid heating to the temperature of a given peak followed by a cool-down to 90K for an optical measurement. The temperatures of those peaks coincide with the temperatures at which the thermally-increased range of the F photocurrent begins[2.32]. Consequently, these F' peaks arise from the thermal ionization of the F'-centers. In the experiment of the thermal bleaching of the optical absorption band, the bleaching curve drops steeply in the vicinity of a specific temperature (T_{KCl}=200K[2.33] for example), undoubtedly due to the thermal release of F' electrons to the conduction band.

The thermal ionization energy is defined as the energy difference between the F' ground state and the F ground state[2.10]:

$$E_{th}(F') = E_g(F') - E_g(F) + \chi \qquad (2.66)$$

Based on the energy cycles (2.65) and (2.66), we calculated the optical binding energy E_{opt} and the thermal ionization energy E_{th} of F'-centres for NaCl, KCl, NaBr and NaI. All results are listed in Table 2.9. In this Table, the F-centre energies are calculated by dropping all terms associated with the second electron. For NaCl, it is seen that the three observed binding energies given in the Table show a fair amount of discrepancy.

On the other hand, many theoretical estimations have been made based on various models. Some of them deviate from experiment relatively far, and we only present some results which fit the experiment to some extent. Also we take NaCl as an example, using the continuum approach, Ostroukhov & Tomasevich[2.40] obtained a threshold optical energy of 1.27eV. Lynch & Robinson[2.4], based on a semi-continuum model, obtained 1.72eV. Arora & Wang's[2.7] polaron approach gave the value 1.70eV. By a point-ion model, Berezin[2.41] had 1.1eV. Another point-ion calculation of La and Bartram[2.10] gives 2.43eV. Their calculations including some other crystals fit the absorption band peak very well. The question arises as to how the binding energy should be defined. It seems, in most cases, the binding energy is identified with the experimental optical absorption edge[2.4]. Therefore a theoretical calculation of the absorption edge should be made. In terms of the binding energy, our calculated values for NaCl, KCl and NaI are in reasonably good agreement with observed ones. For NaBr, we have not found the observed electron affinity, but compared to KCl and NaI, it can be reasonably assumed to be somewhere between 0.5-1.0 eV. If this is true, the calculated optical binding energy for this material also fits well with experiment. On the other hand, given the observed optical binding energy, we can estimate the electron affinity though

eq.(2.65), and the value turns out to be 0.71eV.

The thermal dissociation energies shown in Table 2.9 are the extremes out of many observed data. Basically, different experimental methods lead to different observed values for the same material. Normally, as far as those available data are concerned, the thermal dissociation energy varies by a factor of about two in magnitude (such as NaF: 0.72-1.50eV, KCl: 0.35-0.60eV, KBr: 0.24-0.63eV)[2.9]. Also the recombination of electrons released with activators affects the measurement as well. In addition, the concentrations of both F-centre and F'-centre may not be exactly controlled so that the comparison between the two may lead to some errors. Strictly speaking, the electron affinity involved in the process of thermal ionization should not be the same as that of an optical process. Unfortunately, there have been no reported values. We used the electron affinity from optical experiments to calculate the thermal dissociation energies. As shown in Table 2.9, the calculated value of NaCl is reasonably good. We shall say that the value of NaI is also quite good; even though we have not found the observed data yet, the experimental data of KI should be a good reference. The values of KCl and NaBr are not as good as the two mentioned above. Both do not show thermal binding because of small positive values of this energy, but they are still in the right range.

Table 2.9

Experimental and Calculated Energies (eV) for F'-centres

	NaCl	KCl	NaBr	NaI
E_g (F ')	3.90	3.68	3.45	0.26
E_g (F*)	5.48	5.35	5.71	4.02
E_g (F)	4.00	3.92	3.43	2.28
χ	0.0[2.34]	0.41[2.12]	(1.0)*	1.50[2.34]
E_{opt} (F ') (cal.)	-1.58	-1.26	-1.26	-2.26
E_{th} (F ') (cal.)	-0.1	0.17		-0.52
E_{opt} (F ') (expt.)	-1.20[2.1] -1.72[2.4] -1.10[2.2]	-0.90[2.4] -1.00[2.36]	-1.55[2.35]	-1.90[2.35]
E_{th} (F ') (expt.)	-0.5[2.35] -1.1[2.38]	-0.4[2.37] -0.35[2.39]		(-0.47)[2.52]**

* Due to the unavailability of the electron affinity of NaBr, we assume it is around one eV.

** There has not been observed a thermal disassociation energy for NaI; we take that of KI as a reference because of their close similarity.

2.3.2 Excited States of F'-centres

The excited states of F'-centres are examined by our method. For NaCl, our calculation shows that there is very shallow F' binding, and the existence of a bound excited state is highly improbable. To examine this, we construct the basis to simulate the lowest excited state, triplet $(1s2p)^3$ state, and then perform the energy minimization and basis optimization. We find that the distortion field of this state has lower symmetry (D_{4h}) than that of ground state (O_h). The lowest energy we could get is still higher than its ionization limit, so no bound state could be formed. This result agrees with a previous estimation[2.25] in which the calculations were made based on the same lattice configuration as for the ground state. Our excited state obtained with an appropriate lattice configuration seems to be more reliable.

NaI and NaBr constitute two notable exceptions from other crystals. The F' band in these materials is more bell-shaped, and its halfwidth is strongly temperature-dependent. Both the position of the F' band (on the high-energy side of the F band) and its rather narrow symmetric shape are unusual features compared to the usual broad, unsymmetric low-energy F' absorption in other alkali halides. The shape of the band suggests that optical absorption does not lead directly into conductive states but into a bound singlet state of the system, which becomes auto-ionized after lattice relaxation[2.30]. The experimental evidence shows that both NaBr and NaI have an unusually low lying ground state[2.5]. The basic results from experiment can be summarized as follows: 1) there exists a low lying stable F' singlet ground state, and also a bound triplet state which would not be suppressed but enhanced by spin-polarization; 2) a bound singlet excited state is also highly possible; 3) the optical transition from the deep F' singlet level into a

shallow excited singlet state produces the 2.4 eV F' absorption; the transition from the higher F' triplet state into the conduction band yields the 1.45 eV infrared band[2.5]. These are shown clearly in Fig. 2.1 and 2.2. Using the optimized 1s2p basis which is a linear combination of three sets of bases like eq.(2.65), we calculated the excited triplet state $(1s2p)^3$ energy and singlet state $(1s2p)^1$ energy with their own relaxed lattice configuration. In addition, the F-center energy is calculated with the excited $(1s2p)^3$ state lattice distortion. Hence we can list these energies in Table 2.10. As was shown in eq.(2.65), each set of basis is identified by two parameters, and the optimized parameters are also presented in Table 2.10. Note that F* represents the F-centre calculated at $(1s2p)^3$ lattice distortion, and transition energies are defined as:

$$E_{(1s1s)^1 \rightarrow (1s2p)^1}(F') = E_g(F') - E_{(1s2p)^1}(F') \qquad (2.67)$$

$$E_{(1s2p)^3 \rightarrow cond}(F') = E_{(1s2p)^3}(F') - E(F^*) + \chi \qquad (2.68)$$

This calculation indicates that there is no doubt about the existence of bound excited triplet and excited singlet states. The calculated transition energy from F' ground state to the excited singlet state, and as well as the optical binding energy of the triplet state fit the experimental data quite well.

We can't say much about NaBr without corresponding experimental work. Our estimation can only provide some qualitative understanding. The results imply that the ground state is not as low as the paper[2.5] predicted, but rather somewhere between NaCl and NaI. It is found that a very shallow bound triplet excited state could be formed, and the excited singlet state is not bound.

In principle, the present method is capable of dealing with the ionized state. It interested us to try this idea at the very beginning. Unfortunately we failed to

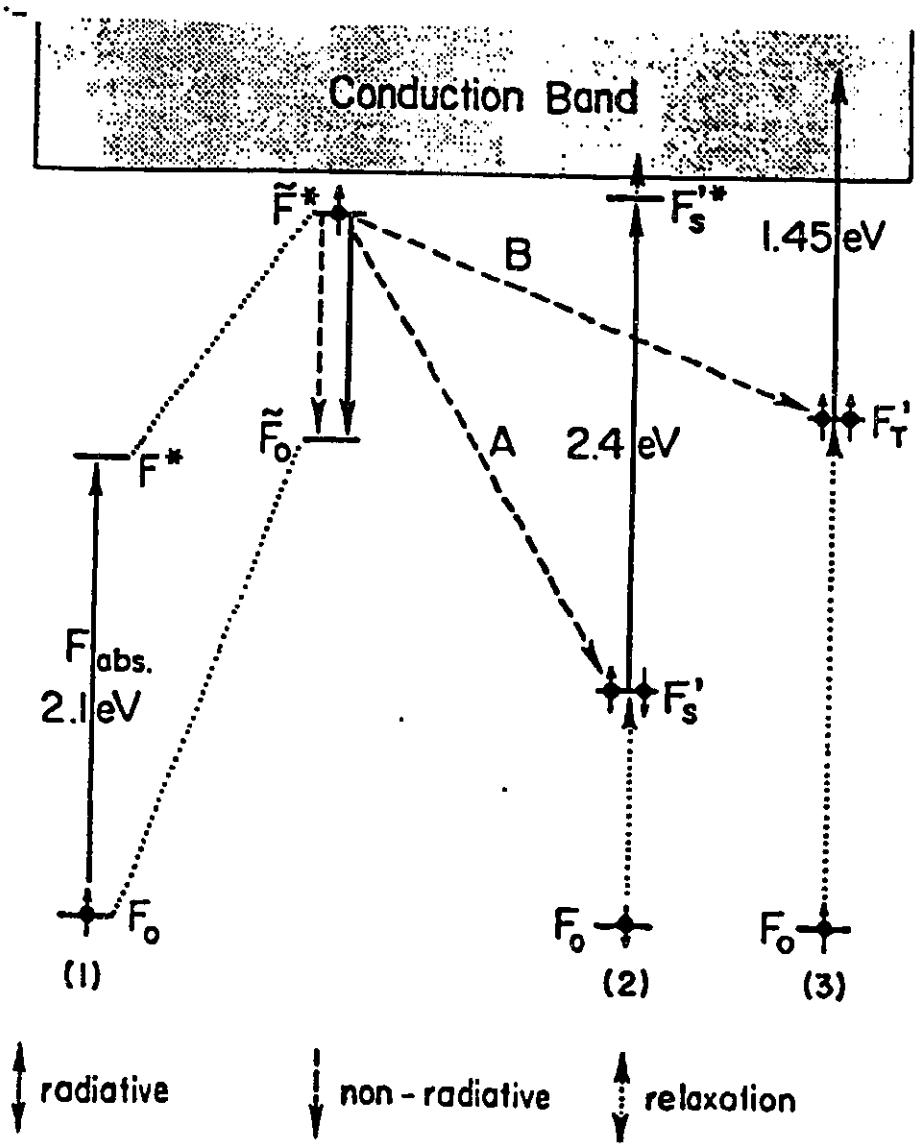

Fig 2.1 Electronic energy level diagram with illustration of radiative, nonradiative and relaxation transitions. The electron of the optically excited F centre (1) can tunnel into a neighbouring F centre of opposite (2) or equal (3) spin-orientation, forming the singlet or triplet F' states.

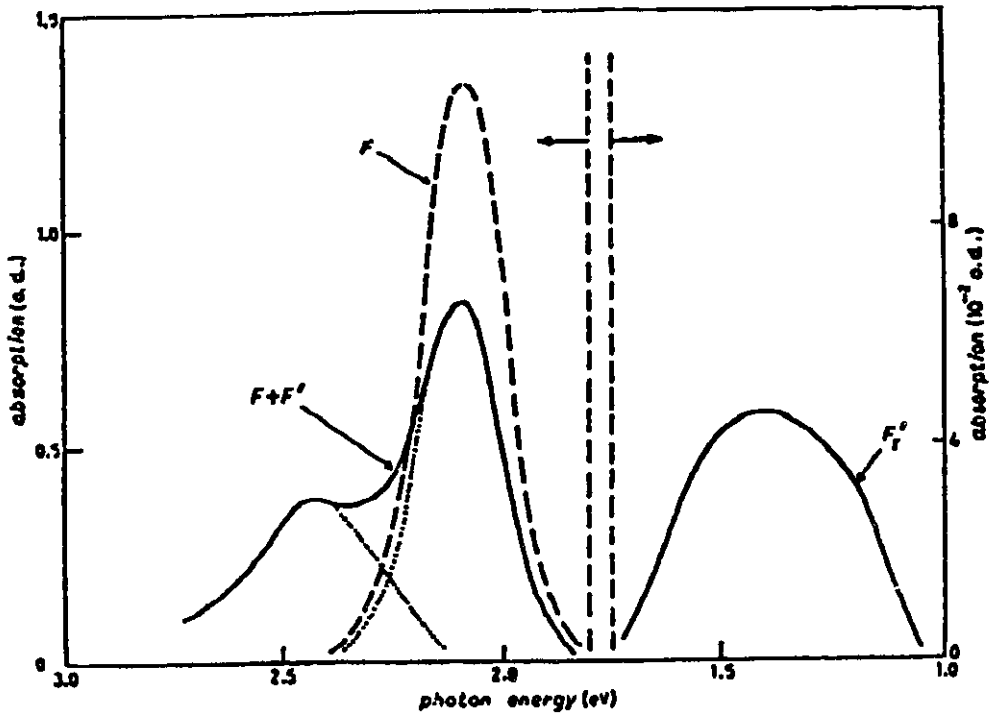

Fig. 2.2 Absorption spectrum in coloured NaI at 1.9 K. The crystal contains initially only F-centres, whose absorption (dashed curve) is centred around 2.08 eV. Upon irradiation at 6328 A, the F-band absorption decreases, while two new bands appear around 2.45 eV and 1.4 eV (continous curve). Note difference o.d. scale in the two parts.

Table 2.10

Experimental and Calculated Transition Energies (eV) for NaI and NaBr.

	E_g	$E_{(1s2p)^1}$	$E_{(1s1s)^1 \rightarrow (1s2p)^1}$	$E_{(1s2p)^3}$	E(F*)	$E_{(1s2p)^3 \rightarrow cond}$
NaI(cal.)	0.26	2.60	-2.34	1.38	3.48	-0.6
NaI(exp.)			-2.4 [2.5]			-1.45 [2.5]
NaBr(cal.)	3.45	7.02		4.97	5.13	

get a good result, but this has enabled us to clarify somewhat our understanding in this subject. If a reliable ionized state could be obtained, we would be able to calculate the optical binding energy directly without making use of the electron affinity χ, i.e.,

$$E_{opt}(F') = E_g(F') - E_g(F^* + e) \tag{2.69}$$

In this way, the conduction electron can be treated inside the cluster. What we do is use very diffuse Gaussians to represent the conduction electron. Because the cluster model used has a limited size of 619 ions, the diffuseness of Gaussians is restricted by this size. It is assumed that 80% of the charge remaining inside the cluster still gives a good description, the decay factor of Gaussians is found to be 0.002 while for the ground state they are around 0.06 a.u.. In the ionized state the defect is electrically neutral, and the polarization is calculated simply like that for an F-centre. For NaCl, the calculated value is $E_g(F^* + e) = 7.70$ eV. This yields an optical binding energy of 3.80 eV, which is very much high and is worse than we expected. We can imagine there are sources of errors. First, the diffuse Gaussians do not seem to give a good description of a conduction electron which, actually, should be represented by a linear combination of plane waves. Second, while the diffuse Gaussians extend into the cluster, the number of cores used to calculate H_{12} only runs up to the fourth shell which could be far insufficient. Third, those terms neglected in H_{12} are no longer small, because the estimation was made based on normal Gaussians ($0.02<\alpha_i<0.12$ a.u.) It seems that we can not do anything to improve the first and the third, but for the second we still can try to improve. What we do is enlarge the sub-cluster in the H_{12} calculation. As seen in Appendix 2.3, the calculation of H_{12} involves the summations over core

orbitals. For a normal Gaussian wave function, we can cut the summation to a sub-cluster of 24 ions due to the fast convergence. But for a diffuse Gaussian wave function, the convergence is slow and the enlargement of this sub-cluster makes a considerable difference. When this sub-cluster is changed from 24 ions to 300 ions, the corresponding energy is improved by about half an eV. This implies that a better result could be obtained by taking a still larger summation, but the work is limited by CPU time. At least this is the right trend. By the way, the binding energy is still 2 eV higher than that of experiment. What is a proper way of defining and evaluating the ionization limit of a defect seems to be an interesting project to study[2.29].

2.3.3 Negative-U effect of the F'-centre

Experimental observations have shown that in the group II materials such as NaI and NaBr, F' ground state is deeply bound. With well controlled experimental conditions, the conversion from F band to F' band can be observed[2.5]. The F' band appears upon annealing in 1:1 correspondence with the disappearance of the F band. The two bands have significant difference in nature, but they are associated with the same defect. This is very similar to the observations made in crystalline silicon with lattice vacancy, and interstitial boron. The two defects have been demonstrated to have negative-U properties[2.43]. A defect has negative-U properties if it can trap two electrons (or holes) with the second bound more strongly than the first[2.44]. On the basis of the results presented in 2.3.1, we can speculate that F' centre in group II materials also has negative-U properties, while the F' centre in group I materials shows the normal positive-U behaviour. So far there has been no report on negative-U properties for defects in alkali halide crystals.

To examine the negative-U properties of these crystals from a theoretical aspect, we compared the ground state energies of F' and F centres obtained in this work. Actually, we needed to investigate the three charge states: V^+, V^0, and V^-, corresponding to an anion vacancy, F-centre, and F'-centre, respectively. From Table 2.9, we estimated the negative-U of 2 eV for NaI. This value is quite large compared to ones (less than 0.5 eV) obtained in semiconductors. We believe that this is mainly due to the large band gap of the insulator. For NaBr, our calculation showed a borderline case, with U ~ -0.02 eV.

In our work the lattice distortion and electron correlation were evaluated during a self-consistent minimization of the defect system energy. These are the two key factors leading to the negative-U ordering. Thus, we can explain the deeply bound F'-centre as a negative-U centre. In NaI, and possibly in NaBr also maginally, a negative-U ordering arises when the second electron is bound more strongly than the first (to form F-centre). The remarkable feature of a defect with negative-U properties is that there is an effective attractive interaction between the two electrons at the defect. In a sense, this is an 'extrinsic Cooper pair' , the two electrons pairing at the defect.

2.4 Discussions

The aim of the present work was to study the F'-centres in alkali halides. Most of our results are in reasonable agreement with experimental observations. We found that, in NaI (and maginally also in NaBr), the calculated ground state energy of the F'-centre is deeper than that of F-centre. The lattice relaxation energy of two electrons together overcomes their Coulomb repulsion, providing a

lower energy state than the F-centre. On this ground, we proposed that the F'-centre in type II materials has negative-U effect. The advantage of our method is the ease with which it may be applied to similar defect electron systems. We treated the lattice distortions induced by the defect and the electron wavefunction. The defect electron wavefunction is recalculated at each step by a hybrid pseudo-potential scheme as the total energy of the system is minimized with respect to each ion position. The exclusive use of floating 1s Gaussians for electron basis sets allows calculations to be easily and efficiently carried out. The flexibility in choosing basis sets not only brings us electron correlations which improve the results substantially, but also makes it convenient to construct any electron orbital of interest.

The disadvantage of this method is the difficulty of optimizing the basis. When many basis functions are employed, there exists a considerable number of variational degrees of freedom to be optimized. To get better electron orbitals, one has to search extensively to locate the true minimum. Especially for excited states, it is not always easy to find the true minimum. We have used various interpolation formulae in the evaluation of the electron energy. We found that the RMS deviation of a least squares fit was less than 10^{-3} in all cases. It is true that such fittings introduce uncertainty in those individual terms. Because the cancellation of Coulomb and exchange terms with overlap terms normally makes the precision of energy calculation one order of magnitude worse, we expect the error introduced into the electron energy due to these approximations to be on the order of 0.2 eV. Those off-center terms in H_{12} were not precisely treated and can be further improved. The neglect of overlap of core orbitals in dealing with the polarization energy has to be addressed too in order to improve the method.

Appendix 2.1

A Gaussian is defined as:

$$G_i(r_i) = e^{-\alpha_i r_i^2}, \quad (\alpha_i > 0) \qquad \text{(A2.1.1)}$$

where the Gaussian is centred at R_i and $r_i = r - R_i$. The product of two Gaussians centred at any two sites, is itself a Gaussian centred at a third site:

$$G_i(r_i)\,G_j(r_j) = K G_k(r_k) \qquad \text{(A2.1.2)}$$

where

$$K = e^{-\frac{\alpha_i \alpha_j}{\alpha_i + \alpha_j}|R_i - R_j|^2}, \qquad R_k = \frac{\alpha_i R_i + \alpha_j R_j}{\alpha_i + \alpha_j}. \qquad \text{(A2.1.3)}$$

The overlap integral of two Gaussians is

$$\langle G_i(r_i) | G_j(r_j) \rangle = \left(\frac{\pi}{\alpha_i + \alpha_j}\right)^{\frac{3}{2}} e^{-\frac{\alpha_i \alpha_j}{\alpha_i + \alpha_j}|R_i - R_j|^2} . \qquad \text{(A2.1.4)}$$

The kinetic energy term is:

$$\langle G_i(r_i)|T|G_j(r_j)\rangle = \int e^{-\alpha_i r_i^2}\left(-\frac{1}{2}\nabla^2\right)e^{-\alpha_j r_j^2}\,d\tau$$

$$= \frac{\alpha_i \alpha_j}{\alpha_i + \alpha_j}\left(3 - 2\frac{\alpha_i \alpha_j}{\alpha_i + \alpha_j}|R_i - R_j|^2\right)\left(\frac{\pi}{\alpha_i + \alpha_j}\right)^{\frac{3}{2}} e^{-\frac{\alpha_i \alpha_j}{\alpha_i + \alpha_j}|R_i - R_j|^2} \qquad \text{(A2.1.5)}$$

The point-ion potential energy is given by:

$$\langle G_i(r_i)|\frac{Z_\gamma}{|r - R_\gamma|}|G_j(r_j)\rangle = \sum_\gamma \int e^{-\alpha_i r_i^2}\frac{Z_\gamma}{|r - R_\gamma|}e^{-\alpha_j r_j^2}\,d\tau$$

$$= \sum_\gamma Z_\gamma\left[\frac{2\pi}{\alpha_i + \alpha_j}F_0\left((\alpha_i + \alpha_j)|R_k - R_\gamma|^2\right)e^{-\frac{\alpha_i \alpha_j}{\alpha_i + \alpha_j}|R_i - R_j|^2}\right] \qquad \text{(A2.1.6)}$$

where Z_γ is the net charge on ion γ, R_k is defined as in equation (A2.1.3) and

$$F_0(t) = \frac{1}{2}\sqrt{\frac{\pi}{t}}\,\mathrm{erf}(\sqrt{t}). \qquad \text{(A2.1.7)}$$

For ions in their perfect lattice positions the sum of equation (A2.1.6) is evaluated by the Ewald method. For ions that have been displaced from their perfect lattice positions the point-ion potential energy is evaluated using equation (A2.1.6), without the sum over γ.

Appendix 2.2

Assuming that ϕ_i is slowly varying, we can expand it in a multipolar series:

$$\phi_i(\mathbf{r}-\mathbf{R}_i) = 2\pi \sum_l F_l(\mathbf{r},\mathbf{R}_i) \sum_m Y_l^m(\theta_r,\varphi_r)^* Y_l^m(\Theta_{R_i},\Phi_{R_i}) \qquad \text{(A2.2.1)}$$

where

$$F_l(\mathbf{r},\mathbf{R}_i) = \int \phi(\mathbf{r}-\mathbf{R}_i) P_l(\cos\Omega)\, d(\cos\Omega) \qquad \text{(A2.2.2)}$$

where Ω is the angle between $\mathbf{r}$ and $\mathbf{R}_i$..Then we can expand F_l in a Taylor's series about $\mathbf{R}_i$ resulting finally in:

$$\phi_i(\mathbf{r}-\mathbf{R}_i) = 2\pi \sum_l \left[\sum_n F_l^{(n)}(0,\mathbf{R}_i) r^n\right] \sum_m Y_l^m(\theta_r,\varphi_r)^* Y_l^m(\Theta_{R_i},\Phi_{R_i}) \qquad \text{(A2.2.3)}$$

Here $F_l^{(n)}$ is the n^{th} derivative of F_l , and P_l are the Legendre polynomials.

Using this expression for ϕ, the overlap contribution of a core can be expressed into a convenient form. We give an example of one of the factors which is expanded up to the first order terms:

$$\langle G_i(r_i) | \chi_\lambda(\mathbf{r})\rangle = 2\pi \langle F_{i0}(0,\mathbf{R}_i) Y_0^0(\theta_r) Y_0^0(\varphi_{R_i})^*$$

$$+ \frac{r^2}{2} F_{i0}^{(2)}(0,\mathbf{R}_i) Y_0^0(\theta_r) Y_0^0(\varphi_{R_i})^* + r F_{i1}^{(1)}(0,\mathbf{R}_i)\left[Y_1^0(\theta_r,\varphi_r) Y_1^0(\Theta_{R_i},\Phi_{R_i})^*\right]$$

$$+ r F_{i1}^{(1)}(0,\mathbf{R}_i)\left[+ Y_1^1(\theta_r,\varphi_r) Y_1^1(\Theta_{R_i},\Phi_{R_i})^* + Y_1^{-1}(\theta_r,\varphi_r) Y_1^{-1}(\Theta_{R_i},\Phi_{R_i})^*\right] | \chi_\lambda(\mathbf{r})\rangle \qquad \text{(A2.2. 4)}$$

For the moment let us restrict ourselves to a single principal quantum number.

The sum over λ will consist of one s orbital and three p orbitals. d orbitals do not participate in first order terms. For each λ, different expansion terms vanish from symmetry. When λ = s, the surviving terms are:

$$\left[2\pi F_{i0}(0, \mathbf{R}_i) \langle Y_0^0(\theta_r, \varphi_r) | \chi_s \rangle Y_0^0(\Theta_{R_i}, \Phi_{R_i})^* + 2\pi F_{i0}^{(2)}(0, \mathbf{R}_i) \langle Y_0^0(\theta_r, \varphi_r) \frac{r^2}{2} | \chi_s \rangle Y_0^0(\Theta_{R_i}, \Phi_{R_i})^* \right] \times$$

$$\left[2\pi F_{j0}(0, \mathbf{R}_i) \langle \chi_s | Y_0^0(\theta_r, \varphi_r) \rangle Y_0^0(\Theta_{R_j}, \Phi_{R_j}) + 2\pi F_{j0}^{(2)}(0, \mathbf{R}_j) \langle \chi_s | Y_0^0(\theta_r, \varphi_r) \frac{r^2}{2} \rangle Y_0^0(\Theta_{R_j}, \Phi_{R_j}) \right] \tag{A2.2.5}$$

since

$$Y_0^0(\theta_r, \varphi_r) = Y_0^0(\Theta_{R_i}, \Phi_{R_i}) = Y_0^0(\Theta_{R_j}, \Phi_{R_j}) = \frac{1}{\sqrt{4\pi}} \tag{A2.2.6}$$

we get

$$\frac{1}{4} F_{i0} F_{j0} \left(\int \chi_s \, d\tau \right)^2 + \frac{1}{8} \left[F_{i0} F_{j0}^{(2)} + F_{i0}^{(2)} F_{j0} \right] \left(\int \chi_s \, r^2 \, d\tau \right)^2 \tag{A2.2.7}$$

where the $F_{i0}^{(2)} F_{j0}^{(2)}$ is dropped because it becomes a 2nd order term. For a p orbital, say the one with Y_1^0 symmetry, only one term survives:

$$2\pi F_{i1}^{(1)}(0, \mathbf{R}_i) \langle Y_1^0(\theta_r, \varphi_r) r | \chi_{p0} \rangle Y_1^0(\Theta_{R_i}, \Phi_{R_i})^* \times$$

$$2\pi F_{j1}^{(1)}(0, \mathbf{R}_j) \langle \chi_{p0} | Y_1^0(\theta_r, \varphi_r) r \rangle Y_1^0(\Theta_{R_j}, \Phi_{R_j}) \quad . \tag{A2.2.8}$$

Substituting

$$Y_1^0(\theta_r, \varphi_r) = \sqrt{\frac{3}{4\pi}} \cos\theta \tag{A2.2.9}$$

we get

$$3\pi \, F_{i1}^{(1)} F_{j1}^{(1)} Y_1^{(0)}(\Theta_{R_i}, \Phi_{R_i})^* Y_1^{(0)}(\Theta_{R_j}, \Phi_{R_j}) \left(\int r \cos\theta \, \chi_{p0} \, d\tau \right)^2 \tag{A2.2.10}$$

For the two other p orbitals, similar expressions are obtained, with all the factors being the same except the spherical harmonic product. Summing the three expressions, one gets:

$$\frac{9}{4} F_{i1}^{(1)} F_{j1}^{(1)} (e_{R_i} \cdot e_{R_j}) \left(\int r \cos\theta \chi_p \, d\tau \right)^2 \qquad \text{(A2.2.11)}$$

where the spherical harmonic addition theorem was used:

$$\sum_{m=-l}^{l} Y_l^{(m)} (\theta_r, \varphi_r)^* Y_l^{(m)} (\theta_{r'}, \varphi_{r'}) = \frac{(2l+1)}{4\pi} P_l (e_r \cdot e_{r'}) \qquad \text{(A2.2.12)}$$

The s and p orbitals of different principal quantum number are easily included since their contributions are simply summed together. The factorization of these terms results in the ion-size parameters B, K' and K exactly as defined in equations (2.26), (2.27) and (2.28). The whole procedure can be repeated for matrix elements of the Coulomb and exchange integrals, giving the parameters A, J' and J.

We can also represent the expansion coefficients into the following form:

$$f_1 = \frac{1}{4} F_{i0} (0, R_i) F_{j0} (0, R_j) \qquad \text{(A2.2.13)}$$

$$f_2 = \frac{1}{8} F_{i0} (0, R_i) F_{j0}^{(2)} (0, R_j) + \frac{1}{8} F_{i0}^{(2)} (0, R_i) F_{j0} (0, R_j) \qquad \text{(A2.2.14)}$$

$$f_3 = \frac{9}{4} F_{i0}^{(1)} (0, R_i) F_{j0}^{(1)} (0, R_j) \qquad \text{(A2.2.15)}$$

which are used in Eq.(2.36) and Eq.(3.45).

Appendix 2.3

The full expression of the matrix elements of Hamiltonian H_{12} in two-particle wave functions involves 16 terms which are given as follows:

$$(H_{12})_j = \langle G_i(1) G_i(2) | H_{12} | G_j(1) G_j(2) \rangle$$

$$- \sum_{\gamma,\lambda} \langle \chi_{\gamma\lambda} | G_j(2) \rangle \langle G_i(1) G_i(2) | H_{12} | G_j(1) \chi_{\gamma\lambda} \rangle$$

$$- \sum_{\gamma,\lambda} \langle \chi_{\gamma\lambda} | G_j(1) \rangle \langle G_i(1) G_i(2) | H_{12} | \chi_{\gamma\lambda} G_j(2) \rangle$$

$$- \sum_{\gamma,\lambda} \langle G_i(2) | \chi_{\gamma\lambda} \rangle \langle \chi_{\gamma\lambda} G_i(1) | H_{12} | G_j(1) G_j(2) \rangle$$

$$- \sum_{\gamma,\lambda} \langle G_i(1) | \chi_{\gamma\lambda} \rangle \langle G_i(2) \chi_{\gamma\lambda} | H_{12} | G_j(1) G_j(2) \rangle$$

$$+ \sum_{\gamma,\lambda,\mu,\nu} \langle G_i(2) | \chi_{\gamma\lambda} \rangle \langle \chi_{\mu\nu} | G_j(2) \rangle \langle \chi_{\gamma\lambda} G_i(1) | H_{12} | G_j(1) \chi_{\mu\nu} \rangle$$

$$+ \sum_{\gamma,\lambda,\mu,\nu} \langle G_i(1) | \chi_{\gamma\lambda} \rangle \langle \chi_{\mu\nu} | G_j(1) \rangle \langle \chi_{\gamma\lambda} G_i(2) | H_{12} | G_j(2) \chi_{\mu\nu} \rangle$$

$$+ \sum_{\gamma,\lambda,\mu,\nu} \langle G_i(1) | \chi_{\gamma\lambda} \rangle \langle G_i(2) | \chi_{\mu\nu}) \rangle \langle \chi_{\mu\nu} \chi_{\gamma\lambda}) | H_{12} | G_j(1) G_j(2) \rangle$$

$$+ \sum_{\gamma,\lambda,\mu,\nu} \langle G_i(1) | \chi_{\gamma\lambda} \rangle \langle \chi_{\mu\nu} | G_j(2) \rangle \langle G_i(2) \chi_{\gamma\lambda} | H_{12} | G_j(1) \chi_{\mu\nu} \rangle$$

$$+ \sum_{\gamma,\lambda,\mu,\nu} \langle G_i(2) | \chi_{\gamma\lambda} \rangle \langle \chi_{\mu\nu} | G_j(1) \rangle \langle G_i(1) \chi_{\gamma\lambda} | H_{12} | G_j(2) \chi_{\mu\nu} \rangle$$

$$+ \sum_{\gamma,\lambda,\mu,\nu} \langle \chi_{\gamma\lambda} | G_j(1) \rangle \langle \chi_{\mu\nu} | G_j(2) \rangle \langle G_i(1) G_i(2) | H_{12} | \chi_{\gamma\lambda} \chi_{\mu\nu} \rangle$$

$$- \sum_{\gamma,\lambda,\mu,\nu,\alpha,\beta} \langle G_i(2) | \chi_{\gamma\lambda} \rangle \langle \chi_{\alpha\beta} | G_j(1) \rangle \langle \chi_{\mu\nu} | G_j(2) \rangle \langle G_i(1) \chi_{\gamma\lambda} | H_{12} | \chi_{\alpha\beta} \chi_{\mu\nu} \rangle$$

$$- \sum_{\gamma,\lambda,\mu,\nu,\alpha,\beta} \langle G_i(1) | \chi_{\gamma\lambda} \rangle \langle \chi_{\alpha\beta} | G_j(1) \rangle \langle \chi_{\mu\nu} | G_j(2) \rangle \langle G_i(2) \chi_{\gamma\lambda} | H_{12} | \chi_{\alpha\beta} \chi_{\mu\nu} \rangle$$

$$- \sum_{\gamma,\lambda,\mu,\nu,\alpha,\beta} \langle G_i(1) | \chi_{\gamma\lambda} \rangle \langle \chi_{\alpha\beta} | G_j(2) \rangle \langle G_i(2) | \chi_{\mu\nu} \rangle \langle \chi_{\gamma\lambda} \chi_{\mu\nu} | H_{12} | G_j(1) \chi_{\alpha\beta} \rangle$$

$$- \sum_{\gamma,\lambda,\mu,\nu,\alpha,\beta} \langle G_i(1) | \chi_{\gamma\lambda} \rangle \langle \chi_{\alpha\beta} | G_j(1) \rangle \langle G_i(2) | \chi_{\mu\nu} \rangle \langle \chi_{\gamma\lambda} \chi_{\mu\nu} | H_{12} | G_j(2) \chi_{\alpha\beta} \rangle$$

$$+ \sum_{\gamma,\lambda,\mu,\nu,\alpha,\beta,\pi,\delta} \langle G_i(1) | \chi_{\gamma\lambda} \rangle \langle \chi_{\alpha\beta} | G_j(1) \rangle \langle \chi_{\pi\delta} | G_j(2) \rangle \langle G_i(2) | \chi_{\mu\nu} \rangle \langle \chi_{\gamma\lambda} \chi_{\mu\nu} | H_{12} | \chi_{\pi\delta} \chi_{\alpha\beta} \rangle$$

Appendix 2.4

The matrix element of the two-particle interaction term can be calculated by using Gaussian wave functions as:

$$\langle G_i(r_{1i})\,G_i(r_{2i}) \left| \frac{1}{r_{12}} \right| G_j(r_{1j})\,G_j(r_{2j}) \rangle = \frac{2\pi^{5/2}}{(\alpha_i^1+\alpha_j^1)(\alpha_i^2+\alpha_j^2)\sqrt{\alpha_i^1+\alpha_j^1+\alpha_i^2+\alpha_j^2}} \times$$

$$F_0\left[\frac{(\alpha_i^1+\alpha_j^1)(\alpha_i^2+\alpha_j^2)}{\alpha_i^1+\alpha_j^1+\alpha_i^2+\alpha_j^2}\overline{PQ}^2\right] e^{-\frac{\alpha_i^1\alpha_j^1}{\alpha_i^1+\alpha_j^1}\left|R_i^1-R_j^1\right|^2} e^{-\frac{\alpha_i^2\alpha_j^2}{\alpha_i^2+\alpha_j^2}\left|R_i^2-R_j^2\right|^2} \qquad \text{(A2.4.1)}$$

The points P and Q lie on $\left|R_i^1 - R_j^1\right|$ and $\left|R_i^2 - R_j^2\right|$, respectively, and are given by,

$$P = \frac{\alpha_i^1 R_i^1 + \alpha_j^1 R_j^1}{\alpha_i^1+\alpha_j^1} \qquad Q = \frac{\alpha_i^2 R_i^2 + \alpha_j^2 R_j^2}{\alpha_i^2+\alpha_j^2} \quad . \qquad \text{(A2.4.2)}$$

Reference 2

2.1 H. Pick, Ann. Physik. 31. 365 (1938)

2.2 N. F. Mott & R. W. Gurney, Electronic Processes in Ionic Crystals, (Oxford 1964)

2.3 J. D. Kingsley, Phys. Rev. 122,772 (1961)

2.4 D. W. Lynch & D. A. Robinson, Phys. Rev. 174, 1050(1968)

2.5 G. Baldacchini, G. P. Gallerano, U. M. Grassano & F. Luty, Radiation Effects, 72, 153(1983)

2.6 L. Pincherle, Proc. Phys. Soc. Sect, A64, 648(1951)

2.7 H. L. Arora & S. Wang, J. Phys. Chem. Solids, 30, 1649(1969)

2.8 H. J. Raveche, J. Phys. Chem. Solids, 26, 2085(1965)

2.9 M. Georgiev, F'centers in Alkali Halides (Springer-Verlag, Berlin, Heidelberg 1988)

2.10 S. Y. La & R. H. Bartram, Phys. Rev. 174, 11050(1968)

2.11 J. A. Krumhansl & N. Schwartz, Phys. Rev. 144, 670(1966)

2.12 J. A. Strozier & B. G. Dick, Phys. Stat. sol. 31,203(1969)

2.13 C. H. Leung & K. S. Song, Can. J. Phys. 58, 412 (1980)

2.14 K. S. Song, L. Emery, G. Brunet & C. H. Leung, Nucl. Instrum. Methods B1, 456(1984)

2.15 C. H. Leung, G. Brunet & K. S. Song. J. Phys. C18,4459(1985)

2.16 K. S. Song, C. H. Leung & R. T. Williams, J. Phys. Cond. Matter, 1, 683(1989)

2.17 C. H. Leung & K. S. Song, Physica, 114B, 323(1982)

2.18 J. R. Reitz, R. N. Seitz & R. W. Genberg, J. Phys. Chem. Solids, 19, 73(1961)

2.19 E. Clementi & C. Roewtti, At. Data Nucl. Data Tables, 14(1974)

2.20 R. H. Barram, A. M. Stoneham & P. Gash, Phys.Rev.176, 1014 (1968)

2.21 R. D. Zwicker, Phys.Rev.B18, 2004(1978)

2.22 N. F. Mott & M. J. Littleton, Tran. Faraday Soc.34,485(1938)
J. R. Hardy & A. B. Lidiard, Phil. Mag. 15,825(1967)

2.23 S. D. Druger & R. S. Knox, J. Chem. Phys, 50,3143(1969)

2.24 B. Szigeti, Proc. Roy. Soc. (London) A204,51(1950)

2.25 M. Born & K. Huang, Dynamical Theory of Crystal Lattice (Oxford Clarndon Press 1954)

2.26 J. R. Hardy & A. N. Caro, The Lattice Dynamics and Statics of Alkali Halide Crystals (Plenum Press, 1979) p.162

2.27 G. Brunet, C. H. Leung & K. S. Song, Solid State Commun. 53,607(1985)

2.28 A. A. Berezin, Sov. Phys. sol. St. 9,2170(1967)

2.29 A. M. Stoneham, Theory of Defects in Solids, p.598,(Clarendon Press, Oxford, 1975)

2.30 G. Baldacchini, D. S. Pan & F. Luty, Phys.Rev.B24,2174(1981)

2.31 T. Todorov, N. Koralov & M. Georgiev, Optics Commun. 13,439(1975)

2.32 F. Seitz, Rev. Modern Phys. 18,384(1946)

2.33 A. Halperin, A. A. Braner, M. Schlesinger & N. Kristianpoller, Proc. Internat. Conf. on Semiconductor Phys. Prague, p.724(1960)

2.34 J. E. Eby, K. J. Teegaeden & D. B. Dutton, Phys. Rev. 116,1099(1959)

2.35 A. Serpi & M. P. Serpi, J. Luminescence, 5,361(1972)

2.36 F. Luty, Halbleiterprobleme 5, 238(1961)

2.37 Y. V. G. S. Murty & K. R. N. Murthy, J. Phys. C: Solid State Phys.7,1918(1974)

2.38 M. R. Chandratillake, G. W. A. Newton, S. F. Patil, V. J. Robinson & M. A. J. Rodger, J. Chem. Soc. Faraday II, 74, 480(1978)

2.39 A. Rascon & J. L. Alvarez Rivas, J. Phys. C: Solid State Phys. 16,241(1983)

2.40 A. A. Ostroukhov & O. F. Tomasevich, Ukrain. Fiz. Zhur.(USSR), 3,449(1958)

2.41 A. A. Berezin, Fiz. Tverd. Tela (USSR) 9,2756(1967)

2.42 G. Baldacchini, G. P. Gallerano, U. M. Grassano & F. Luty, Lett. Nuovo Cimento, 36,495(1983)

2.43 R. D. Harris, J. L. Newton & G. D. Watkins, Phys. Rev. Lett. 51,1722(1983)

2.44 P. W. Anderson, Phys. Rev. Lett. 34,953(1975)

Chapter 3 Positron Centres In Ionic Crystals

Introduction

Positron physics is concerned with the interaction of low-energy positrons with matter. Positron studies provide us information on the concentration and properties of various kinds of defects in solids. Researches in this field have been actively performed for a few decades. We became interested in this field about two years ago. Shortly after we started work on this subject, we found the method we developed to study F'-centres could be applied to this project after some modifications. The newly developed model based on that structure is used to investigate various positron related defect systems. It comes out with plenty of useful results. We shall report them in this part of our work.

In Section 3.1, we present the background in this field. It contains six sub-sections. In 3.1.1 and 3.1.2, we introduce some basic data on positrons and positronium as well as their properties. In 3.1.3, we give a historic view of this field. In 3.1.4, we describe experimental techniques such as lifetime measurements, angular correlation measurements, line-shape measurements and magnetic field effect measurements. In 3.1.5, we summarize previous experimental and theoretical works in the field of our interest. In 3.1.6, we describe our work briefly.

In Section 3.2, the basic points of our theoretical approach are described in detail. It is composed of five sub-sections. 3.2.1 describes the electronic structure including localized Ps states and delocalized Ps states. 3.2.2 describes the treatment of lattice energies such as Coulomb energy, short-range repulsive energy and polarization energy. 3.3.3 explains the energy minimization

procedure. 3.3.4 and 3.3.5 present the lifetime calculation and angular correlation calculation, respectively.

Finally in Section 3.3, results on various defect systems and Ps states are presented, followed with discussions.

3.1 Background

3.1.1 Positron

The existence of the positron was first predicted theoretically by Dirac in 1930[3.1] and observed experimentally by Anderson in 1933[3.2]. The positron, the antiparticle of the electron, may be considered as a positive electron. It has the mass and spin characteristics of the electron but carries a unit positive charge. In most cases positrons are obtained by the radioactive decay of certain naturally occurring nuclei. When high-energy positrons of several hundred KeV enter the sample they rapidly slow down to thermal energy ($k_BT \sim 1.00*10^{-3}$ a.u.= 0.0272 eV) through ionizations and collisions. Positrons approaching thermal energies may annihilate either in a free state or in a bound state.

3.1.2 Positronium

Positronium (Ps) is the bound state of an electron and a positron. Ps is formed when a positron captures an electron from the surrounding medium. The energetics of Ps formation is described by the Ore model[3.3]. It states that Ps formation is most probable when the positron energy during its slowing down lies within a gap where no other electronic energy transfer process is possible. Assume that E_i is the electron ionization energy, E_{ex} the lowest electronic

excitation energy, and E_b the Ps binding energy which is 6.8 eV in vacuum and may be smaller in the medium; then Ps formation is most probable with the energy in the range

$$E_i - E_b \leq E \leq E_{ex} .$$

Ps can also be visualized as an analog of the hydrogen atom, in which the proton is substituted by a positron, and thus can be considered as the lightest isotope of hydrogen with binding energy of 6.8 eV. However, in contrast to the hydrogen atom which behaves like a one-centre system, the equal masses of the electron and positron make the positronium a two-centre system, which leads to drastic differences in the physics.

Ps exists in two ground states, the singlet (para) Ps with antiparallel spin orientation, and the triplet (ortho) Ps with parallel spin orientation. Ortho and para Ps are formed normally in the ratio of 3:1[3.4].

Ps is unstable with regard to positron-electron annihilation into gamma quanta. Quantum electrodynamic selection rules permit rapid annihilation of para-Ps into two gamma quanta, each of energy mc^2 = 0.511 MeV, with the rate $8.0*10^9$/sec[3.4]. They permit ortho-Ps to annihilate only into three gamma quanta, with the slow rate $7.05*10^6$/sec[3.4]. Since annihilation rates decrease rapidly with the nubmer of emitted photons, only two and three photon annihilation occurs in practice[3.5].

3.1.3 Brief History

The study of Ps in alkali halides has a history of more than thirty years. In 1959 Ferrell[3.3] predicted that the bound pair of a positron and an electron would not be stable in perfect alkali halide crystals. The experiment at room

temperature of Stewart and Pope[3.6], in which no narrow peak (Ps peak) was observed in the angular correlation curves (ACCs) of alkali chlorides and sodium halides, seemed to support this argument. A narrow peak characterizes the formation of a Ps state. It is understood that Ps is such a light particle that it is hard to be restricted in a small region of space, and therefore the extended state of Ps leads to a sharp narrow peak in angular correlation curve. Later, Bisi et al[3.7,3.8], measured positron lifetime spectra for some alkali halides and obtained results that suggested the formation of Ps or Ps-like states in the specimen, i.e., the existence of multiple lifetime components and the magnetic field effect on the longer-lived component because a magnetic field mixes the singlet and triplet (with magnetic quantum number m = 0) Ps states and leads to an increase of the number of two-photon decays. It is for this reason that an increase in the intensity of the narrow component can be observed by applying a static magnetic field (magnetic quenching). On the other hand, Herlarch[3.9] showed by comparing the data with and without magnetic field that a narrow component was in fact contained in the apparently smooth ACC of KCl. Following this observation, Dannefaer and Smedskjaer[3.10,3.11] made multiple component parameter-fittings to the ACCs of NaCl and KCl and were able to correlate their narrowest component with the decay of singlet Ps.

In the early 1970's[3.12-3.16], a great deal of experimental work was conducted to study positron annihilation from alkali halides with substantial concentrations of F-centres. The significant change in the angular distribution of two photon annihilation was found and attributed to annihilation of positrons trapped by F-centres. Positron annihilation associated with various types of vacancies was studied actively during that period of time.

The research in this area has been enhanced after Hyodo and Takakusa[3.17] discovered that Ps does exist in a delocalized state in NaF and NaCl at low temperatures. The evidence for delocalized Ps was provided by angular correlation measurements with a very narrow peak in the momentum distribution of the annihilation photon pair at sufficiently low temperature; such narrowness results only when the wave function of the Ps is extended over the crystal as a Bloch wave. Arefiev et al[3.18-3.20] repeated the observation for NaCl and some other features such as purity and magnetic effect were demonstrated. Similar studies have shown that delocalized Ps also is formed in several other alkali halides such as KBr[3.17], KI[3.21], NaI[3.21], RbCl[3.22], and KCl[3.23]. It has been shown that above a characteristic temperature the narrow para-Ps peak in the angular correlation curve broadens drastically. This broadening was interpreted as the result of localization of Ps in a meta-stable, self-trapped state[3.24]. Therefore the Ps atom may reside in either a delocalized or a localized state with the energy level of the localized state assumed to lie higher than the bottom of the delocalized Bloch band. At low temperature Ps will be mainly in the delocalized state but will, with rising temperature, start to populate the localized states. Because every cell has several potential localization sites in the interstices (the number of the possible trapping sites is assumed to be two per unit cell, or eight per usual FCC cube), the broadening of the sharp Ps peak develops quickly[3.43]. This effect has been attributed to a temperature induced transition of the Ps to a self-trapped state.

3.1.4 Experimental Techniques

i) Introduction

When energetic positrons from a radioactive source are injected into a condensed medium they slow down to thermal energies in a very short time of the order of 1 ps[3.4]. The mean implantation range varying from 10 to 1000 μm guarantees that the positrons reach the bulk of the sample material. Finally, after staying in thermal equilibrium, the positron annihilates with an electron from the surrounding medium dominantly into two 511 keV gamma quanta. The average lifetime of positrons is characteristic of each material. The positron technique has many advantages in the study of matter and positron annihilation has proven useful as a nondestructive probe for the study of solids and defects in solids, because the information is carried out of the material by gamma radiation. No special sample preparation is necessary and some applications on dynamic phenomena at elevated temperatures are possible. The longer-lived positron lifetime components are sensitive to the nature of the annihilation site in solids. Very low concentrations of radiation-induced defects can have a profound effect upon the formation of Ps in solids. Both the positron and the Ps atom are light particles and thus are difficult to be confined in a small region of space according to the Heisenberg uncertainty principle. They will, therefore, sample large regions of their surrounding structure and are thus versatile probes.

Most of the experiments on positron annihilation in ionic solids have been performed in accordance with standard techniques, namely: measurements of lifetime spectra, angular correlation curves and Doppler-broadened annihilation line shapes. The knowledge in this area has been accumulated continuously.

ii) Lifetime Measurements

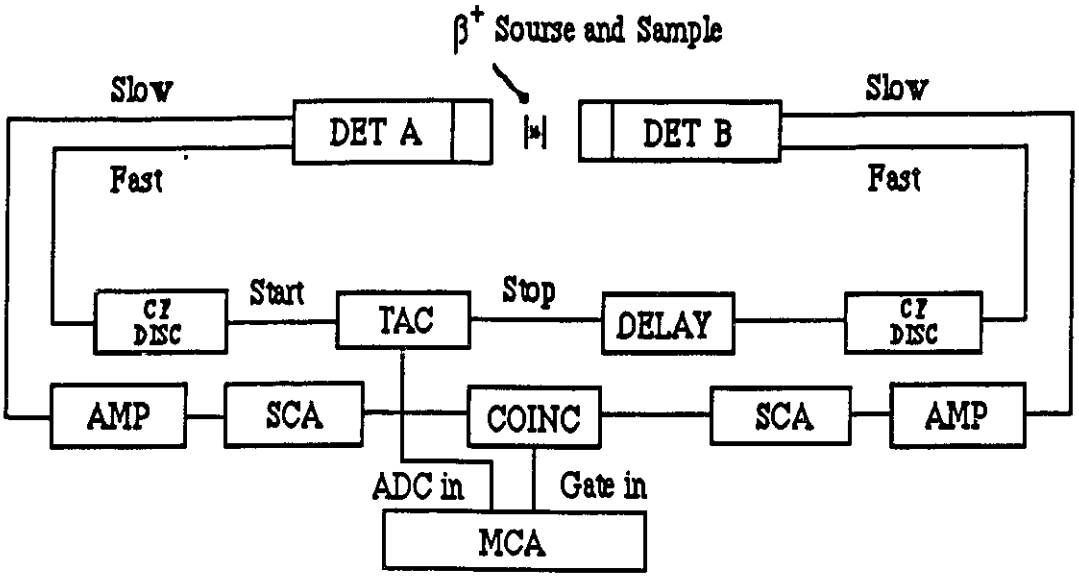

Fig. 1. Schematic diagram of the fast-slow coincidence system used in the positron lifetime measurement. CF DISC: constant-fraction-timing discriminator; TAC: time-to-amplitude converter; AMP: amplifier; SCA: single-channel analyzer; COINC: coincidence circuit; MCA: multichannel analyzer

The lifetime spectrometer is shown schematically in Fig.1. It is a fast-slow coincidence system conventionally used in nuclear spectroscopy. The detectors consist of fast plastic scintillators coupled to fast photomultiplier tubes. The energy windows of the single-channel analyzers in the slow channels are adjusted so that the detector A registers the birth of positrons, while the annihilation of positrons is counted via detector B. The fast signals from the anodes of the photomultipliers are fed to constant-fraction-timing discriminators to produce time signals. These are then led to a time-to-amplitude converter (TAC), the output of which is proportional to the time interval between the start

and stop signals. The output pulses from the (TAC) are then transferred to a multichannel analyzer through a linear gate driven by the coincidences in the slow channel, i.e., the output pulses are accepted only if the corresponding start and stop signals have correct energy values determined by the windows of the single-channel analyzers. A time resolution of 300 ps (full width at half maximum, FWHM) is typically obtained with available commercial equipment and it is of the same order of magnitude as the lifetimes to be measured. The resolution is mainly limited by the decay time of the light centres in the scintillators and by the transit time spread of electrons in the photomultipliers.

Usually positrons annihilate from different states in the sample, so the result is a multi-exponential lifetime spectrum of the form $\exp(-\lambda_i t)$. The corresponding lifetime τ_i is the inverse of λ_i. This is normally analyzed by computers in order to extract values of τ_i and relative intensities I_i associated with the different components.

iii) Angular Correlation Measurements

Angular-correlation measurements in long-slit geometry are a widely used method to study defects in thermal equilibrium. We have sketched in Fig.2 the geometry of the usual angular-correlation experiment. In the centre-of-mass frame the two photons are emitted at an angle of 180°, with total energy $E = 2mc^2 - E_b$, where E_b is the binding energy of the electron and positron in the system and c the velocity of light. In the laboratory frame the two photons are not anticolinear because of the finite momentum **p** to be conserved, and their energy is Doppler shifted. Given a typical atomic momentum **p** ($|p| \sim 10^{-2}mc$), the angle between the

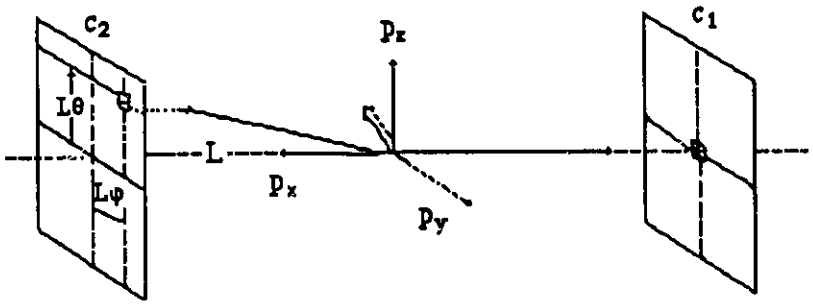

Fig.2 Geometry of the 2γ angular-correlation experiment. The double arrow presents the momentum **p** to be conserved by the two annihilation γ 's.

two photons deviates from 180° only by a few milliradians. If the first photon is detected at the origin of counter plane c_1, then the second correlated photon will hit the counter plane c_2 at the coordinates ϑL and φL (L is the distance of the counter plane from the annihilation centre), since ϑ and φ are only a few milliradians. Thus we obtain $p_z = \vartheta mc$ and $p_y = \varphi mc$, to a good approximation. The third component p_x(as shown in Fig.2, the main direction is taken along x axis) parallel to the main direction of the quanta can be measured by observing the energy of the two photons, E_1 or E_2. We obtain $E_{1,2} = mc^2 - E_b/2 \pm cp_x/2$ (again for $|p| \leq mc$). Typical atomic momentum leads to Doppler shifts of a few keV; thus we can neglect in most measurements the smaller E_b term. In order to maximize the

count rate, the long-slit setup uses two long counters behind long collimating slits, thus integrating over one of momentum components, say p_y (corresponding to long horizontal counters in Fig.2). A typical apparatus is shown schematically in Fig 3.

The gamma-ray detectors are usually long, cylindrically shaped NaI(Tl) scintillators, behind lead slits that define the resolution width Δp_z of the apparatus. To measure true 1D projections, the length of the crystals has to be sufficient to submit an angle φ much larger than the typical width of ~0.5 mrad of an angular distribution. One detector is mounted on a moving arm and is stepped automatically for measuring the coincidence rate as a function of the angle ϑ. The lack of energy measurement means an automatic integration over the p_x component. Thus, for a given momentum density $P(\mathbf{p})$, the long-slit geometry setup measures, for perfect resolution, a coincidence rate proportional to the projection of the momentum distribution

$$N(p_z) = \int P(\mathbf{p})\, dp_x dp_y$$

We call $N(p_z)$ the one-dimensional angular-correlation of the annihilation radiation (ACAR) curve. The form of such angular distribution curves provides a basis for conclusions regarding the various annihilation mechanism.

iv) Line-Shape Measurements

The motion of the electron-positron pair causes a Doppler shift on the energy of the annihilation radiation. As a consequence, the line shape gives the distribution of the longitudinal momentum component of the annihilating pair,

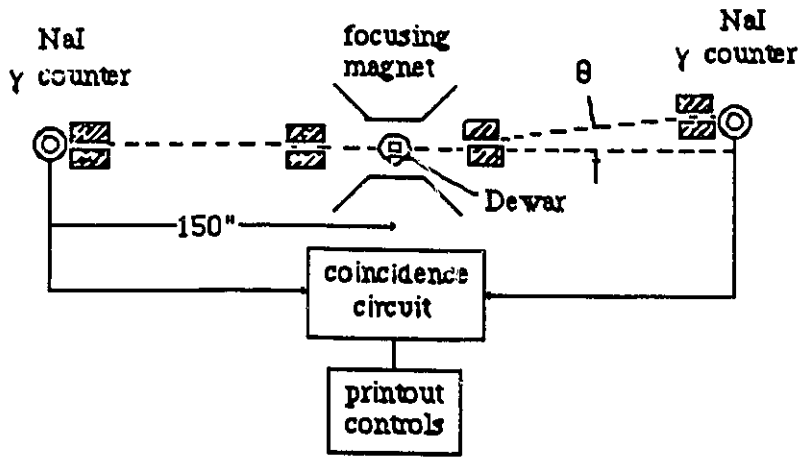

Fig. 3 Sketch of apparatus used for one-dimensional long-slit ACAR (angular correlation annihilation radiation) measurements; the NaI γ counters consist of long cylindrical scintillators positioned perpendicular to the plane of the sketch. The shaded areas are the long lead slits, defining the angle ϑ and the effective resolution $\Delta\vartheta$.

i.e., the distribution of p_x in the coordinate system of Fig.2. This measurement is performed on the above mentioned main direction and other directions are assumed integrated. The energy measurement of one of the annihilation gammas is equivalent to a 1D ACAR measurement, yielding $N(p_x) = \int P(\mathbf{p})\, dp_y dp_z$. From p_x, the energy can be found to be $E_{1,2} = mc^2 - E_b/2 \pm cp_x/2$. In principle, the energy measurement can be performed by a bent-crystal spectrometer to a high

precision; the efficiency of such spectrometers is, however, very low and one thus requires a very large β^+ source. In practice, Doppler spectrometry is performed more commonly with the use of Ge(Li) or intrinsic Ge gamma-ray spectrometers. The advantage of such spectrometers over performing 1D ACAR measurements is in their efficiency; one can accumulate the equivalent of a full ACAR spectrum simultaneously by using a multichannel energy analyzer. On the other hand, the essential drawback in the Doppler-broadening technique is the limitation in the obtainable energy resolution. At present the best Ge spectrometers have an effective resolution of ~ 1 KeV, corresponding in an ACAR setup to an effective momentum resolution of ~ $4mc*10^{-3}$, i.e., an angular resolution of ~ 4 mrad. Thus the effective momentum resolution is about a factor of ten worse than the usual ACAR resolution.

v) Magnetic Field Effect Measurements

This is a very important experimental technique for the study of Ps or quasi-Ps(qPs). The so-called magnetic-quenching experiment is based on the effect the application of a magnetic field has on the annihilation characteristics of correlated e^-e^+ pairs. When an external magnetic field is applied on a correlated e^-e^+ pair, the triplet state is mixed with the singlet state for m = 0. Actually, the orbital magnetic moment, which in ordinary atoms is associated with the electronic motion, is absent in Ps, where no electric current flows. Therefore, the interaction of Ps with a constant field H modifies the Ps Hamiltonian only by a spin-dependent term[3.4]:

$$H' = g\mu_B H (\sigma_z^- - \sigma_z^+)$$

where g is the gyromagnetic ratio of the electron and of the positron, μ_B is the

Bohr mageton, and σ_z^- , σ_z^+ are Dirac spin matrices along the quantization axis set by H. The operator H′ acts only on the spin function $|s, m_s\rangle$, giving

$$H' |s, m_s\rangle = 2\mu_B H \delta_{m_s,0} |1 - s, 0\rangle$$

where s is a spin quantum number and m_s is its projection along the axis set by H. Non-vanishing matrix elements of H' between eigenfunctions of the basis $|n, s, l, j, m\rangle$ connect singlet and triplet states belonging to the same set of quantum numbers n,l,m. Note that this eigenvector is labelled with five quantum numbers(q.n.) : n (principal q.n.), s (spin q.n.), l (orbital q.n.), j (total angular momentum q.n.), m (magnetic q.n.). Thus, in the presence of H, two out of four stationary spin states are singlet-triplet mixtures; this has observable consequences for the energy levels and the annihilation rates of these states. The mixing ratio is higher at higher fields. At sufficiently high field strengths this effect leads to a one-third reduction of the long-lived ortho-Ps component in the lifetime spectrum and to a doubling of the para-Ps component in the angular correlation curve[3.25]. This occurs only because the positron is bound to an electron having unpaired spin. Thus the observation of the magnetic field effect gives the experimental proof of Ps or qPs formation; but there is more than this: the quantitative analysis of the experimental data can lead to determination of the density parameter which represents the electron density seen by the positron, the key quantity that characterizes the internal wave function of qPs.

3.1.5 Summary of Previous Experimental and Theoretical Works

i) Annihilation Centres in Alkali Halides

Annihilation centres are bound states of the positron at lattice defects.

Their existence was predicted by Goldanskii and Prokopev [3.26]. They are formed upon positron trapping[3.27], a process possible whenever the binding energy of the system is positive relative to deposition of the positron in its lowest propagating state in a perfect lattice. Several examples of positrons trapped at negatively charged and neutral defects associated with vacancies are known. A brief description is given of those centres for which the theoretical models are developed.

a) Fe+-Centre

This system is a positron-electron pair trapped by an anion vacancy and can be schematically represented as in Fig.4.

It is by far the best known annihilation centre, and is easily observed in additively coloured and heavily irradiated crystals. It can be formed in ortho and in para states, and is affected by static magnetic fields. Its ortho state contributes a long-living component to lifetime spectra, and the para state a narrow component to momentum distributions. Such components are easily resolved, and the accurate determination of their characteristics is possible. On the other hand, the short-lived contribution of the para state to lifetime spectra has never been singled out.

An excellent fit for the narrow component observed in angular correlation experiments on additively coloured KCl is provided by a model that represents the centre of mass as a particle contained in a rigid cubic cavity. The Ps wave function inside the cavity was assumed to be a standing wave whose wave vector was expressed only as a function of the length of L the edge of the cavity. The Fourier transform of the wave function provided the angular momentun distribution. Herlach & Heinrich[3.30] treated L as an adjustable parameter to fit

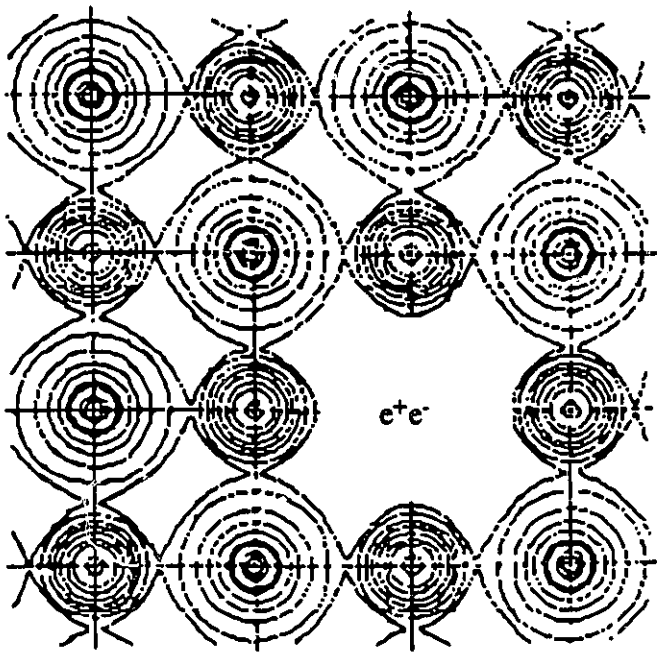

Fig. 4 Model of the Fe+ centre in NaCl viewed in the (100) plane. Constructed from experimental results of Witte and Wolfel [J. Phys. Chem. 3(1955)296] with no allowance for distortion or polarization effects near the anion vacancy.

the angular momentum distribution with the corresponding experimental observations, and evaluated it to be L=5.68 A.

Calculations for the wave function of the system, and for its binding, have been performed by Farazdel & Cade[3.29], Herlach[3.30], Berezin[3.31,3.32] and Hautojarvi[3.33]. Their main conclusions can be briefly given as:

1. explicit consideration of the electron-positron correlation is mandatory not only

for reasonable lifetime calculations but also for energy calculations; the inclusion of this correlation lowers the calculated energy by 1-2 eV[3.29];

2. the stability of the system against the dissociation

Fe^+ centre ---------- e^+ + F centre

is in general easily determined; the situation is more critical when considering the dissociation reaction

Fe^+ centre ---------- $e^+ e^-$ + anion vacancy.

It becomes essential to take into account the lowering of the binding energy of the delocalized e^+e^- pair, which is due to its interaction with the lattice[3.32];

3. the calculated values of the binding energy are markedly influenced by the choice of the model potential; therefore the regular trends that the theory predicts are more significant than the absolute values. In fact, Farazdel & Cade[3.29] showed that the binding energy of the positron to the F-centre increases with both anion and cation sizes.

b) F_{anti} - centre

The F_{anti}-centre is formed by a positron trapped at an empty cation vacancy and is viewed as the antimorph of the F-centre. It has been invoked to explain the complexity of annihilation spectra and the effects of irradiation. Having identified the origin of the long-living intense component in lifetime spectra for uncoloured crystals with Ps in a Bloch state intrinsic to perfect crystals, no direct evidence for F_{anti}-centres seems to remain. However, thermal treatments produce definite changes in the short-living spectral component; this is probably a manifestation of the increased trapping probability in thermally generated cation vacancies. According to this hypothesis Dannefaer et al. deduced from lifetime measurements a mean life of 340 ps for F_{anti}-centres[3.28]. So far no detailed

calculation of the binding energy E_b of the system has been made, though by analogy with F centres one expects this to be of the order of a few eV; Farazdel and Cade[3.29] estimated $E_b = 4 - 6$ eV.

c) F'_{e^+} -centre

This neutral centre comprises two electrons and a positron at an anion vacancy; it is formed by the capture of a delocalized positron in an F'-centre. It is likely to contribute to the short-living part of lifetime spectra and to the small-momentum region in momentum distributions. Although spectral components related to this centre have not been experimentally observed, the evidence of the existence of the centre is quite convincing. Berezin[3.32] has estimated that the positron affinity to the F'-centre is almost twice as great as the positron affinity to the F-centre. In point of fact, after the capture of the positron by an F'-centre, the system will tend to dissociate into an F-centre plus a delocalized Ps; however, annihilation probably occurs before dissociation.

ii) Ps States in Intrinsic Alkali Halides

a) Ps Self-Trapped at an Interstice

Some crystals, e.g., ice and alkali halides, show evidence of both free and localized Ps atoms[3.25]. The Ps atom tends to localize in regions of low electron density away from the ion cores. The exchange repulsion, combined with electrical forces, will favour Ps localization in the interstices and cavities. Bound states will actually be formed when the attracting potential is large and extended enough: for orientation we may recall from elementary quantum mechanics that bound states of a particle of mass M are formed in a square three-dimensional

well of radius r when $Vr^2 > h^2/8M$. The studies on NaF and KCl revealed that Ps became localized at high temperatures($T_{NaCl} = 63K$, $T_{KCl} = 65K$, $T_{NaF} = 150K$, $T_{KI} = 50K$) (3.23,3.24,3.34). The nature of the localization is not understood but some speculation about the site may be made. The localization of the Ps cannot be attributed to trapping at thermally created defects. The effect of such defects has been observed only at much higher temperatures($T > 250K$). It cannot be attributed to temperature activated reaction of the accumulated radiation damage either, because the measurements for KI were performed from room temperature downwards without any heating up and yet the localized Ps disappeared at temperature below 22K(3.22). It is also to be remembered that the temperature region for the transition was the same in the other series of measurements with a different temperature cycle. It is not likely a vacancy for several reasons: The lifetime of trapped Ps is usually longer(3.10,3.11,3.13,3.35,3.36), the number of vacancies is usually not so much a function of temperature in this temperature range as of composition(3.37), and the positron irradiation did not seem to influence the results. A more likely site may be the tetrahedral interstice of the crystal. Kasai and Fujiwara(3.22) suggested that the wave function of the Bloch positronium may have a large amplitude in this region. Ps could be self-trapped there if the volume were expanded by moving ions in the soft (111) directions. It may be pointed out that the tetrahedral interstice is fairly large even before any deformation; if the usually accepted ion radii are assumed, the inscribed spheres to the interstice in most alkali halide crystals have a diameter larger than the Bohr radius of the free Ps in vacuum, 1.06 A. The coupling of Ps to phonons gives rise to a metastable self-trapped state placed about 0.1 eV above the delocalized state. The filling of the metastable state sets in rather abruptly at temperatures <

0.1 eV/k due to the very large number of possible final states (every crystal cell is a potential trapping site). In addition, at the higher temperature the increased trapping probability causes faster Ps localization and hence all para-Ps may end up in the localized state before it decays.

b) Ps in a Free State

The formation of a Ps like system in ionic crystals has for a long time been a debated problem[3.25]. Delocalized Ps states were detected for the first time in quartz by the observation of narrow peaks at the maximum of the annihilation-radiation correlated curves (ARCC) having a width of one mrad, which we shall henceforth refer to as the Ps peak, and on the projections of the corresponding reciprocal-lattice vectors[3.38]. The translational symmetry and width of the observed peaks in the ARCC indicate the delocalized nature of the corresponding state. When a static magnetic field was applied, the intensity of the given peaks in the ARCC increased, which directly indicates the Ps-like nature of the peaks[3.39]. Since that time similar delocalized Ps states have been found in MgF_2 and ice[3.40]. In alkali halide crystals in which positron annihilation has been investigated since the 1950s, delocalized Ps was detected in 1977 by Hyodo et al[3.17] through the observation of a well-defined narrow Ps peak in ARCC when the specimens were cooled down to liquid nitrogen temperature or lower. The temperature dependence of the ACC was further investigated[3.18-3.24,3.41-3.46] and analyses came to the following results:

1. the temperature dependence of the narrow peaks originates from the self-annihilation of singlet Ps;

2. in the lower temperature region, the peak width increases at a rate which shows that the Ps is in a free state;

3. in the higher temperature region, the peak width increases more rapidly than in the lower temperature region, which indicates that a number of the Ps are trapped in some localized state;

4. the temperature region where the rapid broadening of the Ps momentum distribution occurs is different for different substances.

In an attempt to interpret those fascinating observations, a model was proposed by Hyodo et al[3.24] in which the Ps atoms in alkali halides have two kinds of states, delocalized and localized, and the energy level of the localized state is assumed to be a little higher than the bottom of the delocalized band. This observed transition of Ps from Bloch state to localized state can be most naturally understood in terms of thermally activated self-trapping. In alkali halide crystals, the exciton consisting of an electron bound to a self-trapped hole through the Coulomb attraction is self-trapped. Importance of the interaction between the particles and the acoustic phonons for the appearance of the self-trapped state was discussed by Toyozawa[3.53]. Toyozawa and Sumi[3.54] showed that for a certain range of the coupling strength of the interaction, the free and the self-trapped state might coexist as local energy minima with respect to the lattice distortion. Which of the two states is the ground state depends on the strength of the coupling with the acoustic phonons as well as that with the optical phonons. They also explained the temperature dependence of the drift mobility of holes by proposing the possibility of a metastable self-trapped state. The idea of a metastable self-trapped state can also be applied to explain the anomalous temperature dependence of the momentum distribution of Ps annihilation. A possible situation is shown schematically in Fig.5[3.47,3.48].

Figure 5(a) depicts the lowest Ps band in a perfect lattice as a function of the

translational wave vector **k**, while Fig.5(b) shows the energy of the Ps-lattice system as a function of a symbolical configuration coordinate Q of the local lattice distortion around the Ps. The short range interaction causes a bound state to split off the continuum of the free states represented by the thin lines in Fig.5(b). When the interaction is strong enough, the lowest state can form a local minimum at $Q=Q_t$ which is lower by ε than the level of the lowest free state in the deformed lattice. This minimum represents the self-trapped state. The free state and the self-trapped state are separated by a potential barrier of height U. The level of the trapped state, E, is determined by the competition between the energy gained by the delocalization, B, and that gained by the lattice relaxation, E_{LR}, and can be higher or lower than the lowest free state in the undeformed lattice.

At sufficiently low temperature the Ps atoms will populate mainly the delocalized states. Since at very low temperatures no phonon could exist, the particle is unable to overcome the potential barrier to reach the self-trapped state and thus can decay only from the free state. As the temperature is raised, however, they tend to populate in the localized state because of the large number of sites in the crystal available for the localization, which causes a remarkable broadening in the momentum distribution. The agreement between this model and the experiment is fairly good, and the energy difference between the two states and the effective mass are estimated through fitting experimental data.

3.1.6 Present Work

Generally speaking, the progress in experimental research in this area has been quite impressive, going far ahead of theoretical studies. There have been very few theoretical work involving a detailed calculation of Bloch states of Ps and

meta-stable self-trapped Ps. This is one of the stimulii for our present work. The

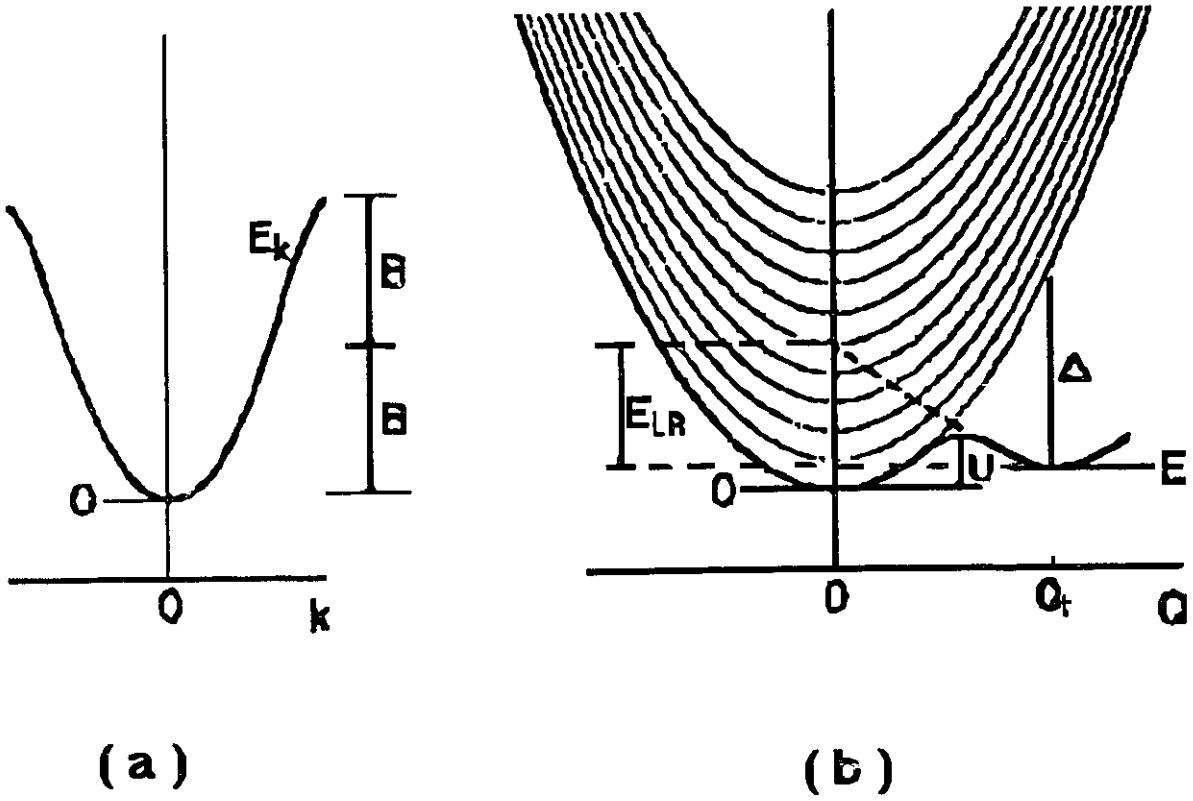

Fig.5. Illustration of (a) the lowest Ps band in a perfect lattice and (b) the Ps-lattice system as a function of a configuration coordinate Q representing the local lattice distortion around the Ps. The mimimum at Q=Qt corresponds to a possible self-trapped state of the Ps. The free and the self-trapped state are separated by a potential barrier of height U. See text for the definition of the other symbols[3.47,3.48].

new approach is developed to study the positron annihilation from various states.

Our hybrid pseudopotential approach described previously in F'-centre work is modified to apply to this new system. Both electron and positron are represented by a linear combinations of floating 1s Gaussian wave functions. Only the electron wave function needs to be orthogonalized to the core orbitals of the surrounding ions because of Pauli's exclusion principle. On the other hand, positron itself does not need to be constrained by such a requirement. The electron-positron correlation is partly represented in the basis function of Ps we have employed. This is believed to be an essential character of the problems in question. The rest of the treatment follows a line similar to the case of the F'-centre.

Three crystals, NaF, NaCl and KCl are studied in the present work, simply because more information has been gathered on them than on all other compounds. Fortunately our method reveals a great advantage in dealing with the problem. Not only those results obtained before by others can be reexamined, but all those different systems can be studied extensively based on the same theoretical approximations. Furthermore, the most exciting part of this work is that those recent experimental observations about the small energy gap (0.1 eV) between a localized Ps state and a delocalized Ps state and the transition between them can also be explained. As a matter of fact, our study agrees with the analyses of experiment reasonably well. The calculated lifetimes for Ps in intrinsic crystals are, however, one order of magnitude larger than observed ones. This could be attributed to the limitation of our Ps wavefunction in which the relative motion of the positron and electron is not completely decoupled from the centre of mass motion. Further discussion on this particular problem will be given later.

3.2 Method of Calculation

3.2.1 Electronic Structure

When we are dealing with defect systems involving either a positron or Ps, the interactions of a positron with electrons of a medium must be treated by taking into consideration the whole positron-multi-electron system because of the indistinguishability of electrons. We know from general principle, that the wave function of such a system must be antisymmetric with respect to electron exchange. To simplify the many-body problem, a basic assumption has to be introduced: the average distance between the pair of particles of a Ps is small compared to the lattice constant; and the positron-electron interaction is the dominant factor and the medium just presents a small external perturbation.

This assumption enables us to treat a few-particle defect system separately from the many-electron medium. A Hartree-Fock single particle approximation is employed and the effect of medium electrons on the defect system is taken care of by orthogonalization of defect electron wave function to the valence electron orbitals.

Orthogonalization is essential, because it introduces nodes in the wave function of the correlated pair taken for $\mathbf{r}_+=\mathbf{r}_-=\mathbf{r}$; the zero amplitude of wave function means that when the positron enters the volume region occupied by core orbitals, the correlated electron can not follow. In other word, the exchange between defect electron and core electrons keep the correlated pair outside the region of core orbitals, thus reducing pick-off and partly preserving the e^-e^+ correlation.

Basically, the defect systems under study are composed of two particles. In

the approach we have developed, the two particle basis is represented by a product wave function of two single particle Gaussian basis function. In the following, we present the relation between our basis and a more conventional basis in which the center of mass and relative motions are explicitly described. For an arbitrary two particle product Gaussian basis of the form, centred at **A** and **B**, (normalization constants are not considered):

$$\exp\left[- \alpha (r_1 - A)^2 \right] \exp\left[- \beta (r_2 - B)^2 \right] \tag{3.1}$$

We transform the coordinates into a C.M. coordinate system by defining

$$r = r_1 - r_2 \ , \qquad R = \frac{1}{2}(r_1 + r_2) \tag{3.2}$$

Then eq.(3.1) can be written as:

$$\exp\left[- \alpha (\frac{1}{2} r + R - A)^2 \right] \exp\left[- \beta (R - \frac{1}{2} r - B)^2 \right] = G(R)\, G(r) \tag{3.3}$$

where

$$G(R) = \exp\left[- \frac{\alpha \beta}{\alpha + \beta} (2R - A - B)^2 \right] \tag{3.4}$$

$$G(r) = \exp\left[- (\alpha + \beta) \left\{ \frac{1}{2} r - \frac{\alpha A - \beta B + (\beta - \alpha) R}{\alpha + \beta} \right\}^2 \right] \tag{3.5}$$

Here one of the properties of Gaussian functions has been used in which a product of two Gaussians can be contracted into a new Gaussian with a new decay factor and at new position. Apparently, the basis decouples into the product of C.M. and relative motions partly, which means that the present Gaussian basis can be used to represent the two particle systems. This can be seen more transparently by assuming that the Gaussians have a common decay factor ($\alpha = \beta$), and their positions are chosen in such a way that **A=B** or **A=-B**, then eq.(3.3) becomes either of the following forms:

$$G(R)\,G(r) = \exp\left[-2\alpha(R-A)^2\right]\exp\left[-\frac{\alpha}{2}(r)^2\right] \tag{3.6}$$

$$G(R)\,G(r) = \exp\left[-2\alpha(R)^2\right]\exp\left[-\frac{\alpha}{2}(r-2A)^2\right] \tag{3.7}$$

Later on, the usefulness of these relations will be further examined.

As mentioned before, we are going to study four distinct systems in this part of the work. Obviously, they have quite different electronic structures one from another, hence their Hartree-Fock Hamiltonians will be described separately.

i) Fe^+-center

For this system, the defect is composed of an anion vacancy plus an electron-positron pair. The HF Hamiltonian is

$$H = H^- + H^+ + H^{+-} \tag{3.8}$$

where H^{+-} is the coulomb interaction between the electron and positron, and H^+ , H^- are, respectively, the single particle positron, electron Hamiltonian of the form

$$H^+ = -\frac{1}{2}\nabla_+^2 - V_{pi}(r_+) - V_{sc}(r_+) \tag{3.9}$$

$$H^- = -\frac{1}{2}\nabla_-^2 + V_{pi}(r_-) + V_{sc}(r_-) + V_{ex}(r_-) \tag{3.10}$$

where H^- has the same expression as eq.(2.5) of the F'-centre. H^+ also has a similar form to eq.(2.5), except that there is no exchange interaction and it has opposite sign for both point-ion potential and screened Coulomb interaction. The wave function can be expressed as a linear combinations of two particle wavefunctions

$$\psi(r_+, r_-) = \sum_i C_i\,\phi_i(r_+)\,\phi_i(r_-) \tag{3.11}$$

where $\phi_i(r_+)$ and $\phi_i(r_-)$ are single particle wave function for positron and electron. They have the form of

$$|\phi_i(r_-)\rangle = |G_i(r_-)\rangle - \sum_{m\lambda} |\chi_{m\lambda}(r_-)\rangle\langle\chi_{m\lambda}(r_-)|G_i(r_-)\rangle \qquad (3.12)$$

$$|\phi_i(r_+)\rangle = |G_i(r_+)\rangle \qquad (3.13)$$

where G_i is a normalized floating 1s Gaussian. The electron pseudo-wavefunction is orthogonalized to the core orbitals $\chi_{m\lambda}$ (**m** and λ label the core sites and orbitals, respectively). The positron wavefunction (3.13) is simpler without orthogonalization.

Here we have to consider the spins of the Ps pair. In a nonrelativistic approach, the energy levels are degenerate with regard to spin and angular momentum states. In the Russell-Saunders coupling, the spatial and spin parts of wave functions are chosen to be eigenstates of the parity operator and of the spin exchange operator, respectively; a generic complete eigenvector $|ns\mathit{l}jm\rangle$ is labelled with five quantum numbers (q.n.): n (principal q.n.), s (spin q.n.), l (orbital q.n.), j (total angular momentum q.n.), m (magnetic q.n.); each Russell-Saunders eigenstate is an eigenstate of the charge conjugation operator, belonging to the eigenvalue $(-1)^{\mathit{l}+s}$. For a spherically symmetric state (s-state, l=0), then we have a singlet state $(-1)^{s=0}$ and a triplet state $(-1)^{s=1}$. Due to the independence of the Hamiltonian on spin, we do not need to give spin explicitly in the wave function. As we have seen with our study of the F'-centre in 2.2.3, the diagonalization of the Hamiltonian results in symmetric space wavefunctions which take care of singlet and triplet states automatically.

The energies and the eigenfunctions may be obtained by solving the secular determinant

$$\left| H_{ij} - E S_{ij} \right| = 0 \tag{3.14}$$

where

$$S_{ij} = \langle \phi_i(r_+)\, \phi_i(r_-) \,|\, \phi_j(r_+)\, \phi_j(r_-) \rangle \tag{3.15}$$

$$\begin{aligned} H_{ij} = {} & \langle \phi_i(r_-) \,|\, H^- \,|\, \phi_j(r_-) \rangle \langle G_i(r_+) \,|\, G_j(r_+) \rangle \\ & + \langle \phi_i(r_-) \,|\, \phi_j(r_-) \rangle \langle G_i(r_+) \,|\, H^+ \,|\, G_j(r_+) \rangle \\ & + \langle G_i(r_+)\, \phi_i(r_-) \,|\, H^{+-} \,|\, G_j(r_+)\, \phi_j(r_-) \rangle \end{aligned} \tag{3.16}$$

The calculation of single particle terms $\langle \phi_i(r_-) \,|\, H^- \,|\, \phi_j(r_-) \rangle$ and $\langle G_i(r_+) \,|\, H^+ \,|\, G_j(r_+) \rangle$ is straightforward following the approach adopted in dealing with the F'-centre which was explained in 2.2.3. The most complicated term is the matrix element of the positron-electron interaction Hamiltonian, i.e., the last term in (3.16) which can be further written as

$$\begin{aligned} H_{ij}^{+-} = {} & \langle G_i(r_+) G_i(r_-) \,|\, H^{+-} \,|\, G_j(r_+) G_j(r_-) \rangle \\ & - \sum_{m\mu} \langle G_i(r_-) \,|\, \chi_{m\mu}(r_-) \rangle \langle G_i(r_+) \chi_{m\mu}(r_-) \,|\, H^{+-} \,|\, G_j(r_+) G_j(r_-) \rangle \\ & - \sum_{m\mu} \langle \chi_{m\mu}(r_-) \,|\, G_j(r_-) \rangle \langle G_i(r_+) G_i(r_-) \,|\, H^{+-} \,|\, G_j(r_+) \chi_{m\mu}(r_-) \rangle \\ & + \sum_{n\nu} \sum_{m\mu} \langle G_i(r_-) \,|\, \chi_{m\mu}(r_-) \rangle \langle \chi_{n\nu}(r_-) \,|\, G_j(r_-) \rangle \langle G_i(r_+) \chi_{m\mu}(r_-) \,|\, H^{+-} \,|\, G_j(r_+) \chi_{n\nu}(r_-) \rangle \end{aligned} \tag{3.17}$$

Compared to the F'-centre, here the H_{ij}^{+-} has a much simpler form. As shown above, there are only 4 terms (i.e., one 0χ,, two 1χ, and one 2χ Coulomb-like) instead of 16 terms in the F'-centre. This is due to the absence of the positron-electron exchange. Similar to the F'-centre, the contributions of the deep core orbitals are neglected, and contributions from the outer s and p shells are fitted into single Gaussians. Those fitted parameters were given in Table 2.6. Thus the calculations only involve Gaussians and are made analytically as in the case of the F'-centre. The total overlap matrix element (3.15) can be written as

$$S_{ij} = \langle G_i(r_+)\, G_i(r_-) \mid G_j(r_+)\, G_j(r_-) \rangle - \sum_{m\lambda} \langle G_i(r_-) \mid \chi_{m\lambda}(r_-) \rangle \langle \chi_{m\lambda}(r_-) \mid G_j(r_-) \rangle \langle G_i(r_+) \mid G_j(r_+) \rangle \tag{3.18}$$

Its calculation is quite the same as eq.(2.16). The eigenvalues and eigenfunctions can be obtained simultaneously by solving the secular determinant (3.14) once all matrix elements are available.

ii) F_{anti}-centre

This system is simpler to treat due to its single particle character. The defect positron Hamiltonian is

$$H^+ = -\frac{1}{2}\nabla_+^2 - V_{pi}(r_+) - V_{sc}(r_+) \tag{3.19}$$

and the wavefunction is a linear combination of single particle Gaussians:

$$\psi(r_+) = \sum_i C_i\, G_i(r_+) \tag{3.20}$$

Practically this is an anti-F-centre system. All the matrix elements can be evaluated without any difficulty. Our cluster model is designed to have options to handle different systems. In the case of the F_{anti}-centre, instead of having an anion vacancy, a cation vacancy is created, then a Gaussian basis representing a positron is sited around the vacancy. Initially one optimized basis is used to minimize the lattice and obtain the relaxed lattice configuration. Then many bases are employed to get the best ground state energy. The positron binding energy to the vacancy is estimated. Further a full comparison is made to the F-centre.

iii) Self-Trapped Ps

As mentioned earlier, Ps could be self-trapped at an interstitial site of the

perfect lattice above a certain characteristic temperature. Right after Ps is trapped, the ions around experience displacements and the lattice readjusts itself to achieve new equilibrium through the electron-phonon interaction. Fortunately the method developed to treat the Fe^+-center can also be applied to this new system.

Ps, being a bound electron-positron pair, has a very light mass so that it is difficult to be confined in a small space region. The theoretical model should be made flexible to account for this feature. Two different approaches are tried in this part of the work. The first one considers the Ps to be fairly well localized in the small region around an interstice. Therefore, the problem is quite similar to that of the Fe^+-center. The matrix elements of the Hamiltonian and the total overlap are:

$$H_{ij} = \langle \phi_i(r_+)\,\phi_i(r_-) \mid H \mid \phi_j(r_+)\,\phi_j(r_-) \rangle \qquad (3.21)$$

and

$$S_{ij} = \langle \phi_i(r_+)\,\phi_i(r_-) \mid \phi_j(r_+)\,\phi_j(r_-) \rangle \qquad (3.22)$$

respectively, with $\phi_i(r_+)$ and $\phi_i(r_-)$ defined in eq.(3.12) and (3.13). Though the Hamiltonian shows the same form as (3.8), (3.9) and (3.10) in appearance, the point-ion potential here is not that important due to the absence of a charged vacancy where the potential well is usually formed. Here, the potential produced by an infinite lattice at the interstice is rather flat. The electron wave function is made orthogonal to all core orbitals of the lattice ions. We place the trial wave function at an interstice, then the energy minimization process provides the ground state energy, the eigenfunctions and the corresponding lattice configurations. Compared to the Fe^+-centre, this defect has Ps trapped at an interstice and therefore the interaction with surrounding ions is stronger due to

the shorter distance in between. More ions may be affected by the existence of the defect. To cope with this situation, the number of ions which are allowed to move has to be increased. Up to the third shell of atoms (relative to the interstitial site) are allowed to relax.

In the second approach, we allow the C.M. of Ps to be more diffuse, extending over a number of unit cells by introducing an envelope function to the basis (3.11) used in the first approach. The reason for this second try is in the nature of the basis we use. As presented earlier, the basis set employed is of the form of a product of two Gaussians, one for each particle. This type of basis provides a separate description of C.M. from relative motion as seen in eq.(3.3), (3.6) and (3.8). Unfortunately, it is found that it does not have fully independent variational degrees of freedom foro the C.M. and the relative motions of the Ps. The difficulty with this choice of basis is that it is not possible to control the C.M. motion of the system independently from the relative motion, while the internal motion of Ps is rather important in determining the lifetime. The theoretical model itself is facing a limitation of basis. One may ask whether this is a problem associated only with the specific system in question? How about those systems discussed previously? To answer the question, we re-examined those previous systems. It is found that there is no serious problem for those well localized defect systems like the Fe^{+}-centre where both C.M. and relative motions are tightly bound at a vacancy by a potential well. It may be a problem for Ps trapped at an interstice, because there is no potential well strong enough to confine the C.M. motion. It is nevertheless a limitation, as we can not determine the C.M. motion of the Ps separately from the relative motion. One device to overcome this is to introduce an envelope function $F(\mathbf{R})$ which describes the amplitude of the basis in

each unit cell. This is an idea which led us to the second approach. Another aspect in favour of a more diffuse C.M. motion of Ps is that with a strongly localized Ps wave function, the calculated angular momentum correlation curve was found to be rather broad compared to experimental data.

Now we describe this approach in detail. The idea is similar to that which describes the exciton in solids[3.49], and the wave function of the system can be written as:

$$\psi(r_+, r_-) = \sum_i C_i \sum_{\mathbf{R}} \exp(-\alpha_R R^2)\,\phi_i(r_+ - \mathbf{R})\,\phi_i(r_- - \mathbf{R}) \qquad (3.23)$$

Here $\mathbf{R}$ represents the position of the unit cell, and the summation over $\mathbf{R}$ runs over all unit cells. As we can see a Gaussian like envelope function is proposed. In other words, the envelope function allows the C.M. of the Ps to spread over like a wave packet and the decay parameter is determined via energy minimization. If we limit $\mathbf{R}$ to zero, then eq.(3.23) goes back to the wave function (3.11). After introducing the envelope function, the wave function of the self-trapped Ps system is improved. Finally the Hamiltonian matrix element for this system can be expressed as

$$\begin{aligned} H_{ij} &= \langle \sum_{\mathbf{R}} F(\mathbf{R})\,\phi_i(r_+ - \mathbf{R})\,\phi_i(r_- - \mathbf{R}) \,|\, H \,|\, \sum_{\mathbf{R}'} F(\mathbf{R}')\,\phi_j(r_+ - \mathbf{R}')\,\phi_j(r_- - \mathbf{R}') \rangle \\ &= \sum_{\mathbf{R}\mathbf{R}'} F(\mathbf{R}')\,F(\mathbf{R})\,\langle \phi_i(r_+ - \mathbf{R})\,\phi_i(r_- - \mathbf{R}) \,|\, H \,|\, \phi_j(r_+ - \mathbf{R}')\,\phi_j(r_- - \mathbf{R}') \rangle \end{aligned} \qquad (3.24)$$

The total overlap matrix element is

$$S_{ij} = \sum_{\mathbf{R}\mathbf{R}'} F(\mathbf{R}')\,F(\mathbf{R})\,\langle \phi_i(r_+ - \mathbf{R})\,\phi_i(r_- - \mathbf{R}) \,|\, \phi_j(r_+ - \mathbf{R}')\,\phi_j(r_- - \mathbf{R}') \rangle \qquad (3.25)$$

The meaning of the above expressions is clear: inside any unit cell the C.M. envelope function is multiplied by the matrix elements (3.15) and (3.16). A Gaussian type of envelope function presents no further difficulty in calculation. Now the only problem is the increased computing time.

iv) Bloch-like Positronium State

Our approach was originally developed to treat well localized states. To our best knowledge, no theoretical work has been done to treat a Bloch-like state of Ps. Here we propose a way to calculate the Bloch state of the Ps through generalization of our present scheme to the extended state. It turns out that the approach with a floating 1s Gaussian basis has a significant potential even in an energy band calculation[3.50]. Because a form of pseudo-potential is used, we note that only excited states are accessible to this method. The valence bands are considered flat, which is an acceptable approximation since more precise self-consistent calculations demonstrate rather flat valence bands[3.50].

Since the interaction of a correlated Ps with a periodic lattice is invariant under translation by a lattice vector, the total crystal momentum of the Ps is a good quantum number to label the eigenstates of the system and the corresponding energy eigenvalues.

We formulate a Bloch function for the Ps which satisfies the Bloch theorem:

$$\psi(\mathbf{r}_+ + \mathbf{d}, \mathbf{r}_- + \mathbf{d}) = e^{i\mathbf{k}\cdot\mathbf{d}}\psi(\mathbf{r}_+, \mathbf{r}_-) \tag{3.24}$$

for an arbitrary lattice vector **d**. Such a Bloch function can be expressed in the following form:

$$\psi_i(\mathbf{r}_+, \mathbf{r}_-) = \frac{1}{\sqrt{N}}\sum_{\mathbf{L}} e^{i\mathbf{k}\cdot\mathbf{L}}\left[G_i(\mathbf{r}_- - \mathbf{L}) - \sum_{m\lambda} \langle \chi_{\lambda,m}(\mathbf{r}_-) | G_i(\mathbf{r}_-) \rangle \chi_{\lambda,\mathbf{L}+m}(\mathbf{r}_-) \right] G_i(\mathbf{r}_+ - \mathbf{L}) \tag{3.26}$$

Here $\chi_{\lambda,m}(\mathbf{r}_-)$ represents a core orbital λ centred at **m**. Thus the wave function can be constructed from a Bloch sum by using a floating Gaussian basis

$$\psi(\mathbf{r}_+, \mathbf{r}_-) = N^{-\frac{1}{2}}\sum_i C_i \sum_{\mathbf{L}} e^{i\mathbf{k}\cdot\mathbf{L}}\left[G_i(\mathbf{r}_- - \mathbf{L}) - \sum_{m\lambda} \langle \chi_{\lambda,m}(\mathbf{r}_-) | G_i(\mathbf{r}_-) \rangle \chi_{\lambda,\mathbf{L}+m}(\mathbf{r}_-) \right] G_i(\mathbf{r}_+ - \mathbf{L}) \tag{3.27}$$

where N is the number of unit cells, G_i is the floating Gaussian, **k** is the Bloch

state positronium wavevector, and **L** is an atomic site. Summation over **L** runs over all unit cells. It also appears that eq.(3.27) approaches the localized case when the sum over **L** is limited to one unit cell.

We are interested in the behaviour of the delocalized Ps state at the centre of the Brillouin zone, so the wavevector **k** can be simply taken to be zero. Now we introduce an abbreviation $G_i^+ \equiv G_i(r_+)$ to avoid writing those long expressions. The Bloch wave function (3.27) yields the Hamiltonian matrix element of the form:

$$H_{ij} = H_{ij}^- + H_{ij}^+ + H_{ij}^{+-} \tag{3.28}$$

where

$$\begin{aligned} H_{ij}^- = & \sum_{\mathbf{L}} \langle G_i^- | H^- | G_j^-(\mathbf{L}) \rangle \langle G_i^+ | G_j^+(\mathbf{L}) \rangle \\ & - \sum_{m\mathbf{L}\lambda} \varepsilon_{\lambda m+\mathbf{L}} \langle G_i^- | \chi_{\lambda m+\mathbf{L}} \rangle \langle \chi_{\lambda m} | G_j^- \rangle \langle G_i^+ | G_j^+(\mathbf{L}) \rangle \\ & - \sum_{m\mathbf{L}\lambda} \varepsilon_{\lambda m} \langle G_i^- | \chi_{\lambda m} \rangle \langle \chi_{\lambda m} | G_j^-(\mathbf{L}) \rangle \langle G_i^+ | G_j^+(\mathbf{L}) \rangle \\ & + \sum_{\lambda\lambda'\mathbf{L}mm'} \varepsilon_{\lambda' m'} \langle G_i^- | \chi_{\lambda' m'} \rangle \langle \chi_{\lambda m} | G_j^- \rangle \langle \chi_{\lambda' m'} | \chi_{\lambda m+\mathbf{L}} \rangle \langle G_i^+ | G_j^+(\mathbf{L}) \rangle \end{aligned} \tag{3.29}$$

Here $\varepsilon_{\lambda m}$ is the same core energy as explained in the discussion of the F'-centre and as a result of translational symmetry, one of the summations over **L** drops and cancels 1/N. Before going further to write down the detailed expressions for the remaining two terms in (3.28), we simplify (3.29) first. The orthogonality of different core orbitals results in

$$\langle \chi_{\lambda' m'} | \chi_{\lambda m+\mathbf{L}} \rangle = \delta_{\lambda\lambda'} \delta_{m' m+\mathbf{L}} \tag{3.30}$$

The use of this equation reduces the multiple summations in the last term of (3.29), which then becomes

$$\sum_{\lambda\mathbf{L}m} \varepsilon_{\lambda m+\mathbf{L}} \langle \chi_{\lambda m} | G_j^- \rangle \langle G_i^- | \chi_{\lambda m+\mathbf{L}} \rangle \langle G_i^+ | G_j^+(\mathbf{L}) \rangle \tag{3.31}$$

Note that (3.31) cancels the second term in (3.29), so (3.29) reduces to

$$H_{ij}^{-} = \sum_{L} \langle G_i^{-} | H^{-} | G_j^{-}(L) \rangle \langle G_i^{+} | G_j^{+}(L) \rangle - \sum_{m L \lambda} \varepsilon_{\lambda m} \langle G_i^{-} | \chi_{\lambda m} \rangle \langle \chi_{\lambda m} | G_j^{-}(L) \rangle \langle G_i^{+} | G_j^{+}(L) \rangle \tag{3.32}$$

Following the same procedure, we have matrix element for the positron Hamiltonian

$$H_{ij}^{+} = \sum_{L} \langle G_i^{-} | G_j^{-}(L) \rangle \langle G_i^{+} | H^{+} | G_j^{+}(L) \rangle - \sum_{L \lambda m} \langle G_i^{-} | \chi_{\lambda m} \rangle \langle \chi_{\lambda m} | G_j^{-}(L) \rangle \langle G_i^{+} | H^{+} | G_j^{+}(L) \rangle \tag{3.33}$$

The matrix element of the interaction Hamiltonian has a complicated form

$$\begin{aligned} H_{ij}^{+-} &= \sum_{L} \langle G_i^{+} G_i^{-} | H^{+-} | G_j^{+}(L)\, G_j^{-}(L) \rangle \\ &- \sum_{L \lambda m} \langle \chi_{\lambda m} | G_j^{-} \rangle \langle G_i^{-} G_i^{+} | H^{+-} | \chi_{\lambda m+L}\, G_j^{+}(L) \rangle \\ &- \sum_{L \lambda m} \langle G_i^{-} | \chi_{\lambda m} \rangle \langle G_i^{+} \chi_{\lambda m} | H^{+-} | G_j^{+}(L)\, G_j^{-}(L) \rangle \\ &+ \sum_{L} \sum_{\lambda \lambda' m m'} \langle G_i^{-} | \chi_{\lambda' m'} \rangle \langle \chi_{\lambda m} | G_j^{-} \rangle \langle G_i^{+} \chi_{\lambda' m'} | H^{+-} | G_j^{+}(L)\, \chi_{\lambda m+L} \rangle \end{aligned} \tag{3.34}$$

The total overlap matrix element is

$$S_{ij} = \sum_{L} \langle G_i^{-} | G_j^{-}(L) \rangle \langle G_i^{+} | G_j^{+}(L) \rangle - \sum_{L \lambda m} \langle G_i^{-} | \chi_{\lambda m} \rangle \langle \chi_{\lambda m} | G_j^{-}(L) \rangle \langle G_i^{+} | G_j^{+}(L) \rangle \tag{3.35}$$

We have derived these general expressions for various matrix elements. Let us go back to (3.32) and work out details of them one by one. In expression (3.32), the first term can be simply written as

$$\sum_{L} [\, T_{ij}^{-}(L) + V_{ij}^{ec}(L) + V_{ij}^{ex}(L)\,]\, S_{ij}^{+}(L) \tag{3.36}$$

in which the kinetic energy operator integral is

$$\begin{aligned} T_{ij}^{-}(L) &= \langle G_i^{-} | T^{-} | G_j^{-}(L) \rangle \\ &= N_i^{-} N_j^{-} \left(3 - \frac{2\,\alpha_i^{-}\alpha_j^{-}}{\alpha_i^{-} + \alpha_j^{-}} R_{-}^{2} \right) \exp\left(- \frac{\alpha_i^{-}\alpha_j^{-}}{\alpha_i^{-} + \alpha_j^{-}} R_{-}^{2} \right) \end{aligned} \tag{3.37}$$

where

$$R_-^2 = \left| a_i^- - (L - a_j^-) \right|^2 \tag{3.38}$$

and N_i, N_j are the normalization constants of Gaussians; the positron overlap integral is

$$S_{ij}^+(L) = \langle G_i^+ | G_j^+(L) \rangle = N_i^+ N_j^+ \exp\left(- \frac{\alpha_i^+ \alpha_j^+}{\alpha_i^+ + \alpha_j^+} R_+^2 \right) \exp\left(- (\alpha_i^+ + \alpha_j^+)(R_K^+)^2 \right) \tag{3.39}$$

where

$$R_+^2 = \left| a_i^+ - (L - a_j^+) \right|^2 \tag{3.40}$$

$$R_K^+ = \frac{\alpha_i^+ a_i^+ + \alpha_j^+ (L - a_j^+)}{\alpha_i^+ + \alpha_j^+} \tag{3.41}$$

The integral of the short range potential is

$$V_{ij}^-(L) = \langle G_i^- | V_{sc} + V_{ex} | G_j^-(L) \rangle \tag{3.42}$$

This integral can be divided into a deep core part and an outer shell part as in the F'-centre calculation. The deep core contribution is formulated in a similar way after making a multipolar expansion:

$$\begin{aligned} V_{ij}^-(L) &= \frac{1}{4} F_{i0}(0, a_i^-) F_{j0}(0, L + a_j^-) A_0 \\ &+ \frac{1}{8} \left(F_{i0}(0, a_i^-) F_{j0}^{(2)}(0, L + a_j^-) + F_{i0}^{(2)}(0, a_i^-) F_{j0}(0, L + a_j^-) \right) J_0' \\ &+ \frac{9}{4} F_{i1}^{(1)}(0, a_i^-) F_{j1}^{(1)}(0, L + a_j^-) \frac{a_i^- \cdot (L + a_j^-)}{|a_i^-| |L + a_j^-|} J_0 \end{aligned} \tag{3.43}$$

where A_0, J_0' and J_0 have been defined in (2.26), (2.27) and (2.28), and expansion coefficients have no difference for those appearing in (2.26). Similarly the deep core part of the second term of (3.32) comes out to be

$$\frac{1}{4} F_{i0}(0, \bar{a_i}) F_{j0}(0, L + \bar{a_j}) \sum_{s\text{-core}} \varepsilon_\lambda^0 B_\lambda$$

$$+ \frac{1}{8} \left(F_{i0}(0, \bar{a_i}) F_{j0}^{(2)}(0, L + \bar{a_j}) + F_{i0}^{(2)}(0, \bar{a_i}) F_{j0}(0, L + \bar{a_j}) \right) \sum_{s\text{-core}} \varepsilon_\lambda^0 K'_\lambda \qquad (3.44)$$

$$+ \frac{9}{4} F_{i1}^{(1)}(0, \bar{a_i}) F_{j1}^{(1)}(0, L + \bar{a_j}) \frac{\bar{a_i} \cdot (L + \bar{a_j})}{|\bar{a_i}| |L + \bar{a_j}|} \sum_{p\text{-core}} \varepsilon_\lambda^0 K_\lambda$$

Note that we have not multiplied the positron overlap by this term and we will do it in the final step. We find that the same ion-size parameters as defined in (2.29), (2.30) and (2.31) of the F'-centre can also be used in this work, because (3.43) and (3.44) have similar pseudo-potential terms. When we factorize them, the familiar ion-size terms are obtained. Thus the incorporation of overlap energy terms with the short range potential terms gives the ion-size correction of the electron Hamiltonian matrix element. Now we can write down the final form of (3.32):

$$\sum_L T_{ij}^-(L) S_{ij}^+(L) +$$

$$\sum_{Lm} S_{ij}^+(L) \left[f_1(L) A_m + f_2(L) J'_m + f_3(L) J_m - \Delta\varepsilon_m \left\{ f_1(L) B_m + f_2(L) K'_m + f_3(L) K_m \right\} \right] \qquad (3.45)$$

The ion-size parameters A, B, J, K, J' and K' have the same form of (2.29), (2.30) and (2.31) and their values are given in Table 2.3. f_1, f_2, f_3 are the simplified notations of expansion coefficients which are given in Appendix 2.2, i.e. (A2.2.13), (A2.2.14) and (A2.2.15).

The above technique can also be applied to calculate the matrix element (3.33). The first term is

$$\sum_L [T_{ij}^+(L) - V_{ij}^{sc}(L)] S_{ij}^-(L) \qquad (3.46)$$

Here the positron kinetic energy term takes the same expression as that of the electron (3.37), except that the variable R^2 has to be replaced by

$$R_+^2 = |a_i^+ - (L - a_j^+)|^2 \qquad (3.47)$$

Similarly, the electron overlap also has a form similar to (3.39); we only need to change $R_{\pm}^2$ into R^2 of (3.38) and change $R_K^{\pm}$ into

$$R_K^- = \frac{\alpha_i^- a_i^- + \alpha_j^- (L - a_j^-)}{\alpha_i^- + \alpha_j^-} \tag{3.48}$$

As we know, the positron does not have an exchange interaction, hence the short range potential contains only the coulomb interaction. The deep core part of this potential is similarly expressed as

$$\begin{aligned} V_{ij}^+(L) &= \frac{1}{4} F_{i0}(0, a_i^+) F_{j0}(0, L + a_j^+) A_0^+ \\ &+ \frac{1}{8}\left(F_{i0}(0, a_i^+) F_{j0}^{(2)}(0, L + a_j^+) + F_{i0}^{(2)}(0, a_i^+) F_{j0}(0, L + a_j^+)\right) J_0^{+'} \\ &+ \frac{9}{4} F_{i1}^{(1)}(0, a_i^+) F_{j1}^{(1)}(0, L + a_j^+) \frac{a_i^+ \cdot (L + a_j^+)}{|a_i^+||L + a_j^+|} J_0^+ \end{aligned} \tag{3.49}$$

where

$$A_0^+ = \int V_{sc}\, dr \tag{3.50}$$

$$J_0^+ = \int V_{sc}\, (r \cos\theta)^2\, dr \tag{3.51}$$

$$J_0^{+'} = \int V_{sc}\, (r)^2\, dr \tag{3.52}$$

are the ion-size parameters for the positron Hamiltonian. The positron interacts with core electrons through the coulomb interaction only. This is why these parameters are different from their counterpart for the electron. The ion-size parameters of the positron for different ions are shown in Table 3.1.

The second term of (3.33) is the product of a positron term and two electron overlap terms. The positron term has been calculated above, so we concentrate on the electron overlaps. They are:

$$\frac{1}{4} F_{i0}(0, \bar{a_i}) F_{j0}(0, L + \bar{a_j}) B$$

$$+ \frac{1}{8} \left(F_{i0}(0, \bar{a_i}) F_{j0}^{(2)}(0, L + \bar{a_j}) + F_{i0}^{(2)}(0, \bar{a_i}) F_{j0}(0, L + \bar{a_j}) \right) K' \qquad (3.53)$$

$$+ \frac{9}{4} F_{i1}^{(1)}(0, \bar{a_i}) F_{j1}^{(1)}(0, L + \bar{a_j}) \frac{(\bar{a_i}) \cdot (L + \bar{a_j})}{|\bar{a_i}||L + \bar{a_j}|} K$$

where B, K' and K are the same ion-size parameters as those defined in (2.22), (2.23) and (2.24), which are also given in Table 3.1. The above work brings (3.33) to the final form:

$$H_{ij}^{+} = \sum_{L} \left[S_{ij}^{-}(L) - \sum_{m} \left\{ f_1(L) B_m + f_2(L) K_m' + f_3(L) K_m \right\} \right] \times \left[T_{ij}^{-}(L) - f_1(L) A_0^{+} - f_2(L) J_0^{+'} - f_3(L) J_0^{+} \right] \qquad (3.54)$$

The contributions from outer s and p electrons are calculated separately. We go over the above terms again to find out the outer shell contributions. For the electron Hamiltonian with the short range potential terms, (3.42), the same interpolation scheme as presented in the F'-centre is used. The relevant interpolated parameters for screened Coulomb and exchange were given in Table 2.4.

The electron overlap integrals of eq.(3.32) are calculated through interpolated formulae as were described for the F'-centre in Chapter 2. The values of the fitted overlap parameters were listed in Table 2.5. Once the outer shell overlaps are evaluated, the overlap energy terms in (3.32) are easily calculated:

$$\sum_{L} \varepsilon_s \, ss\sigma ov(\bar{a_i}) \, ss\sigma ov(L + \bar{a_j}) + \sum_{L} \varepsilon_p \left[sp\sigma ov(\bar{a_i}) \frac{\bar{a_{ix}}}{|\bar{a_i}|} sp\sigma ov(L + \bar{a_j}) \frac{L_x + \bar{a_{jx}}}{|L + \bar{a_j}|} \right] +$$

$$\sum_{L} \varepsilon_p \left[sp\sigma ov(\bar{a_i}) \frac{\bar{a_{iy}}}{|\bar{a_i}|} sp\sigma ov(L + \bar{a_j}) \frac{L_y + \bar{a_{jy}}}{|L + \bar{a_j}|} + sp\sigma ov(\bar{a_i}) \frac{\bar{a_{iz}}}{|\bar{a_i}|} sp\sigma ov(L + \bar{a_j}) \frac{L_z + \bar{a_{jz}}}{|L + \bar{a_j}|} \right] \qquad (3.55)$$

where $ss\sigma ov$ and $sp\sigma ov$ were defined in (2.28).

Table 3.1

Deep core ion-size parameters of positronium for several ions (a.u.).

Ion	A_0^+	B	J_0^+	K	$J_0^{+'}$	K′
Na^+	-0.70817	0.186	-0.00345	0.0000	-0.01702	0.007
K^+	-7.70759	2.080	-0.4832	0.2300	-0.66771	0.370
Cl^-	-10.2873	3.143	-0.89779	0.5870	-1.18961	0.679
F^-	-1.07022	0.34943	-0.00794	0.0000	-0.03998	0.02252

In calculating the outer shell part of the term (3.33), we have only a short range Coulomb interaction for the positron Hamiltonian which is evaluated by an interpolation scheme as above and there are no new parameters involved. The overlaps in (3.33) are much easier to calculate following the same procedure as above.

As in the case of the Fe^+-centre, the problem resides in the most complicated interaction term (3.34). In this matrix element, the first term comes out immediately, due to the availability of the analytical expression for this sort of integral as presented in appendix 2.4. The remaining terms involve cores. Because of the compact character of core orbitals, we can reasonably assume that the outer shells make significant contributions, and the neglect of the deep core part shall not produce a serious problem. We interpolate outer s and p shells into single Gaussians respectively with fitted parameters characterizing the different ion and orbital, and then perform the same calculation as those similar terms in the Fe^+-centre. Those fitted parameters for various orbitals are the same as those of the F'-centre and they were listed in Table 2.6. Technically, we shall not encounter any new difficulty, all integrals simply involve Gaussians only. The only problem may be the last one containing two cores that seems troublesome. In dealing with it, we have to not only count all different combinations of orbitals , but also the triple summations over the lattice site. In principle, a large cluster would result in a more precise energy value, but computation time could be a problem. The economic way of doing it is to try a different size of the sub-cluster, until the possible smallest cluster is reached with satisfactory energy convergence.

The calculation of the total overlap matrix element (3.35) is much simpler.

Since the overlaps between Gaussian and core are calculated above, following the above procedure we obtain its ion-size correction and outer shell part with ease. Details are not necessary to be presented again. We finally solve the secular equation by substitution of H_{ij} and S_{ij} into (3.7).

3.2.2 Lattice Energy

The lattice energy includes the coulomb energy between ions considered as point charges, the short range repulsive energy and the polarization energy. For those systems under study, the difference between them mainly comes from the defect structure, and their lattice environments are quite similar. It is convenient to use the same method as used in the F'-centre to calculate the lattice energy of these new systems.

It is known that the intrinsic Ps state exhibits a temperature effect. Basically, our approach can not handle temperature explicitly. But we still develop a way to estimate those results at different temperatures indirectly. In fact, some basic quantities like lattice parameter, and Born-Mayer parameters are determined based on room temperature observations, therefore using those parameters results in the calculations which are valid only at room temperature. We can extend our method to other temperature ranges provided that the parameters are available. As a useful try, an extreme case of zero temperature is examined. We simulate the zero temperature lattice environment by, first, using the low temperature lattice parameters, and, second, refitting Born-Mayer parameters based on low temperature observations. These parameters are shown in Table 2.2. The other concerned properties are, we believe, not sensitive to temperature. Repeating the same procedure as that of room temperature, we

obtained low temperature results.

Polarization effects depends very much on the defect charge. Its calculation is subject to rough approximations and assumptions. In our approach, we adopt the Mott-Littleton method to estimate the polarization effect. For the Fe+-centre, the system has a net charge of +e. This means that the polarization effect may need to be treated by a more sophisticated method, but a substantially more accurate calculation will present considerable complexity as discussed in 1.1.3. A method of treating the F'-centre having a net charge of -e rather than +e developed previously can still be taken as an acceptable approximation. So the same scheme is applied to the new system. A little modification of the program yields the polarization energy. Systems such as the F_{anti}-centre and Ps self-trapped at an interstice are charge neutral defects, and the polarization effects turn out to be quite small. Their calculations are therefore similar to that of the F-centre.

The Bloch-like state of the Ps also does not have a bnet charge, but behaves in a slightly different way because of translational symmetry. Polarization effects are to be treated also based on the lowest order Mott-Littleton method. We give below more details. The normalized Bloch-like wavefunction from (3.27) is

$$\psi(r_+, r_-) = \frac{1}{\sqrt{N}} \sum_i C_i \psi_i(r_+, r_-) = \frac{1}{\sqrt{N}} \sum_L C_i G_i(r_+ - L) G_i(r_- - L) \qquad (3.56)$$

Note that the orthogonalization correction for the electron wavefunction is ignored for this time. The charge density of Ps is

$$\rho(r) = \int |\psi|^2 [\delta(r - r_+) - \delta(r - r_-)] \, dr_+ \, dr_- \qquad (3.57)$$

$$= \frac{1}{N} \int \left| \sum_i C_i \psi_i(r, r_-) \right|^2 dr_- - \frac{1}{N} \int \left| \sum_i C_i \psi_i(r_+, r) \right|^2 dr_+ = \rho^+(r) - \rho^-(r)$$

The density is the superposition of the positron and electron densities. The full expression of ρ^+ is given by:

$$\rho^+(r) = \frac{1}{N}\sum_{LL'}\sum_{ij} C_i C_j \; G_i(r-L)G_j(r-L') \int G_i(r_- - L)G_j(r_- - L')\,dr_-$$
$$= \frac{1}{N}\sum_{LL'}\sum_{ij} C_i C_j \; G_i(r-L)G_j(r-L')\,S_{ij}^-(L-L') \tag{3.58}$$

If we define the charge enclosed in a sphere of radius $|R_\gamma - R_{ij}^-(L, L')|$ centred at $R_{ij}^-(L, L')$ as:

$$Q_{ij}^+(L, L', R_\gamma) = \int_0^{|R_\gamma - R_{ij}^-(L, L')|} G_i(r-L)G_j(r-L')\,dr \tag{3.59}$$

then the electric field produced by the charge is

$$E^+(R_\gamma) = -\frac{1}{N^2}\sum_{LL'}\sum_{ij} C_i C_j \; S_{ij}^-(L-L')Q_{ij}^+(L, L', R_\gamma)\frac{R_\gamma - R_{ij}^-(L, L')}{|R_\gamma - R_{ij}^-(L, L')|^3} \tag{3.60}$$

Here,

$$R_{ij}^-(L, L') = \frac{\alpha_i^-(L + a_i^-) + \alpha_j^-(L' + a_j^-)}{\alpha_i^- + \alpha_j^-} \tag{3.61}$$

A similar treatment gives us the term

$$E^-(R_\gamma) = -\frac{1}{N^2}\sum_{LL'}\sum_{ij} C_i C_j \; S_{ij}^+(L-L')Q_{ij}^-(L, L', R_\gamma)\frac{R_\gamma - R_{ij}^+(L, L')}{|R_\gamma - R_{ij}^+(L, L')|^3} \tag{3.62}$$

with

$$R_{ij}^+(L, L') = \frac{\alpha_i^+(L + a_i^+) + \alpha_j^+(L' + a_j^+)}{\alpha_i^+ + \alpha_j^+} \tag{3.63}$$

In our extended Bloch state, there are no lattice distortions. Only defect Ps produces the electric field. Therefore, the polarization energy is given by

$$E_{pol} = -\frac{1}{2}\sum_\gamma \alpha_\gamma E^2(R_\gamma) \tag{3.64}$$

where α_γ is the free atomic polarizability of ion γ and the electric field is

$$E(R_\gamma) = E^+(R_\gamma) + E^-(R_\gamma) \tag{3.65}$$

3.2.3 Energy Minimization

Following the energy minimization procedure adopted in the F'-centre calculation, we can minimize the total energy with respect to the ionic positions for various positron centers. We treat at most three degrees of freedom at one time by minimizing each ion individually. Thus the minimization process is carried out in sequence over all ions allowed to move. In this way, lattice relaxations around the defect can be obtained self-consistently.

3.2.4 Lifetime Calculation

The information about the behaviour of the positron in solids is transmitted exclusively by the annihilation radiation. Since the annihilation of Ps into two gamma quanta according to

$$e^+ + e^- \Rightarrow 2\gamma \tag{3.66}$$

is much more frequent than that into three gamma quanta, we confine ourselves entirely to the former process.

The measuring techniques fall into two broad categories, depending on whether they give information on the momentum distribution of the annihilating Ps or on the annihilation rate of the positrons. The annihilation rate is determined by the overlap of the positron wavefunction with the electron wavefunction and is thus closely related to the electron density at the annihilation site. The two photon annihilation rate Γ is related to the electronic structure of the system by the expression[3.27]

$$\Gamma = \frac{1}{\tau} = \pi \alpha^3 \int \psi^*(r^N, r_+) \left\{ \sum_{\mu}^{N} \delta (r_\mu - r_+) \right\} \psi(r^N, r_+) dr^N dr_+ \qquad (3.67)$$

for a closed-shell N electron and one positron system. Here α is the fine structure constant and ψ is the wave function for the N-electron plus one-positron system with r^N representing the space-spin variables of the N electrons and r_+ the space-spin variables of the positron. The rate is given in atomic units. Note that the summation over the delta-function leads to a product of $N^*\delta (r_1 - r_+)$ and then the integration over the space coordinate of electron one can be carried out. The equation (3.67) can be rewritten as:

$$\Gamma = \frac{1}{\tau} = \pi \alpha^3 \int P (r_+) dr_+ \qquad (3.68)$$

where

$$P (r_+) = N \sum_{s_1 \cdots s_N, s_+} \int | \psi(r_1 = r_+, r_2 \cdots r_N, r_+, s_+) |^2 dr_2 \cdots dr_N \qquad (3.69)$$

and spin coordinates are kept in (3.69). Physically $P(r_+)dr_+$ is the spin-averaged probability of finding an electron in the volume element dr_+ around the position of the positron, regardless of the positions and spins of the remaining N-1 electrons. Clearly $P(r_+)dr_+$ is proportional to the annihilation rate due to the electronic charge within the volume element containing the positron (at r_+). For those defect systems discussed in the present work, only the correlation between positron and defect electron is counted and the correlation is perturbed by electrons in the medium. This means that the number of electrons N can be taken as one in our following calculation. The expression is simplified as

$$\Gamma = \frac{1}{\tau} = \pi \alpha^3 \int \psi^*(r_-, r_+) \delta (r_- - r_+) \psi(r_-, r_+) dr_- dr_+ \qquad (3.70)$$

Depending on the different wave functions of various systems, this yields the

values for the lifetime. Now we work out those formula as follows.

i) **Localized States**

By substituting the wave function (3.4) into (3.70), the rate becomes

$$\Gamma = \frac{1}{\tau} = \pi \alpha^3 \sum_{ij} C_i C_j \int \left\{ G_i^- - \sum_{\lambda m} \langle G_i^- | \chi_{\lambda m} \rangle \chi_{\lambda m} \right\} G_i^+ \left\{ G_j^- - \sum_{\lambda' m'} \langle \chi_{\lambda' m'} | G_j^- \rangle \chi_{\lambda' m'} \right\} G_j^+ \, dr$$

$$= \pi \alpha^3 \sum_{ij} C_i C_j \{ \langle G_i^- G_i^+ | G_j^- G_j^+ \rangle - \sum_{\lambda m} \langle G_i^- | \chi_{\lambda m} \rangle \langle \chi_{\lambda m} G_i^+ | G_j^- G_j^+ \rangle \tag{3.71}$$

$$- \sum_{\lambda' m'} \langle \chi_{\lambda' m'} | G_j^- \rangle \langle G_i^- G_i^+ | \chi_{\lambda' m'} G_j^+ \rangle + \sum_{\lambda m \lambda' m'} \langle \chi_{\lambda' m'} | G_j^- \rangle \langle G_i^- | \chi_{\lambda m} \rangle \langle \chi_{\lambda m} G_i^+ | \chi_{\lambda' m'} G_j^+ \rangle \}$$

This expression looks a bit like the matrix element of the interaction Hamiltonian (3.10), but with only a single integration, rather than double integrations, involved, the calculation shall not be so complex. The first term on the right represents the 0th order approximation to the rate and its calculation is straightforward. The remaining terms represent the corrections from consideration of the core effects. We assume that the compact deep core orbitals are less important than outer s and p shells in the lifetime, thereby we avoid treating complicated deep core contributions. The justification of this assumption sounds rather difficult, because the contributions of deep cores are represented by deep core ion-size parameters. We tried an indirect way to see the impact of deep cores on the lifetime. As it is seen in Table 2.4 and Table 2.5, the outer S and P shells are fitted into Gaussians in our approach. The interpolated decay parameters of the Gaussians were made 10 times larger, or, in other words, the diffuse outer shells were made artificially compact, so that they behave somehow like deep cores. The lifetime was recalculated by using such ' deep cores ' and it was found that the lifetime was modified by about 1%. Therefore, we decided to

drop the contributions of the deep cores in (3.71). The second and the third terms are relatively simple, because the three Gaussians can be contracted into a single Gaussian and the core is either S orbital or P orbitals. The interpolation scheme developed before to treat those outer shell overlaps in the F'-centre is applied here to calculate the ion-size correction on the lifetime. The last term involves two cores which can be at different sites. We assume those interpolation formulae are still valid and replace the cores by fitted Gaussians. At this point, we have, basically, the four Gaussian type overlap integrals. We need to work out all configurations regarding the different orbitals and then sum them up. Generally, this term is smaller and as the distance between the two cores increases it decreases fast.

ii) **Bloch State Ps**

The Bloch state has an extended wave function (3.27), so the corresponding probability density is

$$P(r) = \frac{1}{N^2}\sum_{LL'}\sum_{ij} C_i C_j \left\{G_i^-(L) - \sum_{\lambda m}\langle G_i^- | \chi_{\lambda m}\rangle \chi_{\lambda m+L}\right\} G_i^+(L)\times \left\{G_j^-(L') - \sum_{\lambda' m'}\langle \chi_{\lambda' m'} | G_j^-\rangle \chi_{\lambda' m'+L'}\right\} G_j^+(L') \tag{3.72}$$

It is seen that more summations are involved. To serve the purpose of a qualitative estimation of the lifetime, we keep only the first term, which means all influences on lifetime from core orbitals are ignored. Under this approximation the wave function has to be renormalized, and after a little algebra we get the rate

$$\Gamma = \frac{1}{\tau} = \pi \alpha^3 \sum_{ij} C_i C_j N_i^- N_i^+ N_j^- N_j^+ \left(\frac{\pi}{\alpha_i^- + \alpha_i^+ + \alpha_j^- + \alpha_j^+} \right)^{\frac{3}{2}}$$
$$\sum_h \exp\left\{ - \frac{(\alpha_i^- + \alpha_i^+)(\alpha_j^- + \alpha_j^+)}{\alpha_i^- + \alpha_i^+ + \alpha_j^- + \alpha_j^+} \left| R_i^{+-} - R_j^{+-} - h \right|^2 \right\} \tag{3.73}$$

where

$$R_i^{+-} = \frac{\alpha_i^- R_i^- + \alpha_i^+ R_i^+}{\alpha_i^- + \alpha_i^+} \tag{3.74}$$

Our variational wave function is obtained after energy minimization. It is this wave function that we use to calculate the annihilation rate.

3.2.5 Angular Correlation Calculation

We have given a detailed description of the background knowledge and how the observations of angular correlation curves are operated in section 3.1. Now, we intend to develop a theoretical description for the angular correlation curve. Free positrons usually annihilate with electrons located in outer shells of the atom (pick-off), which have a certain momentum. The angle between the two annihilation quanta therefore differs considerably from 180°, and leads to the broad component in the angular distribution curves. The para-Ps, on the other hand, loses most of its kinetic energy very rapidly after its formation and has very little centre of mass momentum left at the instant of annihilation; the photons emitted in this case deviate only slightly from 180° depending upon the kinetic energy of the system and are responsible for the occurrence of the narrow component in the angular distribution curves. The formation of para-Ps can be very readily recognized from the presence of the narrow component. The ortho-Ps annihilates mostly in para-decay (two gamma annihilation) via pick-off of

electrons bound to cores in high momentum states, because the pick-off annihilation is always present when the ortho-Ps atom exists in a medium. In the pick-off process the positron of ortho-Ps annihilates in fast para-annihilation with an electron of the medium. The result is an electron in the conduction band, a hole in the filled valence band and two gamma-rays emerging in opposite directions from the pick-off site[3.25].

Strictly speaking, the momentum density P(**p**) includes the sum of two terms, one corresponding to self-annihilation of the correlated pair and the other one to pick-off annihilation. With our wave function, we are able to give a more detailed discussion on self-annihilation. For singlet states

$$P(\mathbf{p}) = \left| \int e^{i\mathbf{p}\cdot\mathbf{r}_-} \delta(\mathbf{r}_- - \mathbf{r}_+)\, \psi(\mathbf{r}_-, \mathbf{r}_+)\, d\mathbf{r}_-\, d\mathbf{r}_+ \right|^2 = \left| \int e^{i\mathbf{p}\cdot\mathbf{r}} \psi(\mathbf{r}, \mathbf{r})\, d\mathbf{r} \right|^2 = |a(\mathbf{p})|^2 \quad (3.75)$$

where a(**p**) is the Fourier transform of the wave function $\psi(\mathbf{r}, \mathbf{r})$. with present technology, it is not possible to measure P(**p**) directly. For conventional long-slit experiments only the z-component of **p** is measured, regardless of the total momentum of the gamma-ray pair. The one dimensional angular momentum correlation is defined as (in a.u.):

$$N(\vartheta) = \int P\left(p_x, p_y, p_z = \frac{\vartheta}{\alpha}\right) dp_x\, dp_y \quad (3.76)$$

where $p_z = c\theta = \theta/\alpha$ and $\alpha = 1/c$ is the fine structure constant in a.u.. In the following two parts, we derive the angular momentum correlation expressions for localized state Ps and Bloch state Ps separately.

i) **Localized States**

The wave function ψ extends over a region containing a few atoms of the medium. If we assume that ψ is contained in a sphere of radius L, then a(**p**) will extend in the momentum space up to moment of the order of $h / 2\pi L$ in accordance

with the uncertainty principle. The 0th order approximation wave function of (3.4) is chosen (dropping all core related terms) to make an estimation.

$$a(\mathbf{p}) = \sum_i C_i \int e^{-i\mathbf{p}\cdot\mathbf{r}}\; G_i^- G_i^+ \, d\mathbf{r} = \tag{3.77}$$

$$= \sum_i C_i\, N_i^- N_i^+ \left(\frac{\pi}{\alpha_i^- + \alpha_i^+}\right)^{\frac{3}{2}} \exp\left\{- \frac{\alpha_i^-\,\alpha_i^+}{\alpha_i^- + \alpha_i^+} \left|a_i^- - a_i^+\right|^2\right\} e^{-i\mathbf{p}\cdot a_K^i} \exp\left\{- \frac{1}{\alpha_i^- + \alpha_i^+} \left|\frac{\mathbf{p}}{2}\right|^2\right\}$$

where

$$a_K^i = \frac{\alpha_i^- a_i^- + \alpha_i^+ a_i^+}{\alpha_i^- + \alpha_i^+} \tag{3.78}$$

Then the density becomes

$$P(\mathbf{p}) = \sum_{ij} C_i C_j N_i^- N_i^+ N_j^- N_j^+ \left(\frac{\pi}{\alpha_i^- + \alpha_i^+}\right)^{\frac{3}{2}} \left(\frac{\pi}{\alpha_j^- + \alpha_j^+}\right)^{\frac{3}{2}} \exp\left\{- \frac{\alpha_i^-\,\alpha_i^+}{\alpha_i^- + \alpha_i^+} \left|a_i^- - a_i^+\right|^2\right\} \tag{3.79}$$

$$\times \exp\left\{- \frac{\alpha_j^-\,\alpha_j^+}{\alpha_j^- + \alpha_j^+} \left|a_j^- - a_j^+\right|^2\right\} e^{-i\mathbf{p}\cdot(a_K^i - a_K^j)} \exp\left\{- \left(\frac{1}{\alpha_i^- + \alpha_i^+} + \frac{1}{\alpha_j^- + \alpha_j^+}\right) \left|\frac{\mathbf{p}}{2}\right|^2\right\}$$

Integration over p_x and p_y components gives the one dimensional angular momentum distribution:

$$N(\vartheta) = 4\pi \sum_{ij} C_i C_j N_i^- N_i^+ N_j^- N_j^+ \left(\frac{\pi}{\alpha_i^- + \alpha_i^+}\right)^{\frac{3}{2}} \left(\frac{\pi}{\alpha_j^- + \alpha_j^+}\right)^{\frac{3}{2}} \exp\left\{- \frac{\alpha_i^-\,\alpha_i^+}{\alpha_i^- + \alpha_i^+} \left|a_i^- - a_i^+\right|^2\right\} \tag{3.80}$$

$$\times \exp\left\{- \frac{\alpha_j^-\,\alpha_j^+}{\alpha_j^- + \alpha_j^+} \left|a_j^- - a_j^+\right|^2\right\} \left(\frac{1}{\alpha_i^- + \alpha_i^+} + \frac{1}{\alpha_j^- + \alpha_j^+}\right)^{-1}$$

$$\times \exp\left\{- \left(\frac{1}{\alpha_i^- + \alpha_i^+} + \frac{1}{\alpha_j^- + \alpha_j^+}\right)^{-1} \left(a_{KX}^i - a_{KX}^j\right)^2\right\}$$

$$\times \exp\left\{- \left(\frac{1}{\alpha_i^- + \alpha_i^+} + \frac{1}{\alpha_j^- + \alpha_j^+}\right)^{-1} \left(a_{KY}^i - a_{KY}^j\right)^2\right\}$$

$$\times \exp\left\{- \left(\frac{1}{\alpha_i^- + \alpha_i^+} + \frac{1}{\alpha_j^- + \alpha_j^+}\right) \frac{\vartheta^2}{4\alpha^2}\right\} \cos\left\{\frac{\vartheta}{\alpha}\left(a_{KZ}^i - a_{KZ}^j\right)\right\}$$

ii) **Bloch State Ps**

The Fourier transform of the Bloch wave function (3.27) in the 0th order approximation is given as follows (**k** = 0):

$$a(\mathbf{p}) = \frac{1}{N}\sum_{iL} C_i \int e^{-i\mathbf{p}\cdot\mathbf{r}}\; G_i^-(\mathbf{L})\,G_i^+(\mathbf{L})\,d\mathbf{r}$$

$$= \frac{1}{N}\sum_{iL} C_i\; N_i^-\,N_i^+ \left(\frac{\pi}{\alpha_i^- + \alpha_i^+}\right)^{\frac{3}{2}} \exp\left\{-\frac{\alpha_i^-\,\alpha_i^+}{\alpha_i^- + \alpha_i^+}\left|\mathbf{a}_i^- - \mathbf{a}_i^+\right|^2\right\} \times e^{-i\mathbf{p}\cdot(\mathbf{a}_K^i + \mathbf{L})}\; \exp\left\{-\frac{1}{\alpha_i^- + \alpha_i^+}\left|\frac{\mathbf{p}}{2}\right|^2\right\} \tag{3.81}$$

$$= \sum_i C_i\, N_i^-\, N_i^+ \left(\frac{\pi}{\alpha_i^- + \alpha_i^+}\right)^{\frac{3}{2}} \times \exp\left\{-\frac{\alpha_i^-\,\alpha_i^+}{\alpha_i^- + \alpha_i^+}\left|\mathbf{a}_i^- - \mathbf{a}_i^+\right|^2\right\} \times$$

$$e^{-i\mathbf{p}\cdot\mathbf{a}_K^i}\;\delta(\mathbf{p} - \mathbf{G})\exp\left\{-\frac{1}{\alpha_i^- + \alpha_i^+}\left|\frac{\mathbf{p}}{2}\right|^2\right\}$$

where the summation over **L** leads to a delta function which confines the momentum to those reciprocal-lattice vectors **G**. The momentum density in this case turns out to be

$$P(\mathbf{p}) = \sum_{ij} C_i\, C_j\, N_i^-\, N_i^+\, N_j^-\, N_j^+ \left(\frac{\pi}{\alpha_i^- + \alpha_i^+}\right)^{\frac{3}{2}}\left(\frac{\pi}{\alpha_j^- + \alpha_j^+}\right)^{\frac{3}{2}} \exp\left\{-\frac{\alpha_i^-\,\alpha_i^+}{\alpha_i^- + \alpha_i^+}\left|\mathbf{a}_i^- - \mathbf{a}_i^+\right|^2\right\} \times \tag{3.82}$$

$$\exp\left\{-\frac{\alpha_j^-\,\alpha_j^+}{\alpha_j^- + \alpha_j^+}\left|\mathbf{a}_j^- - \mathbf{a}_j^+\right|^2\right\} e^{-i\mathbf{G}\cdot(\mathbf{a}_K^i - \mathbf{a}_K^j)} \exp\left\{-\left(\frac{1}{\alpha_i^- + \alpha_i^+} + \frac{1}{\alpha_j^- + \alpha_j^+}\right)\left|\frac{\mathbf{G}}{2}\right|^2\right\}$$

where the discrete momentum $\mathbf{G}=(2\pi/L)\mathbf{n}$ corresponds to reciprocal-lattice vectors and L stands for lattice parameter. The angular momentum distribution of the z component may be obtained by summing the above equation over the other two components n_x and n_y. Finally we have the angular correlation for Bloch state Ps underthe lowest approximation

$$N(n_z) = 4\pi \sum_{ij} C_i C_j N_i^- N_i^+ N_j^- N_j^+ \left(\frac{\pi}{\alpha_i^- + \alpha_i^+}\right)^{\frac{3}{2}} \left(\frac{\pi}{\alpha_j^- + \alpha_j^+}\right)^{\frac{3}{2}} \exp\left\{-\frac{\alpha_i^- \alpha_i^+}{\alpha_i^- + \alpha_i^+} \left| a_i^- - a_i^+ \right|^2\right\} \tag{3.83}$$

$$\times \exp\left\{-\frac{\alpha_j^- \alpha_j^+}{\alpha_j^- + \alpha_j^+} \left| a_j^- - a_j^+ \right|^2\right\} \left(\frac{1}{\alpha_i^- + \alpha_i^+} + \frac{1}{\alpha_j^- + \alpha_j^+}\right)^{-1}$$

$$\times \sum_{n_x n_y} \exp\left\{-\left(\frac{1}{\alpha_i^- + \alpha_i^+} + \frac{1}{\alpha_j^- + \alpha_j^+}\right) \frac{1}{4} \left(\frac{2\pi}{L}\right)^2 \left[n_x^2 + n_y^2 + n_z^2\right]\right\}$$

$$\times \cos\left\{\frac{2\pi}{L} n_x \left(a_{KX}^i - a_{KX}^j\right) + \frac{2\pi}{L} n_y \left(a_{KY}^i - a_{KY}^j\right) + \frac{2\pi}{L} n_z \left(a_{KZ}^i - a_{KZ}^j\right)\right\}$$

3.3 Results and Discussions

3.3.1 Fe^+ - centres

i) Calculation of the Defect Structure

This system is formed by an F-centre trapping a positron. Both electron and positron are well localized at vacancy. The vacancy itself has the symmetry of point group O_h. The method described in section 3.2.1(i) is used in calculating the electronic structure of Fe^+ - centres. Lattice energies and energy minimization are carried out based on the theory described in section 3.2.2 and 3.2.3 respectively. Our two-particle floating 1s Gaussian representing the electron-positron pair can be placed at any site around the vacancy. At first, we use one basis (two-particle) to minimize the lattice. Generally, a Gaussian representing the electron would have different parameters from that representing the positron. The basis parameters need to be optimized before lattice relaxation. It is found that the lowest ground state energy can be achieved only when the basis is sited right at the centre of the vacancy and decay parameters α^- of the

electron Gaussian and α^+ of the positron Gaussian are identical in the perfect lattice situation. We refer to this type of basis as an on-centre basis. The calculated perfect lattice energies and corresponding parameters are given in Table 3.2. In the process of energy minimization, ions surrounding the defect are moving outward without breaking the O_h symmetry. Up to the fourth shell of ions are relaxed.

The first nearest-neighbour(n-n) ions displace quite an amount due to the stronger polarization effect from the extra charge at vacancy. As the distance from the defect centre increases, ionic displacements are getting smaller. As ions displace, the total energy drops gradually until the new balance is reached. Table 3.2 shows the final lattice distortions of the first n-n ions. The displacements of those ions other than first n-n ions are small and are not presented in the Table. The changes of various energies constituting the total energy are presented in Table 3.2. We define the energy change ΔE as the total energy difference between the perfect lattice and the relaxed lattice to measure energy drops caused by lattice relaxation. It is also listed in the Table.

From Table 3.2, we see that as the anion increases in size, the D_{nn} decreases and so does ΔE. The two features are less sensitive to the size of the cations. It is understood that a smaller anion vacancy provides less room for defect particles, those surrounding ions are closer to the defect and the stronger interaction forces them to move more, thereby the energy changes more. In contrast, the change of cation size seems to affect the energy weakly.

ii) Binding Energy

As mentioned above we use one on-centre basis to obtain the distortion field

Table 3.2

Fe^+-centre ground state lattice relaxation and energy change. D_{nn} represents the coordinates of n-n displacements(a.u.). α^- and α^+ (a.u.) are optimized decay parameters of electron and positron Gaussians, respectively. E_{coul}, E_{rep}, E_{el}, E_{pol} and E_t represent lattice coulomb energy, lattice repulsive energy, electronic energy, polarization energy and total energy(eV), respectively.

	NaF	NaCl	KCl	
Perfect Lattice				
α^-, α^+	0.10	0.08	0.08	
E_{coul}	10.86	8.92	7.99	
E_{rep}	0.00	0.00	0.00	
E_{el}	1.09	-1.38	-1.33	
E_{pol}	-1.05	-1.37	-1.24	
E_t	10.90	6.18	5.42	
Relaxed Lattice				
α^-, α^+	0.10	0.08	0.08	
D_{nn}	0.65	0.55	0.54	(1,0,0)
E_{coul}	6.88	6.08	5.62	
E_{rep}	2.27	1.28	1.01	
E_{el}	0.02	-1.68	-1.77	
E_{pol}	-0.40	-0.52	-0.50	
E_t	8.64	5.16	4.36	
ΔE	2.16	1.02	1.06	

through energy minimization. Addition of more basis functions lowers the total energy significantly. Like the case of the F'-centre, we can construct an off-centre basis (bases are placed around defect on certain directions) which contains the correlation effect between the electron and positron. It is well known that such a correlation plays a very important role in Ps self-annihilation. Generally speaking, more basis functions would give a more accurate description of the electron state and they would bring the system more close to the real ground state. An on-centre basis alone can not improve the energy substantially no matter how many more bases are used. It is the off-centre basis that make significant contributions to the energy improvement. This is simply because only off-centre bases contain the important correlation effect as we have seen in 2.2.6. We can also refer to this type of basis as a correlated basis. Besides a few on-centre bases, more off-centre basis functions are used until the energy is converged. We need to optimize both decay parameters and positions of the off-centre basis. Basically, our wavefunction is a linear combinations of many bases. A large number of basis combinations needs to be tried to search the optimum one. Such a search is time consuming. Experience helps to save time. This is one of disadvantages of our approach. For instance, we can optimize the off-centre basis along the X direction from symmetry considerations. The benefit of using an off-centre basis is to count correlation effects between electron and positron. As we described in an F'-centre work, basis functions need to be placed symmetrically along the X direction and -X direction. The basis is the product Gaussians of electron and positron $G(a^-)^* G(a^+)$; optimization shows that the two always take identical parameters, even though our method has the freedom to optimize them individually. Thus we do not need to distinguish the parameters between the two, and use common symbols

to represent them.

The procedure is first to optimize a pair of basis symmetrically sited on X axis, then repeat the procedure on Y and Z directions. We define 6 such bases as a group basis. We only need two parameters(α,R) to identify a group basis. α is the common decay parameter for all of them and R is the magnitude of basis positions such as: ($\pm a_x$, 0, 0), (0, $\pm a_y$, 0), (0, 0, $\pm a_z$), from the origin. Finally, 16 bases (4 on-centre bases plus 2 groups of off-centre bases) are used to obtained the best ground state energy. Following previous workers, the binding energy of a positron to an F-centre is defined as[3.29]

$$E_b = E(F^*) - E(Fe^+)$$

i.e., the energy difference between the ground state F-centre and the Fe^+-centre. E(F*) represents the F-centre ground state energy calculated at the Fe^+-centre ground state lattice relaxation in accordance with the Franck-Condon principle, because the binding energy here is referred to optical absorption energy. Note the energy in above expression is the total energy.

Our program has an option to perform F-centre calculations. In fact, simply dropping those positron related terms in the theory, all features of the F-centre can be reexamined and will be given in the next section. The F-centre binding energies of three crystals are calculated. The results are shown in Table 3.3. In order to show details of our calculation, we present all constituting terms of the total energy in the Table for both systems. As described in the theory part on polarization, the existence of a net charge in the Fe^+-centre produces a long range interaction, so a modification is introduced to handle the lattice polarization in our scheme in which the lattice is divided into two parts, a discrete part with a limited number of ions and an infinite continuous part, and polarization energy is

calculated for both parts by using a different method. The details have been explained in calculating F'-centre polarization (see section 2.2.4). The evaluated polarization energies are given in Table 3.3. The needed energies of two different defect systems are calculated exactly under the same lattice environment, so the Coulomb energy and repulsive energy are the same for both and therefore they will not affect the binding energy. Their values are shown in Table 3.2. The above binding energy expression can be written as a following equivalent form:

$$E_b = E_{elec}(F^*) + E_{pol}(F^*) - E_{elec}(Fe^+) - E^{I}_{pol}(Fe^+) - E^{II}_{pol}(Fe^+)$$

In this expression, the sub-indices represent electronic energy and polarization energy, respectively and the super-indices represent the discrete part(I), containing 4 shells of the ions, and the continuous part(II) of the polarization energy, respectively. We should mention that the polarization energies shown in Table 3.2 are the polarization energies of the discrete part only which depend on the lattice configuration. To compare with the earlier calculations from Farazdel & Cade[3.29], and Berezin[3.32], part of their results for the binding energy are also listed in Table 3.3. Based on the values in Table 3.3, a few conclusions can be drawn:

a) Positron binding energies to F-centres ranges from 1 to 2 eV for the alkali halides we studied, and as the size of the cation increases, binding gets deeper, which agree generally with previous calculations.

b) The binding mainly comes from the electron positron correlation. Introducing this effect in the wave function, i.e., adding two groups of off-centre bases, lowers the ground state energy by about 1 eV. The binding can not be formed without correlation, because the electronic energy calculated only from the on-centre basis is simply higher than that of the F*-center. The calculation indicates the

Table 3.3

Positron binding energies to the F-centre. (α;R) are the optimum basis parameters(a.u.). Four on-centre bases with four different α's are usually used. Two groups of off-centre bases are used and each group is identified by α and R. E_{el} represents the electronic energy. E_{pol}^{I}, E_{pol}^{II} represent polarization energies, in the case of the Fe^{+}-centre, from the discrete part of lattice and the continuous part of lattice, respectively. ΔE is the electronic energy difference between the uncorrelated basis calculation and the correlated basis calculation. E_b is the positron binding energy to the F-centre. F^* presents the unrelaxed F-centre. The energy unit eV is used. The plus in the correlated basis represents the linear combinations of three group of bases.

	NaF	NaCl	KCl
Fe+-centre			
Basis without correlation			
(α; R)	(0.10;0)	(0.08;0)	(0.08;0)
E_{el}	0.02	-1.68	-1.77
Basis with correlation			
(α_1; R_1)	(0.09-0.12;0)	(0.07-0.10;0)	(0.07-0.10;0)
+(α_2; R_2)	(0.10;0.4354)	(0.09;1.066)	(0.10;0.595)
+(α_3; R_3)	(0.13;1.306)	(0.10;1.599)	(0.11;1.785)
E_{el}	-1.15	-2.86	-2.96
ΔE	1.13	1.16	1.19

E_{pol}^{I}	-0.40	-0.52	-0.50
E_{pol}^{II}	-0.56	-0.38	-0.35

F*-centre

α	0.09-0.12	0.07-0.10	0.07-0.10
E_{el}	-0.51	-2.17	-1.79
E_{pol}	-0.41	-0.39	-0.32
E_b	1.19	1.20	1.70

Results from other sources

E_b(#1) [3.29]	1.09	1.42	1.70
E_b(#2) [3.29]	1.93	2.87	3.38
E_b(#3) [3.29]	-0.12	0.13	0.08
E_b(#4) [3.29]	0.54	1.17	1.26
E_b(#5) [3.29]	0.68	1.56	1.78
E_b(#6) [3.32]		1.40	1.60

Numbers #1 to #6 are results from various models:
#1 represents hydrogenic model potential with uncorrelated wave function;
#2 represents hydrogenic potential with restricted correlated wave function;
#3 represents Krumhansl-Schwartz potential with uncorrelated wave function;
#4 represents K-S potential with restricted correlated wave function;
#5 represents K-S potential with correlated wave function;
#6 represents Hulthen potential used by Berezin

importance of the correlation effect in positron binding.

iii) Lifetime and Angular Correlation

Both lifetime and angular correlation are calculated based on Eq.(3.71) and Eq.(3.79), respectively. Bases which give the best ground state energy are used to perform such calculations. Similar to the above energy calculation, the results are obtained for both correlated basis and uncorrelated basis. We also want to examine the contributions from core electrons to the lifetime. Eq.(3.71) contains several terms among which the first involves pure Gaussian functions only and the remaining terms are related to core orbitals because of orthogonalization. If we keep the first term in the lifetime calculation, then the core effect on lifetime is ignored. More accurate way is to calculate the lifetime by its full expression. By comparing the values from both calculations, we could estimate the influence of the core electrons on the lifetime. Calculated lifetimes and available experimental values are shown in Table 3.4. As in Table 3.3, the values from Farazdel and Cade[3.29] are also given in this Table.

Usually, a few lifetime components with corresponding intensities are observed in experiment. The problem is to isolate the desired component from various annihilation mechanisms. The observed lifetime values in the Table are so-called longer-lived component which is proportional to the F-centre concentration and so is believed to be the lifetime of Ps self-annihilation. Our calculated lifetime values for NaCl and KCl are about twice as long as those observed. Comparing calculated lifetimes with the core effect to the ones without the core effect, we see that taking core orbitals into account does not improve the lifetime appreciably. But introducing the correlation in basis does improve

Table 3.4

Positron lifetimes for Fe^{+}-centres (nsec); τ(ucr) and τ(cr) represent lifetimes calculated with uncorrelated bases and correlated bases respectively, and τ^{*} and τ^{0} refer to the lifetimes calculated with and without counting the core effect. τ_{exp} is the observed lifetimes.

	NaF	NaCl	KCl
τ(ucr)	3.31	4.68	4.65
τ^{0}(cr)	1.90	2.55	2.59
τ^{*}(cr)	1.60	2.20	2.40
τ_{exp}		1.10 (3.10)	1.20 (3.50)
τ(#1)	21.7	18.3	17.4
τ(#2)	1.12	1.02	0.95
τ(#3)	147	153	211
τ(#4)	2.32	2.07	1.89
τ(#5)	0.83	0.61	0.56

Numbers #1 to #5 are results from various models of Farazdel & Cade(3.29):

#1 represents hydrogenic model potential with uncorrelated wave function;

#2 represents hydrogenic potential with restricted correlated wave function;

#3 represents Krumhansl-Schwartz potential with uncorrelated wave function;

#4 represents K-S potential with restricted correlated wave function;

#5 represents K-S potential with correlated wave function;

lifetime significantly.

Angular correlation curves(ACCs) of Ps annihilation are one of the most frequently reported data. The calculated ACCs for NaF, NaCl and KCl are drawn in Fig. 3.8, Fig.3.9 and Fig.3.10, respectively. The experimental measurements for NaCl and KCl[3.29] are also shown in the figures. In order to make a comparison, Farazdel's results for NaCl are also given in Fig.3.11. In Fig.3.9 and 3.10, two calculated curves are displayed in each figure. One is calculated with an uncorrelated wave function, and the other with a correlated wave function. Generally, both agree with experiment. But the correlated wave function improves the calculation very appreciably. Those figures clearly show that the ACCs calculated by a correlated wave function fit the experimental results very well.

iv) Discussion

Positron binding energies to F-centres were estimated before by Berezin[3.32], Farazdel and Cade[3.29]. Berezin used the Hulthen potential approximation to calculate the binding energies for a few alkali halides and those

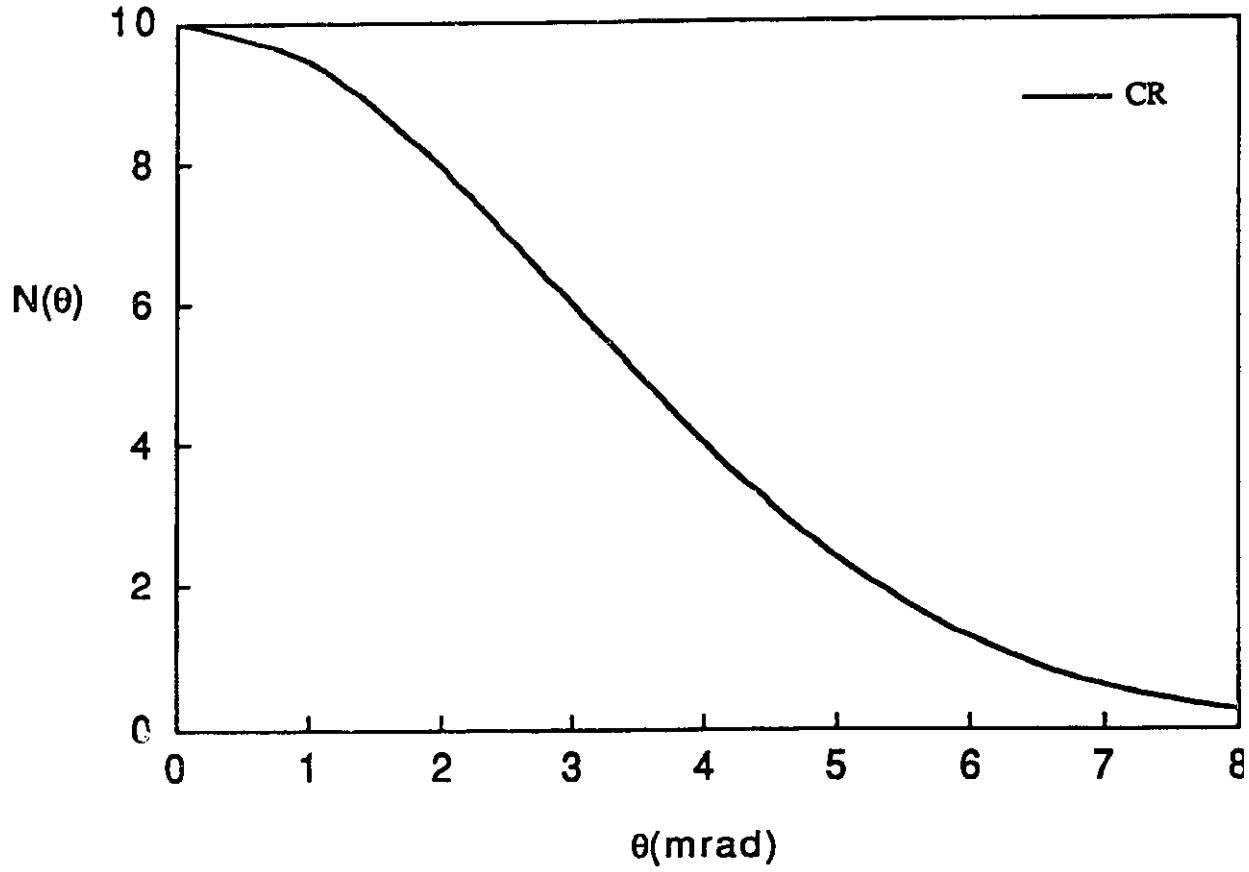

Fig.3.8 Angular distribution for two-photon annihilation N(θ) from F-centres in NaF. Curve shows the theoretical calculation with correlated wave functions. Normalization of N(θ) is made such that N(θ)=10 at θ=0.

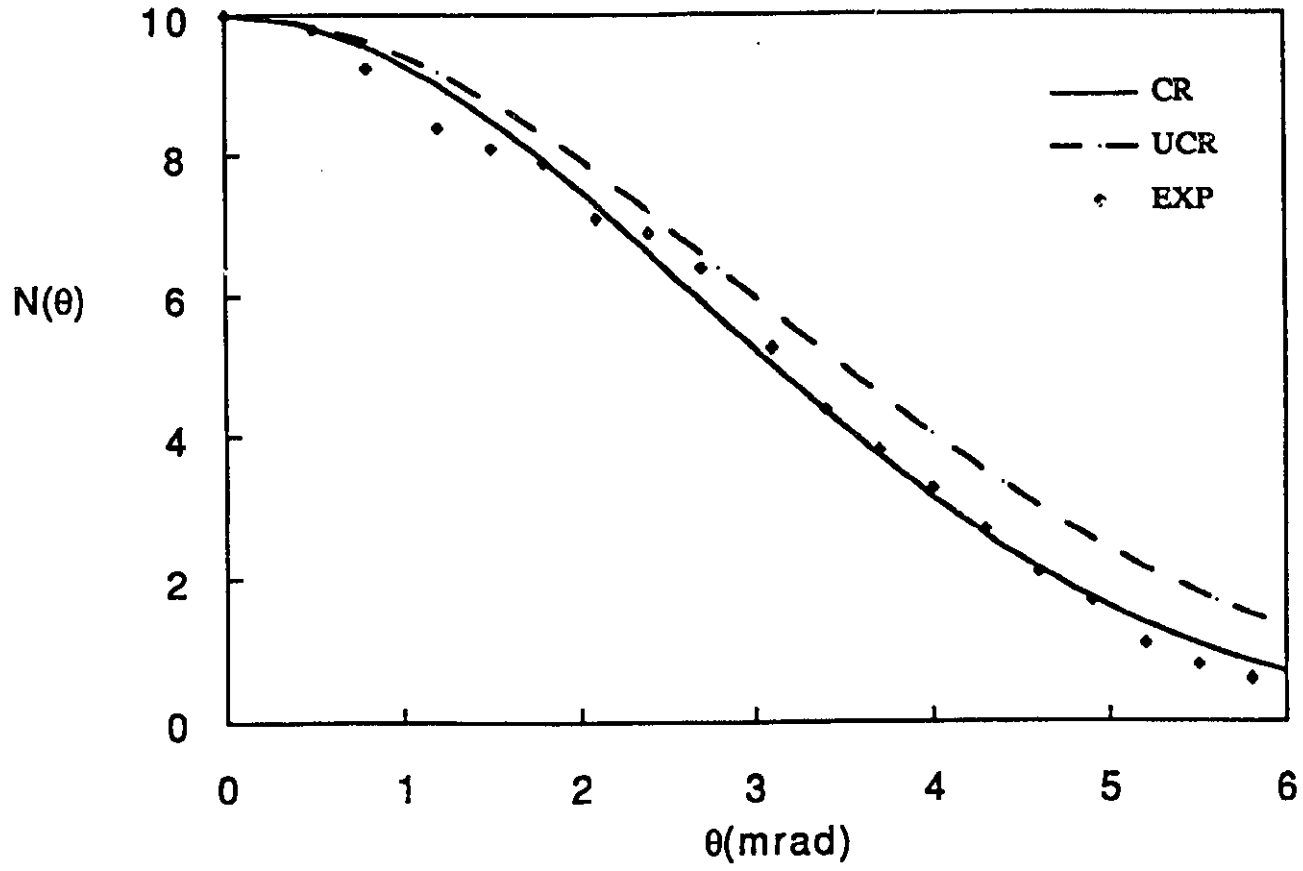

Fig.3.9 Angular distribution for two-photon annihilation N(θ) from F-centres in NaCl. Curves(solid line and dashed line) represent the theoretical calculations with or without correlated wave functions, respectively. Squares are experimental data from Herlach & Oggenfuss[3.29]. Normalization of N(θ) is made such that N(θ)=10 at θ=0.

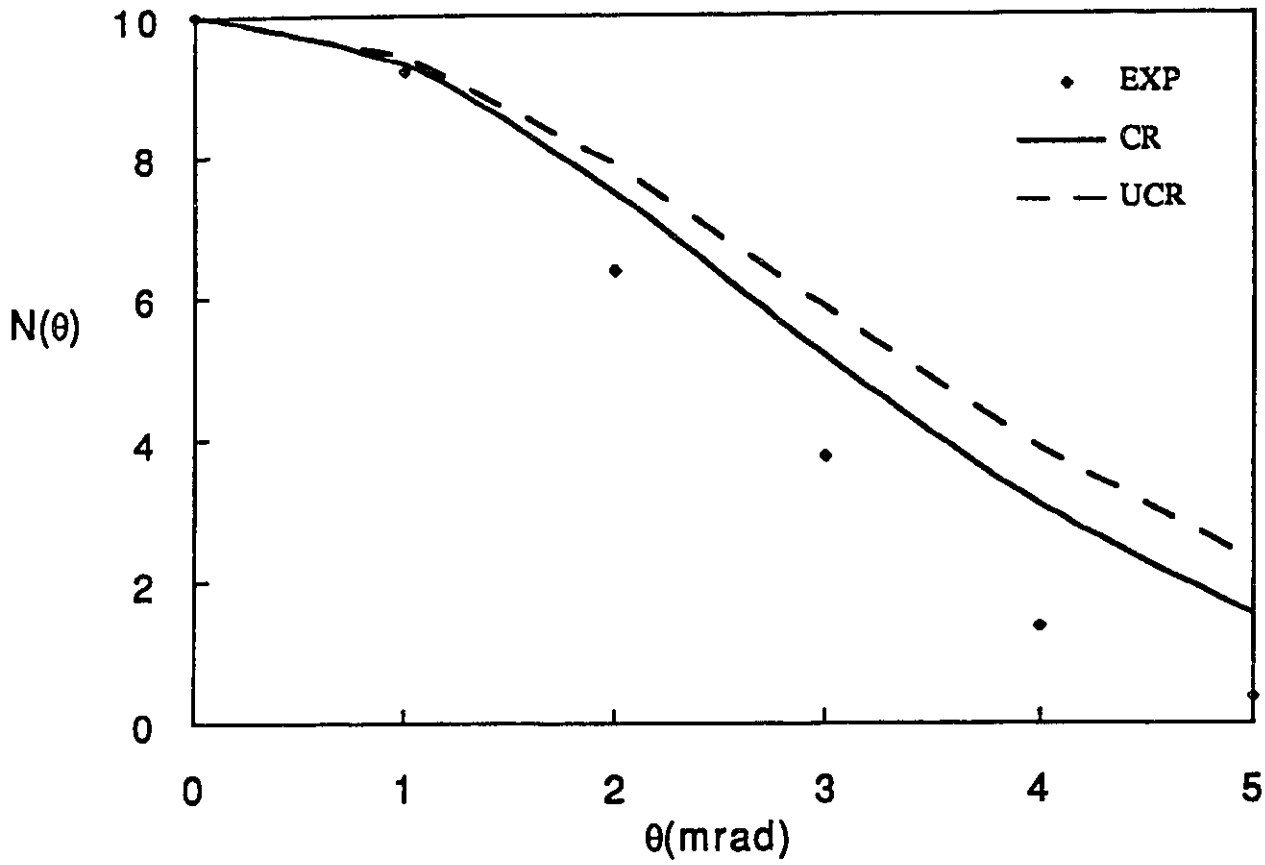

Fig.3.10 Angular distribution for two-photon annihilation N(θ) from F-centres in KCl. Curves(solid line and dashed line) represent the theoretical calculations with or without correlated wave functions, respectively. Squares are experimental data from Herlach & Oggenfuss[3.29]. Normalization of N(θ) is made such that N(θ)=10 at θ=0.

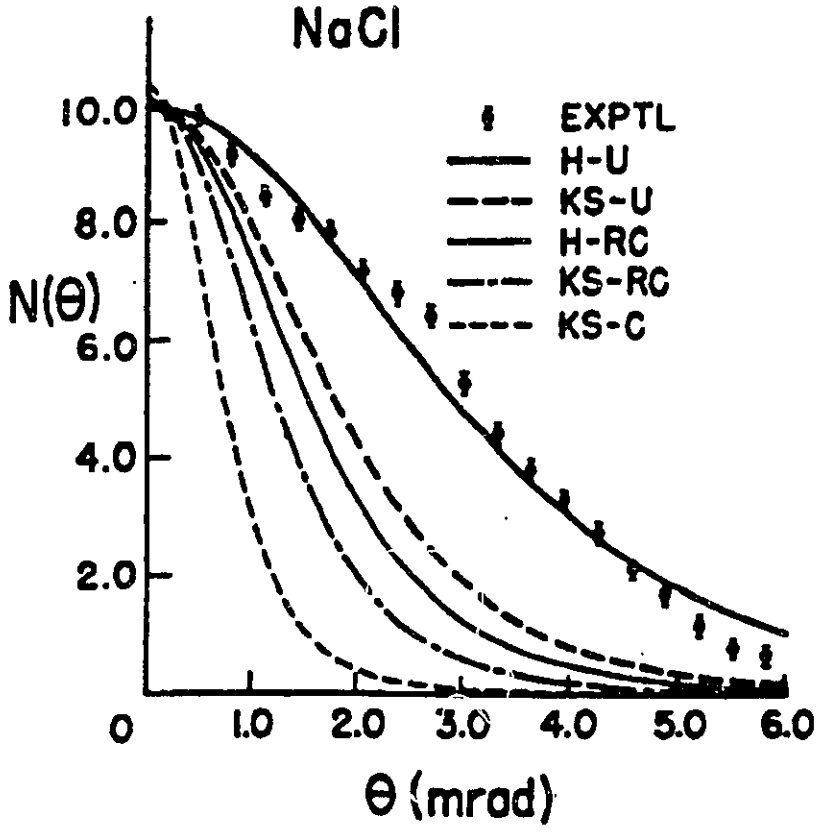

Fig.3.11 Angular distribution for two-photon annihilation N(θ) from F-centres in NaCl. The figure is a scanned copy of Fig.4 from the paper of Farazdel & Cade[3.29]. Theory for various approximate wave functions corresponding to our notation #5, #4, #2, #3, #1, respectively(from bottom to top) and experiment.

values he found were 1.4 eV for NaCl, 1.6 eV for KCl, and 1.7 eV for KBr. The correlation was totally ignored in his calculation. Two model potentials (hydrogenic potential and K-S potential) were used by Farazdel & Cade, and 3 types of trial wave functions (uncorrelated, restricted correlated and correlated) were applied to calculate the binding energies. As we can see from Table 3.3, their binding energies vary considerably depending on the potential and trial wave function used. For both potentials the correlated wave function gave binding energies 1-2 eV larger than the uncorrelated wave function. The model potentials made a large difference. In terms of the uncorrelated wave function, the hydrogenic potential led to quite deep binding energies varying from 1-2 eV for different crystals, while the cavity model potential did not show any sign of binding shown as #3 in Table 3.3.

The binding energies calculated by our model agree with both Farazdel & Cade, and Berezin in the sense that their values are in about the same range. As a matter of fact, our values are closer to what Farazdel & Cade got by using a K-S potential with a correlated wave function (#4 and #5 in Table 3.3). Berezin's treatment is relatively crude due to the lack of a correlation effect. We would imagine that once the correlation is taken into account in his approach, the binding energies could increase and may be comparable with Farazdel's results using the hydrogenic potential. Our wave function does not count correlation fully, thus it is possible that the binding energies are underestimated to some extent. So far there have been no experimental results reported for the binding energy. We have no basis to argue the superiority of different approaches even though the system is better treated in our approach. Our work is the only one involving a detailed lattice environment and both a correlation effect and lattice

relaxation effects can be estimated. In terms of an electron description, our Gaussian wave function is not as good as a Slater wave function, but the linear combinations of many Gaussians make up this shortcoming somehow. The self-consistent treatment of defect and lattice provides information about ion movement around the defect simultaneously. Both the Fe+-centre and the F-centre are treated by exactly the same approach or program, and, certainly, it makes comparison much more meaningful.

As we have done in the F′-centre calculation, a Gaussian basis can be arranged to simulate a p-like state, provided that the first excited state is 1s2p, i.e., the electron is in a 1s ground state and the positron is in the excited p-like state. A specially designed basis based on this configuration can be used to calculate the excited state energy. During the process of energy minimization, ions on the direction of the p state lobe move more. In consequence, the lattice symmetry changes from O_h down to D_{4h} and lattice relaxation and polarization are quite different from those of the ground state. The calculation is tried only for NaCl and the energy obtained is 7.1 eV. The F-centre ground state energy under the same lattice distortion comes to be 5.12 eV(We are simulating the corresponding ionized state). Obviously the binding is impossible, or, in other word, we can say the ground state is the only possible binding state for Fe+-centres.

We now discuss the angular momentum correlation curve. First we examine the calculations made by Farazdel & Cade in Fig.3.11. The figure shows that the best fit comes from an uncorrelated wave function with a hydrogen potential. Even though those restricted correlated and correlated wave functions give a better energy and lifetime, the deviations for ACCs are quite large. The

improvement of energy and ACCs goes in opposite directions. The inconsistency is obviously associated with the method. Our calculation shows that a correlated wave function yields better results not only for ACCs, but also for energy and lifetime. The approach itself shows consistency in dealing with all perspectives of the problem.

It is believed that the centre of mass motion of the Ps pair has an energy distribution which follows a Boltzmann distribution, whereas the distribution of momentum is proportional to $e^{-P^2/2MkT}$. On the other hand, as was shown in 3.2.1, since our basis contains a centre of mass of Ps with a Gaussian wavefunction $e^{-\alpha R^2}$, its Fourier transform results in a similar form, with α being a function of M and T. The use of a Gaussian basis provides an unexpected advantage in representing the distribution of momentum **P**. This was not realized until we analyzed the ACCs for Fe+-centres. As far as we are aware, the best ACCs for the Fe+-centre are obtained from our method.

For lifetime calculations, the results we calculated are not as good as those discussed above. The reason why our calculated lifetimes are somewhat longer than experiment may come from the shortcoming of our approach itself. From the theory part of the lifetime calculation, we have seen that it is the cusp in the relative motion wave function which plays a key role in determining the lifetime. Unfortunately, unlike the Slater wave function, our floating Gaussian basis does not posses such a cusp at $r_+=r_-$. Using many basis functions probably improves the description, but the cusp can never be created this way.

3.3.2 F_{anti}-centres

i) Calculation of the Defect Structure

The defect system is formed when a positron is trapped by a cation vacancy. During the trapping process, our calculation shows that the six n-n anions are moving outward. The defect symmetry remains the same. To compare this anti-F-centre system with its twin F-centre system, calculations for both systems are performed parallely. One optimized on-centre basis is used to relax the lattice for the ground state, and then a few more on-centre bases are added to further improve the energy. There is no need to include an off-centre basis for such a system as was the case in the Fe^+-centre. First shell ion displacements and energy drops are listed in Table 3.5. Ions up to the second n-n are allowed to relax. Generally, the ion displacement is very small.

It is seen from the above Table that lattice relaxation is quite small and about the same for both F-centres and F_{anti}-centres. So far both experiment and theory have agreed that lattice distortion is small in the F-centre ground state. Consequently, the energy is improved very little after lattice relaxation.

ii) Transition Energy and Binding Energy

With the lattice distortion gained above, more on-centre bases are placed at the vacancy to further improve the energy. Usually two or three bases are sufficient to bring the ground state energy to the minimum. Also a p-like basis is constructed to simulate the first excited 2p state and therefore the corresponding energy can be evaluated by using this type of basis. The optical absorption energy is simply the energy difference between the two states. Both calculated ground state energy and excited state energy are shown in Table 3.6. For the F-centre, the experimentally observed absorption energies are available and are also given in

Table 3.5

Lattice relaxations and various energy drops for F and F_{anti} centres. D_{nn} represents the coordinates of relaxed ions (a.u.). E_{coul}, E_{rep}, E_{el}, E_{pol} and E_t represent lattice coulomb energy, lattice repulsive energy, electronic energy, polarization energy and total energy, respectively. ΔE represents the energy difference between the perfect lattice and the relaxed lattice. All energies in the table are in the unit of eV.

	NaF	NaCl	KCl
<u>Perfect Lattice</u>			
α (F)	0.10	0.06	0.06
E_{coul} (F)	10.86	8.92	7.99
E_{rep} (F)	0.00	0.00	0.00
E_{el} (F)	-4.42	-4.82	-4.12
E_{pol} (F)	-0.001	-0.001	-0.001
E_t (F)	6.64	4.11	3.88
α (F_{anti})	0.11	0.09	0.07
E_{coul} (F_{anti})	10.86	8.92	7.99
E_{rep} (F_{anti})	0.00	0.00	0.00
E_{el} (F_{anti})	-3.96	-3.03	-4.12
E_{pol} (F_{anti})	-0.0003	-0.0004	-0.0009
E_t (F_{anti})	6.90	5.89	4.40

Relaxed Lattice

D_{nn} (F)	0.00	0.20	0.10 (1,0,0)
E_{coul} (F)	11.48	10.17	8.55
E_{rep} (F)	-0.03	-0.31	-0.08
E_{el} (F)	-4.90	-5.83	-4.60
E_{pol} (F)	-0.014	-0.04	-0.01
E_t (F)	6.61	4.06	3.85
ΔE (F)	0.03	0.05	0.03

D_{nn} (F_{anti})	0.15	0.18	0.17 (1,0,0)
E_{coul} (F_{anti})	10.04	8.21	7.46
E_{rep} (F_{anti})	0.43	0.36	0.26
E_{el} (F_{anti})	-3.73	-2.85	-3.38
E_{pol} (F_{anti})	-0.01	-0.01	-0.01
E_t (F_{anti})	6.74	5.71	4.34
ΔE (F_{anti})	0.16	0.17	0.06

the Table.

In our model the defect electron or positron is described by a Gaussian basis. To find the binding energy, we need to know the energy associated with the state where the defect particle is ionized to the free state. By assigning a very diffuse Gaussian to the defect particle, it is hoped to simulate the free state, since the diffuse basis extends over a large volume of the crystal. We use this type of basis to estimate the binding energy for both F-centre and F_{anti}-centre.

However, there has been no good model to describe the ionized state so far for such a system. This is a very difficult problem. With the present approach, we hope to obtain some rough idea only. Besides the orthogonalization problem, as far as our model is concerned, there are two problems associated with this treatment. The first is related to the cluster size. Generally, a more diffuse basis would give a better description to the free state, but a too diffuse basis would lead the Gaussian distribution to exceed far beyond the limited cluster boundary. We are facing the restriction of our model cluster.

To solve this problem, we have to find to what extent the diffuse Gaussian basis gives an acceptable description. It seems reasonable to assume that a diffuse Gaussian with 80% of its charge remaining inside the cluster boundary is still an acceptable basis to simulate the free state. Thus the Gaussian decay parameter is determined based on this criterion. It is found that the value of α=0.002 a.u. is compatible with 600 ions in the cluster.

The second problem comes from the interpolation of outer s and p shells. As indicated earlier, those parameters are fitted in the range of a decay factor changing from 0.02-0.12. Outside this range the interpolated formulae do not

break down right away, but they deteriorate gradually, especially for smaller α. The point here is we do not have satisfactory solutions for these problems. But we expect our calculation can serve as a rough estimation. In principle, the extended-ion method can calculate the conduction band(at k=0 for example) energy[3.51]. Here we actually use the conduction band to approximate the ionized state. The calculated values are listed in Table 3.6. Note that both the ground state and the excited state are calculated under the same distortion field, while the Coulomb energy and repulsive energy have the same values which have been given in Table 3.5. We do not need to present them here.

iii) Discussion

The F-centre is a classical defect system of which various features are quite well known. We are not directly interested in this system, but it helps to understand the properties of the F_{anti}-centre due to the similarity of the two systems.

In our calculation of the F-centre, the lattice distortions are quite small. Six n-n cations move outward slightly due to a weak polarization effect. The exception here is NaF which gives no n-n ion displacement. Actually among the three crystals, NaF has a relatively small vacancy region. Our calculation indicates that its optimized Gaussian decay parameter turns out to be 0.10 instead of 0.06 (a.u.) for the other two crystals. This implies the defect charge distribution is more compact and thus the induced electrical potential largely cancels the Madelung potential at the vacancy. Whereas the smaller displacements of n-n cations may be possible.

The calculated F band absorption energies are about 0.8 eV higher than

Table 3.6

Transition energies and binding energies for F and F_{anti} centres (eV). E_g, E_{ex}, E_{iz} and E_{tot} represent ground state energy, first excited state energy, ionized state energy, and total energy, respectively. The extra sub-indexes have the usual meanings defined in those previous tables. (α;R) are basis parameters characterizing the p-like state. E_{1s-2p} and E_{exp} represent the calculated transition energy and observed transition energy, respectively. E_b and $E_{b,exp}$ represent the calculated and observed binding energies, respectively. Plus presents the linear combinations of many basis functions.

	NaF	NaCl	KCl
F-centre			
$(\alpha_1;R_1)$	(0.09;0.4354)	(0.04;0.533)	(0.05;0.119)
$+(\alpha_2;R_2)$	(0.10;0.305)	(0.05;0.160)	(0.06;0.298)
$+(\alpha_3;R_3)$	(0.11;0.1306)	(0.06;0.2665)	(0.07;0.714)
$E_{g,el}$	-4.90	-5.78	-4.60
$E_{g,pol}$	-0.01	-0.04	-0.01
$E_{g.tot}$	-4.91	-5.82	-4.61
$E_{ex,el}$	-0.21	-2.46	-1.85
$E_{ex,pol}$	-0.09	-0.14	-0.13
$E_{ex.tot}$	-0.30	-2.60	-1.98
E_{1s-2p}	4.61	3.22	2.63
E_{exp}[3.50]	3.65	2.67	2.20

$E_{iz,el}$	3.45	0.84	1.58
$E_{iz,pol}$	-1.12	-1.77	-1.55
$E_{iz.tot}$	2.33	-0.93	0.03
E_b	7.22	4.80	4.54
$E_{b,exp}$ [3.51]	***	***	3.60

E_{anti}-centre

$(\alpha_1;R_1)$	(0.10;0.305)	(0.10;0.053)	(0.07;0.357)
$+(\alpha_2;R_2)$	(0.11;0.4354)	(0.11;0.533)	(0.08;0.595)
$+(\alpha_3;R_3)$	(0.12;0.087)	(0.12;0.267)	(0.09;0.179)
$E_{g,el}$	-3.73	-2.85	-3.38
$E_{g,pol}$	-0.01	-0.01	-0.01
$E_{g.tot}$	-3.74	-2.86	-3.39
$E_{ex,el}$	-0.20	-0.20	-1.23
$E_{ex,pol}$	-0.17	-0.10	-0.07
$E_{ex.tot}$	-0.37	-0.30	-1.30
E_{1s-2p}	3.36	2.56	2.09
$E_{iz,el}$	4.46	5.34	5.11
$E_{iz,pol}$	-1.12	-1.93	-1.56
$E_{iz.tot}$	3.34	3.41	3.55
E_b	6.70	6.25	6.93

those of experiment. This is not only a problem for our model. In fact, this is a generally observed trend in most one-electron calculations. The reason is that the F band energy is sensitive to the orthogonalization of the ion cores to each other. Another inadequate treatment in our model may come from a simplified calculation of polarization energy for both ground and excited states. It is known that the two states have quite different polarization. The method we adopt to calculate polarization is not sensitive enough to the states and therefore the polarization of the excited state might be underestimated.

It is understood that ground state lattice relaxation is small for both F-centre and F_{anti}-centre. This is a well-established result for F-centres. This specific feature is clearly caused by two effects. Polarization, on the one hand, is rather weak due to the neutrally charged defect and larger distance between the first shell ions and the vacancy, on the other hand, is very large.

The binding energy which corresponds to the transition energy from the ground state to the conduction band is calculated. Experiments on KCl show that there are a few sub-bands corresponding to the ionized states and the lowest absorption band is 3.60 eV. Our calculation gives 4.54 eV which seems in the right range.

Unfortunately, there has as yet been no experimental observation for the F_{anti}-centre. Our work is the first one to treat this defect systematically. The system behaves very much like an F-centre. Our work shows that six n-n anions are going outward slightly and their displacements are about the same. The calculated absorption energies are smaller than those of F-centres. The degree of accuracy in the absorption energy of the F-centre depends upon the proper treatment of orthogonalization. The difficulty makes all evaluations not so

satisfactory. For positron, there is no orthogonalization requirement, so we expect the calculated transition energies shall be more precise than those of the F-centres. Actually, we can see they fit the observed F-centre transition energies quite well.

It is not surprising to have F_{anti}-centre binding energies being in the same range as those of the F-centre. The calculated binding energies are around 6 eV which agrees generally with the estimations made by Farazdel and Cade[3.29].

3.3.3 Positronium Self-Trapped at an Interstice

i) Calculation Of Defect Structure

The method has been described in 3.1.1. As usual, the lattice relaxation is present in this part. For Ps localized at an interstice, two approaches are applied to this system as described in the theoretical part. We first present lattice distortions obtained from the first approach. The Ps is assumed well localized in the first approach. As indicated by Kasai & Fujiwara[3.31], the largest space in fcc alkali halide crystals which would be favourable for the stay of Ps is found around the centre of every 1/8 cubic cell, and Ps could be self-trapped at an interstice if the volume were expanded by moving ions in soft (1,1,1) directions. We can test this idea by placing an on-centre basis right at an interstice, then relax the lattice through energy minimization. It is found that the relaxed lattice still keeps tetrahedral symmetry. Eight n-n ion displacements and corresponding energy changes are shown in Table 3.7. Ion displacements in the Table show that four cations obviously move more than four anions. Their displacements are symmetric. We only give the cation at (1,1,1) and the anion as (0,0,0) as an

Table 3.7

Lattice relaxation and corresponding energy change of positronium self-trapped at an interstice. D_m represents the coordinate of the displaced ion(a.u.). (α;R) are the optimum basis parameters(a.u.). $E_{perfect}$ and E_{relax} represent the total energy of perfect lattice and relaxed lattice, respectively. The lattice parameter is that at room temperature.

	NaF	NaCl	KCl
(α; R)	(0.12;0)	(0.12;0)	(0.12;0)
D_{nn+}	0.58	0.47	0.33 (1,1,1)
D_{nn-}	0.44	0.24	0.23 (0,0,0)
$E_{perfect}$	9.45	2.52	1.01
E_{relax}	3.26	0.92	0.27

example. In this sense, such directions can be referred to as soft directions.

In the second approach, the extended C.M. envelope function is multiplied by the wave function used in the first approach and is summed over unit cells. This means the Ps is very much less localized. The envelope function is represented by a Gaussian function which is centred at the central unit cell and its decay parameter is determined via energy optimization. In our calculation, it comes to be 0.01 a.u..

Extension of the C.M. motion makes the Ps wave function spread in space. Consequently, the lattice relaxation is very small. Our calculation shows that the displacements of eight n-n ions are about 0.1-0.15 a.u. for the three crystals. Thus, the energy changes caused by lattice relaxation are correspondingly small.

ii) Ground State Energy

In the first approach, once the lattice distortion is determined, we could apply many bases to search for the lowest possible ground state energy. In Table 3.8, we only presented the energy calculated by using a single basis. If a large number of bases were employed, the energy could be lowered by about one eV. The reason why we are not interested in this energy will be explained in the following paragraph.

In the second approach, we could not improve the energy by employing many basis due to the huge CPU time required. From the relevant theory part of section 3.2.1 iii), we see multiple-summations are involved in the calculation and result in expensive computing. In this case, we are restricted to use a single

basis. In Table 3.8, we present those energies calculated by both methods. In order to make a fair comparison between the two, we used the same number of bases, i.e. a single basis to evaluate the ground state energy for both of them.

Kasai & Fujiwara[3.21] proposed the so called crystallographic effect based on their observations on Bloch like state Ps. To be able to examine this effect from our model, we need to rearrange our basis in a certain way. The details about this effect will be explained in the next section. We mention it here simply because we are comparing the extended localized Ps states with Bloch like Ps states. So the same basis arrangement has to be made for both. In every unit cell, there are two interstitial sites: (1/2, 1/2, 1/2), (1/2, 1/2, -1/2), as shown in Fig.3.13. One basis arrangement is to place a basis at only one of the interstitial sites and is defined as a single interstitial basis (S.B). The other is to place bases at the both interstitial sites of the unit cell and is referred to as a pair interstitial basis (P.B). The calculated ground state energies from both types of basis are listed in Table 3.8. The same quality of basis was used to make a fair comparison. It is seen that the energy levels obtained from the first approach are lower than those of the second approach. Such an energy decrease is mainly attributed to the lattice relaxation involved in the first approach, because the lattice relaxation experienced by ions is not very precise in the first approach. On the other hand, the existence of a local minimum is also possible. Furthermore, the (P.B) improves energy compared with the (S.B). Some more discussions on this matter will be given later.

iii) Lifetime and Angular Correlation

Lifetime is a quantity which depends mainly on the relative motion. Theory shows that the extension of C.M. motion does not affect the lifetime calculation. In other word, the two approaches would make no difference in calculating the

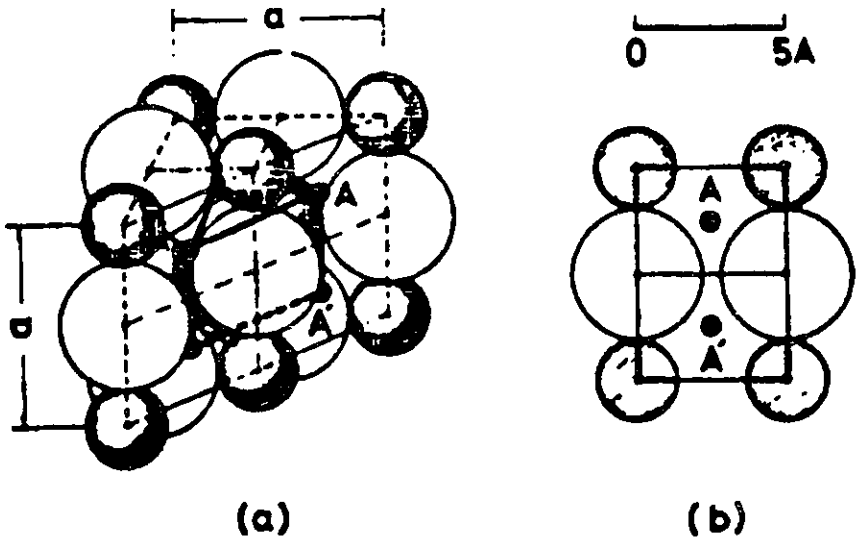

Fig.3.13. Two equivalent lattice sites A and A´ for Ps localization. a is the cation-cation distance. (a) is an illustration of the packing of ions and (b) the arrangement of ions on a (1,1,0) plane.

lifetime. The optimized bases are used to evaluate the lifetimes for localized Ps states. The calculated values of the three crystals are given in Table 3.8. Depending on weather the contributions from core orbitals are included or not, τ and τ_0 are used to represent the lifetime for both treatments respectively. Hyodo & Stewart[3.52] proposed a model to deduce lifetimes of KCl and NaF for both localized and delocalized Ps based on their observations. Though there are some arguments on this model[3.43], we present their values for localized Ps as τ_{exp} in Table 3.8. Compared to those values, our calculated lifetimes are quite large. More comments will be given in the following section of discussion.

ACCs are calculated by using two approaches. The ACCs of KCl calculated by the first approach are shown in Fig.3.14. The observed ACCs of the same

Table 3.8

Calculated ground state energies (eV) at both room temperature and 0K, and lifetime τ (nsec) for localized Ps. $E_{loc}^{\phi 1}$ and $E_{loc}^{\phi 2}$ are the localized Ps energies evaluated by the first and the second approaches, respectively. α is the optimum basis parameter(a.u.). β is the decay parameter of envelope Gaussian. τ and τ_0 represent the lifetimes with or without counting the core effect, while τ_{exp} stands for the experimental data. S.B and P.B are abbreviations of single basis and pair basis.

	NaF	NaCl	KCl
α	0.12	0.12	0.12
$E_{loc}^{\phi 1}$ $(S.B)_{R.T}$	3.26	0.92	0.27
α	0.13	0.14	0.13
β	0.01	0.01	0.01
$E_{loc}^{\phi 2}$ $(S.B)_{R.T}$	8.77	2.47	0.99
$E_{loc}^{\phi 2}$ $(P.B)_{R.T}$	7.85	2.32	0.84
$E_{loc}^{\phi 2}$ $(S.B)_{0.T}$	9.10	2.67	1.13
$E_{loc}^{\phi 2}$ $(P.B)_{0.T}$	8.20	2.59	1.11
τ_0	1.40	1.81	2.23
τ	1.20	1.44	1.78
τ_{exp}	0.10 [3.52]		0.11 [3.52]

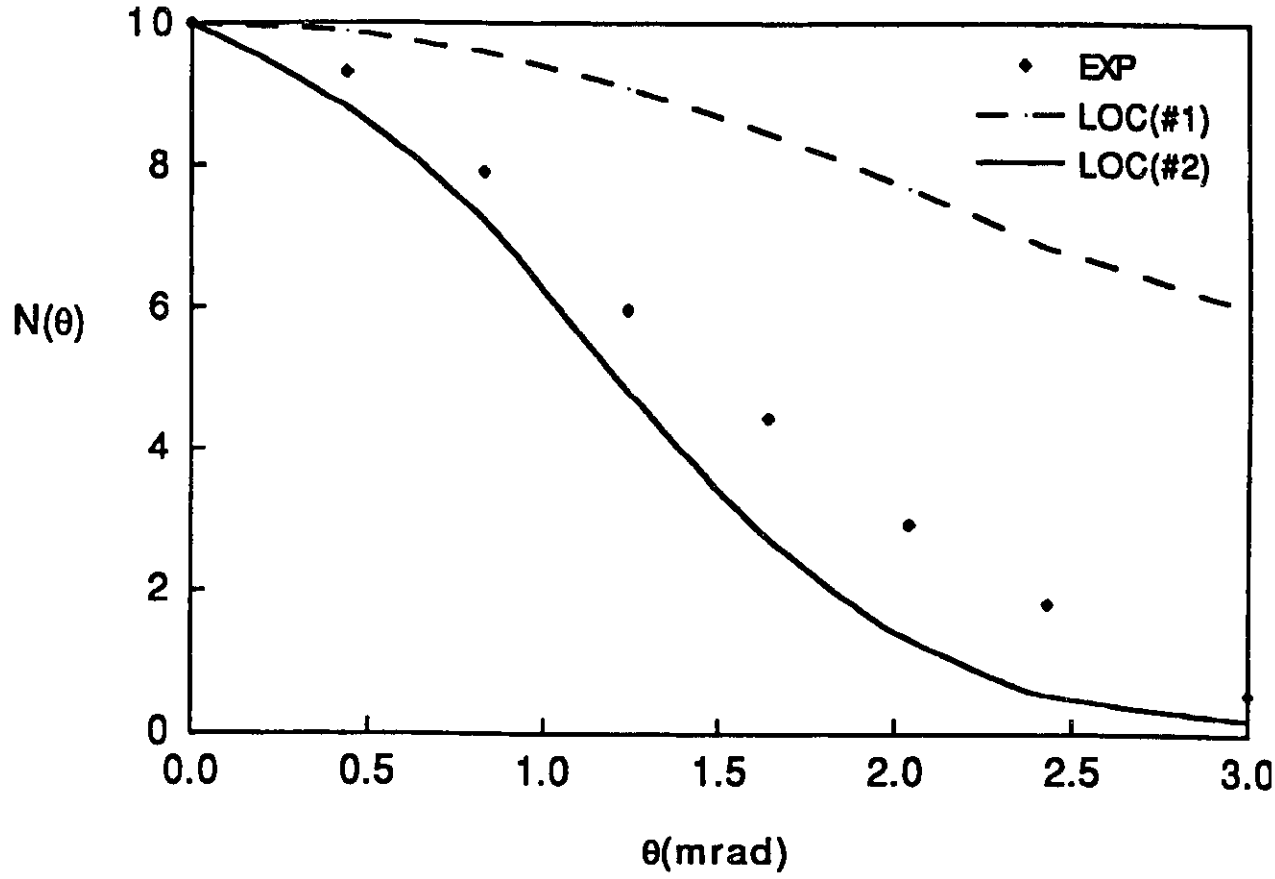

Fig.3.14. Angular correlation curves of localized Ps at an interstice in KCl. Squares are experimental data from Kasai & Hyodo[3.23]. The dashed line is based on the calculation by the first approach and the continuous line is calculated by the second approach. Curves are normalized such that $N(\theta)=10$ at $\theta=0$.

material by Kasai & Hyodo[3.23] are shown in the same Figure. Note that the experimentally observed ACCs are the mixture of two main contributions. One is from the Ps self-annihilation characterizing the temperature sensitive sharp central peak. The other is a temperature insensitive broad component which is believed to be the result of pick-off annihilation[3.23]. We are only interested in the former, so the observed ACCs in Fig.3.14 represent the Ps momentum distribution in KCl obtained by subtracting the broad component.

In the first approach, the Ps atom is assumed well-localized, and the corresponding ACC in Fig.3.14 is rather broad compared to experiment (see dashed line). As a matter of fact, this was one motivation for us to seek the second approach. In this approach, the extended C.M. motion leads to a sharp central peak. The calculated ACCs are also displayed in Fig.3.14. This curve is pretty close to the experimental one (see solid line).

iv) Discussion

As Ps is trapped at an interstice, the lattice experiences expansion. Eight ions around the interstice are moving outward until a new equilibrium configuration is reached. This new configuration keeps T_d symmetry as well. Our calculation indicates that four cations move more than four anions. We attribute this to the polarizability difference for different ions. Generally, the cations move more and therefore are called soft directions proposed by Kasai et al.

From Table 3.7, we can see that F^- in NaF moves more than Cl^- in NaCl

and KCl. This means the lattice expansion also depends on the size of the interstice. To give a clear picture of this effect, now we define a length L which is the distance between a cation and its second n-n anion minus the radii of the two ions to measure the size of the interstice. Actually, we can view L as a diameter of the sphere inscribed in the interstice. As usual we use 'a' to represent the n-n distance; then L can be expressed as

$$L = \sqrt{3}\, a - r^{+} - r^{-}$$

Here r^{+} and r^{-} are radii of cation and anion respectively, and their values are listed: $r^{+}(K^{+})$ = 1.33 A, $r^{+}(Na^{+})$ = 0.98 A, $r^{-}(F^{-})$ = 1.33 A, $r^{-}(Cl^{-})$ = 1.81 A. Then we have:

	NaF	NaCl	KCl
L (A)	1.703	2.094	2.31

After lattice relaxation as a result of the Ps trapping, we estimated the corresponding length L' in order to have some quantitative idea about the volume change at trapping site. Because the eight n-n ions of interstice move outward in the process of Ps trapping, thus the lattice relaxation leads to L':

$$L' = L + \sqrt{3}\,(D_{nn}^{-} + D_{nn}^{+})$$

where relaxed ion coordinates D_{nn} are given in Table 3.7 and the values are found to be:

	NaF	NaCl	KCl
L' (A)	2.638	2.745	2.818

L' appears to be a constant for different crystals. This may imply that Ps localization needs a certain volume. If we define a sphere inscribed in a relaxed interstice, such a sphere would have a radius about 1.37 A regardless of materials. For those crystals having a smaller L, the ions have to displace more to

provide enough space for localization, or, in other words, the crystals having larger L would experience smaller lattice expansion around the trapping site.

There is a similar L which was chosen as a quantity to measure the spatial extension of the C.M. of the self-trapped Ps, and was estimated by several authors before. The wave function of localized Ps extends over a region contained in a sphere of radius L, and thus the Fourier transform of the wave function will extend in the momentum space up to a momentum of the order of $h/2\pi L$ in accordance with the uncertainty principle. Assuming that the Ps pair is represented by a Gaussian wave packet, its Fourier transform and angular momentum distribution can be derived by simply following (3.77) and (3.80). Through fitting the full width at half maximum(FWHM) of the momentum distribution $W_{1/2}$ with observed data, the L can be estimated by a relation:

$$L\,(A) = 10.7*10^{-3}mc/W_{1/2}\,,$$

where m is the mass of the electron and c is the speed of light.

Hyodo, Kasai and Fujiwara[3.24,3.22,3.23] measured angular correlation curves of NaF, KCl, and some other alkali halides as well, successively. Based on their experimental data and the above equation, they drew a conclusion from their estimation of L that the localization length is of the order of the nearest anion-cation distance. For NaF and KCl, they got the values 3.2A and 3.5A, respectively. Comparing with these values, we have a radius, 1.37A from the first approach, which is rather small, meaning that the localization may be overdone. In the second approach, with a decay factor 0.01 a.u., the extension of C.M. is derived following the same way and the value turns out to be 3.7A which fits well with above the estimation.

If we look at the ground state energies calculated from the two approaches

in Table 3.8, energies from the first approach are still lower than those from the second approach. This is mainly due to the large lattice distortion. From the experience in dealing with those proceeding systems, we know that the lattice relaxation can always lower the energy by about one eV. This is the case of NaCl and KCl. NaF behaves rather strangely. The energy drop is quite big and sensitive to the basis parameter, which we have not understood well yet.

The inaccurate lattice distortion of localized Ps puts a question mark on our earlier results. We reexamined the procedure carefully and realized that they are not seriously affected by this effect in terms of our required accuracy. As we have discussed in the theory part, the method we are using does not have separate control on relative motion and C.M. motion. The coupling between the two may lead to a serious impact on the accuracy of our description. In the case of the Fe^{+}-centre, the Ps atom is tightly bound to the defect and therefore both relative motion and C.M. motion are better localized at the defect, so this impact is distinctively reduced. This is why our treatment there yields very good results. The localization characteristic could be different for Ps localized at an interstice. Now there is no strongly attractive centre to bind Ps, and localization would happen in a relatively large space area centred at interstice. That coupling provides us no degree of freedom to minimize the energy in terms of C.M. motion. As a consequence, the localization is overdone. This effect also causes a large deviation in the angular correlation curve seen in Fig.3.14, and brings the energy improperly down to some extent, about which we are still not clear.

We extend the C.M. motion in the second approach and we actually create an extra degree of freedom to minimize the energy with respect to C.M. motion. The price we paid here is that we are unable to minimize the energy by using

many bases. Fortunately, our aim is not to get the real minimum of energy; instead, what we need is to find out the energy difference between the localized Ps state and delocalized Ps state. As long as the same quality of basis are applied to calculate the energy for both states, it makes sense to compare them.

The second approach possess the right spatial extension of C.M. motion, so it should provide more accurate energy. This is true for the angular correlation curve shown in Fig.3.14 where the curve calculated from the second approach fits the experiment reasonably well.

Generally, lifetime calculations are underestimated in our work. Two reasons may be responsible. One is associated with the Hartree-Fock scheme[3.53]. It is known that the electron-positron attraction corresponds to a local maximum in the exact (and unknown) wave function when the positron is close to an electron. This maximum is missed completely by the Hartree-Fock method because it is an independent-particle method, whereas the attraction is a two particle effect. But we shall mention that momentum distributions are still very well given by Hartree-Fock scheme. This is because both the measured and calculated momentum distributions are responsible for the centre of mass of the annihilating particles. The other is that the Gaussian wave function does not have cusp in the relative motion. The result may be slightly worse for the Ps self-trapped at interstice due to the similar reason mentioned before for the energy.

3.3.4 Ps in Bloch-Like States

i) Positronium Energy in a Bloch State

In 3.1.5. ii), we described the existence of two Ps states, delocalized and

localized, in alkali halide crystals. Experimental observations have demonstrated that Ps would mainly stay in the delocalized state at sufficiently low temperature (below liquid nitrogen temperature) and delocalized Ps is formed in the perfect lattice region. Our modified hybrid pseudo-potential scheme allows the energy calculation of the delocalized Ps state. We are interested in the lowest possible energy of such a state at the centre of the Brillouin zone (k=0). Then we place the floating Gaussian basis in the central unit cell. In the first place, one basis is used to calculate the energy. Basis positions are changed inside the unit cell and it is found that the best energy is achieved when the basis is centred at an interstitial site of the unit cell. The calculation is performed both for the lattice constants at room temperature(R.T) and 0K, and results are shown in Table 3.9.

We have mentioned the crystallographic effect previously in 3.1.7. Because this effect is closely related to a Bloch-like state Ps, we would rather give an explanation in detail here. It is known that self-annihilation of Ps from a Bloch state is identified by a series of narrow peaks appearing on the angular correlation curve of annihilation radiation, the positions of which correspond to the projections of the reciprocal lattice vectors onto the scanning directions. Kasai & Fujiwara[3.31] examined the experimentally observed intensities of those satellite peaks and reported a remarkable feature of the Ps-peak patterns. Anomalously weak intensities of the satellite peaks corresponding to the reciprocal lattice points ofodd indices as shown in Fig.3.15 are repeated. They are attributed to the crystallographic effect on the electrostatic lattice potential. Their result with weak intensities of the satellite peaks corresponding to the odd Miller indices imply that the Ps atoms are moving in the crystal, only vaguely distinguishing between the anion and cation, and so experience, in a rough sense

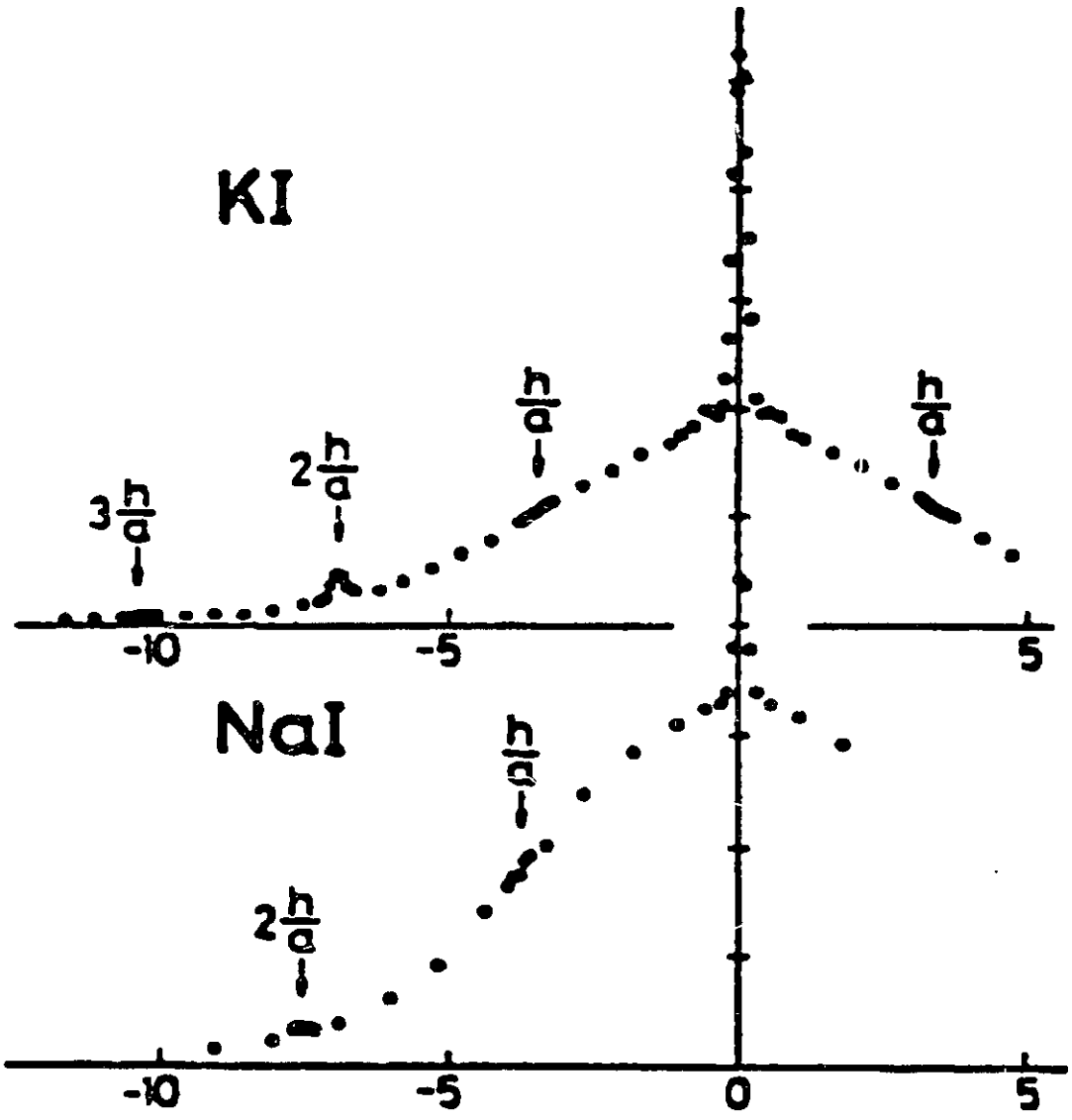

Fig.3.15. The angular correlation of gamma rays from positrons annihilating in single crystals at about 15K of KI and NaI oriented nearly along the (1,0,0) direction. Note the anomalously weak intensities of the first satellite peaks. Resolution:0.178 mc*10^{-3}. The horizontal axis represents momentum in mc*10^{-3}. The figure is from Kasai & Fujiwara[3.31].

Table 3.9

Calculated Bloch-like state Ps energies (eV) at both room temperature and 0K, and lifetime τ (nsec) as well. α is the optimum basis parameter(a.u.). τ_{exp} stands for the experimental data. S.B and P.B are abbreviations for single basis and pair basis.

	NaF	NaCl	KCl
α	0.13	0.14	0.13
$E_{0.T}$ (S.B)	8.95	2.61	1.09
$E_{0.T}$ (P.B)	8.03	2.47	1.04
$E_{R.T}$ (S.B)	8.77	2.43	0.97
$E_{R.T}$ (P.B)	7.64	2.30	0.91
τ	0.95	1.64	1.80
τ_{exp}	0.08 [3.52]		0.09 [3.52]

, the periodicity of a simple cubic lattice of lattice constant a/2 rather than an ordinary fcc lattice of lattice constant a.

There are two interstitial sites in one unit cell(see Fig.3.13). If we place a basis only at one of them, we are assuming that the Ps atoms could distinguish the anion and cation, and experience the periodicity of a fcc lattice. If we want to examine the crystallographic effect, we have to adopt the hypothesis proposed by Hyodo et al, and consider the other equivalent site of the unit cell. The pair basis(P.B), one for each site of a unit cell, has to be employed, then sum over all unit cells. Thanks to the floating Gaussian basis providing such a privilege, we can position our basis flexibly to perform such a calculation. Energy optimization shows that a basis centred right at interstitial sites gives the best energy. In principle, adding more bases at pair sites would improve the energy. Unfortunately, available computer resources restrict such an attempt. Therefore, one pair of on-centre bases is used and calculated energies are presented in Table 3.9. It is interesting to notice that the energies evaluated by the pair basis are slightly lower than those by the single basis (S.B).

ii) Lifetime and Angular Correlation

Lifetimes for three alkali halides are calculated with respect to the Bloch state of Ps. The values are shown in Table 3.9 and they are 0.95 ns, 1.64 ns, and 1.80 ns for NaF, NaCl, and KCl, respectively. There have been no direct observations on lifetimes of the Bloch state of Ps. Hyodo & Stewart[3.52] measured

positron lifetime spectra for NaF and KCl in a certain temperature range. Since many annihilation processes always simultaneously happen in crystals, observed lifetime spectra consist of contributions from various processes. They proposed a model to deduce lifetimes for various annihilations. There are some disagreements about the way they deduced lifetime in the literature[3.43] in which Linderoth et al repeated the similar experiment but were not able to describe their data by the model of Hyodo and Stewart. We could not judge how accurate their lifetime deduction is. As a reference, their deduced lifetimes for Bloch state para-Ps are presented as τ_{exp} in Table 3.9. The lifetimes evaluated from our model are more than ten times larger than their values. Our lifetime calculation is always not satisfactory due to those previously mentioned reasons associated with the weakness of the method in handling the relative motion. So we shall not expect a better result.

In terms of angular correlation, what can be observed from the Bloch state of Ps are the central peak and a few satellite peaks corresponding to the projections of reciprocal lattice vectors onto the scanning directions. For one-dimensional angular correlation, the projections of an arbitrary reciprocal lattice vector G on the z direction (assumed to be the observation direction), G_z determines the positions of those peaks. $G_z=0,\pm1,\pm2,\ldots\ldots$ $(2\pi/a)$ correspond to the central peak, first satellite peaks, second satellite peaks, and so on. Actually, they reflect the periodicity of the lattice. Those peaks are calculated and are listed in Table 3.10.

To examine the interesting crystallographic effect, we can demonstrate this effect through our calculation of angular correlation . We use (P.B), i.e., a pair basis sited at both interstitial sites of a unit cell, to calculate those peaks. Those

Table 3.10

Calculated angular correlation peaks for Bloch state Ps at room temperature. α is the optimum basis parameter(a.u.). S.B and P.B are abbreviations of single basis and pair basis. G_z represents the projections of reciprocal lattice vector on z direction.

	G_z(h/a)	0	1	2	3
NaF(α=0.13)					
	N (S.B)	1.15	0.43	0.09	0.002
	N (P.B)	2.02	$2.0*10^{-20}$	0.14	$2.1*10^{-21}$
NaCl(α=0.13)					
	N (S.B)	1.17	0.45	0.09	0.001
	N (P.B)	2.09	$3.6*10^{-16}$	0.17	$1.5*10^{-16}$
KCl(α=0.14)					
	N (S.B)	1.24	0.60	0.14	0.09
	N (P.B)	2.32	$1.2*10^{-14}$	0.27	$2.5*10^{-16}$
EXP(KI)		1.00		0.067[3.21]	

values are shown in Table 3.10.

It is seen from the above Table that when the P.B are used, the satellite peaks corresponding to odd G_z are dramatically reduced to almost zero. This implies that the Ps atoms seem not to see the difference between anion and cation, and move like they are in the simple cubic lattice with half period of the original fcc lattice. This is the first (we believe) theoretical proof of the observed crystallographic effect, and it is also the one of most exciting results achieved by our model.

In the Kasai & Fujiwara experiment[3.21], they also reported the ratio between the central peak and the first satellite peak of the reciprocal lattice vector of the simple cubic lattice for KI being 15/1(see Fig.3.15). Our calculated ratios for NaF, NaCl, and KCl are 14.4/1, 12.3/1, and 8.6/1, respectively. Apparently, they fit observations very well.

iii) Discussions

So far, many experimental observations have confirmed that the Ps transition from a delocalized state to a localized state happens in most alkali halides except LiF when the temperature is raised. Every alkali halide has its own specific temperature of transition. A model is proposed to interpret this phenomenon. This model was originally developed by Toyozawa[3.48] in explaining some features of the self-trapped exciton. Later the model was first referred to by Hyodo et al in their paper[3.24] in which an anomalous temperature dependence of the width of the Ps peak in NaF was interpreted in terms of a metastable self-trapped state of Ps. In this model, the Ps atoms have two kinds of states, free and self-trapped, which are separated by an adiabatic potential barrier. The barrier

height and energy level E_{st} of the self-trapped state with respect to the lowest free state depend on the bandwidth of the particles, strength of the particle-phonon interaction, and phonon energy[3.44]. The self-trapped state is assumed to be metastable, thus $E_{st}>0$ and tunnelling to the self-trapped state is impossible. In other words, Ps can only decay to the self-trapped state as the result of temperature rising. By using a phenomenological model, experimentalists fitted the model parameters to experimental data, and estimated the energy level of the self-trapped state as being about 0.1 eV above the bottom of the delocalized band[3.24]. We calculated the corresponding energy level by our theoretical model and results we obtained are presented in Table 3.11. From this Table, it is seen that this energy difference is about zero. Because our calculation has uncertainty of about 0.2eV, the conclusion we can make from our calculation is that the energy level of the self-trapped Ps state is very close to that of the Bloch Ps state.

We have carried out the theoretical calculation for both the self-trapped Ps state and the Bloch like Ps state which are displayed in Table 3.8 and Table 3.9, respectively. To make the comparison more transparent, we reorganized those data and filled them in Table 3.11.

It should be mentioned that our approach is not a statistical theory, therefore it can not provide any information about how the energy levels are populated with temperature. Based on this theory, we would not be able to examine those temperature dependent transitions from a localized Ps state to a delocalized Ps state. The point here is our calculation does support the model of a metastable self-trapped state of Ps in the sense that at both room temperature and zero temperature, the calculated energy levels of the self-trapped Ps state E_{st} agree reasonably well with those obtained by experimentalists.

Table 3.11

Calculated lowest energy levels(eV) of localized state Ps and delocalized state Ps. E_{Loc}, E_{Bloch}, and E_{st} represent the localized Ps state energy calculated by the second approach, Bloch state Ps energy, and self-trapped state energy, respectively. S.B and P.B are abbreviations of single basis and pair basis.

	NaF	NaCl	KCl
Room Temperature			
E_{Loc} (S.B)	8.77	2.47	0.99
E_{Bloch} (S.B)	8.51	2.43	0.97
E_{st} (S.B)	0.26	0.04	0.02
E_{Loc} (P.B)	7.85	2.32	0.84
E_{Bloch} (P.B)	7.64	2.30	0.81
E_{st} (P.B)	0.21	0.02	0.03
0K			
E_{Loc} (S.B)	9.10	2.67	1.13
E_{Bloch} (S.B)	8.95	2.61	1.09
E_{st} (S.B)	0.15	0.06	0.04
E_{Loc} (P.B)	8.20	2.59	1.11
E_{Bloch} (P.B)	8.03	2.47	1.04
E_{st} (P.B)	0.17	0.12	0.07
E_{st} (Exp.)	0.10[3.24]		0.05[3.23]

Our results regarding both the localized Ps state and the delocalized Ps state are obtained by utilizing one or two bases. One may wonder what happens when many basis are used? To answer this question, we managed to rerun two jobs by using eight basis function (two on-centre plus six off-centre basis) placed at single interstitial site. Because of the time it requires, only NaCl was tested at room temperature. The values are given as follows:

$E_L = 0.76$ eV, $E_F = 0.56$ eV, $E_{st} = 0.20$ eV .

Generally, many basis functions improve the energy calculation. It is believed that such improvements from both states are going in parallel, and the basic trend shown in the above calculations remain the same. We shall mention that even for eight basis functions the evaluation of the localized state is very expensive. To speed the calculation, some off-diagonal terms which make negligible contributions have to be short cut. Now we can confidently say that once the same quality of basis is used to perform calculations for both states, the result always remains generally true.

3.4 Summary

The goal of this work was to study the structure of the positron and positronium in alkali halide crystals. The systematic investigations resulted in overall features of various systems which are found to be in reasonable agreement with experiment, except the lifetimes in the cases of localized and delocalized Ps states.

The advantage of our method is the ease with which it can be applied to many defect systems such as the F-centre, the anti-F-centre, the Fe^+-centre, localized Ps, free Ps, and even potentially to some other more complicated defect

systems. For well localized positron systems like the anti-F-centre and the Fe^{+}-centre, we calculated the binding energy, angular correlation curve, and lifetime. Although our approach does not have variational degrees of freedom to control both centre of mass motion and relative motion of multi-particle defect systems separately, our results in terms of the above mentioned quantities are satisfactory in general.

Those positronium systems associated with an interstice have been a quite attractive research project. The first approach gave us a strongly localized Ps state with a relatively large distortion, a deep energy level and a poor angular correlation curve. Therefore, our theoretical model had to be modified to be able to handle the centre of mass motion more flexibly. This is how we introduced a new model in which an envelope Gaussian modulates the wave function. Better results are achieved with the improved model, but the lifetime still remains not satisfactory. The model we developed to treat Bloch-like Ps seems adequate in describing free Ps state. It is well established experimentally that the Ps stays in a Bloch state at very low temperature. As the temperature is raised, Ps transits to a self-trapped localized state. The energy difference between the two states is very small. Our calculation presents the energy difference which is in favour of the observations. We shall point out that the well-known observed crystallographic effect can be explained quite successfully by our free state Ps model. The advantage of using a floating Gaussian basis provides us flexibility to position the basis. By placing bases at both interstitial sites of a unit cell, the observed phenomenon is excitingly reproduced, and the detected ratio between those satellite peaks is accurately matched as well.

All in all, we have developed a successful method under the line of an

extended-ion approach in dealing with those complicated defect systems possessing more than one 'electrons'. It has been shown to be efficient and economic. Not only considerable amount of results associated with various positron or positronium systems have been achieved, but several important features of the observations are satisfactorily explained.

References 3

3.1 P. A. M. Dirac, Proc. Cambridge Philos. Soc. 26 (1930) 361

3.2 C. D. Anderson, Phys. Rev. 43 (1933) 491

3.3 R. A. Ferrell, Rev. Mod. Phys. 28 (1956) 308

3.4 W. Brandt, in Positron Solid-State Physics, ed. by W. Brandt & A. Dupasquier (North-Holland Pub. Co. 1983)

3.5 S. Curry, Phys. Rev. A7, 447(1973)

3.6 A. T. Stewart & N. K. Pope, Phys. Rev. 120 (1960) 2033

3.7 A. Bisi, A. Florentini & L. Zappa, Phys. Rev. 122 (1963) 1023

3.8 A. Bisi, A. Florentini & L. Zappa, Phys. Rev. A134 (1964) 328

3.9 D. Herlach, Helv. Phys. Acta 45 (1972) 894

3.10 S. Dannefaer & L. Smedskjaer, J. Phys. C6 (1973) 3536

3.11 L. Smedskjaer & S. Dannefaer, J. Phys. C7 (1974) 2603

3.12 D. Herlach & F. Heinrich, Phys. Lett. A31 (1970) 47

3.13 A. Dupasquier, Nuovo Cimento Lett. 4 (1970) 13

3.14 W. Brandt, H. F. Waung & P. W. Levy, Phys. Rev. Lett. 26 (1971) 496

3.15 W. C. Mallard & F. H. Hsu, Phys. Lett. A38 (1972) 164

3.16 K. P. Arefiev & S. A. Vorobiev, Phys. Lett. A39 (1972) 381

3.17 T. Hyodo & Y. Takakusa, J. Phys. Soc. Jpn. 42 (1977) 1065

3.18 K. P. Arefev, P. V. Kuznetsov & O. V. Boev, Sov. Phys. Solid State 23 (1981) 1098

3.19 K. P. Arefev, O. V. Boev, P. V. Kuznetsov & S. A. Vorobiev, Solid State Commun. 44 (1982) 1067

3.20 K. P. Arefev, O. V. Boev, S. A. Vorobiev & P. V. Kuznetsov, Sov. Phys. Solid

State 26 (1984) 1017

3.21 J. Kasai & K. Fujiwara, J. Phys. Soc. Jpn. 51 (1982) 3077

3.22 J. Kasai, T. Hyodo & K. Fujiwara, J. Phys. Soc. Jpn. 57 (1988) 329

3.23 J. Kasai, T. Hyodo & K. Fujiwara, J. Phys. Soc. Jpn. 52 (1983) 3671

3.24 T. Hyodo, J. Kasai & Y. Takakusa, J. Phys. Soc. Jpn. 49 (1980) 2248

3.25 Positron in Solids, Edited by P. Hautojarvi, (Springer, Berlin 1979), p.197

3.26 V. I. Goldanskii & E. P. Prokopev, Sov. Phys. Solid State 6 (1965) 2641

3.27 W. Brandit, In Positron Annihilation, ed. by A. T. Stewart, L. O. Roellig (Academic Press, New York, London 1967) p.179

3.28 S. Dannefaer, G. W. Dean & B. G. Hogg, Phys. Rev. B13 (1976) 3715

3.29 A. Farazdel & P. E. Cade, Phys. Rev. B9 (1974) 2036

3.30 D. Herlach & F. Heinrich, Helv. Phys. Acta. 43 (1970) 491

3.31 A. A. Berezin & R. A. Evarestov, Phys. Status Solidi B48 (1971)133

3.32 A. A. Berezin, Phys. Status Solidi B50 (1972) 71

3.33 P. Hautojarvi, R. Nieminen & P. Jauho, Phys. Status Solidi B57 (1973) 115

3.34 Y. Takakusa & T. Hyodo, J. Phys. Soc. Jpn. 49 (1980) 2243

3.35 W. Brandt, A. Dupasquier & G. Durr, Phys. Rev. B6 (1972) 3156

3.36 A. Bisi, L. Bosi, A. Dupasquier & L. Zappa, Phys. Status Solidi B68 (1975) 515

3.37 R. G. Fuller, in Point Defects in Solids, ed. by J. H. Crawford, Jr. & L. M. Slifkin (Plenum New York, 1972), Vol.1,p.103

3.38 W. Brandt, G. Coussot & R. Paulin, Phys. Rev. Lett. 23 (1969) 522

3.39 A. Greenberger, A. P. Mills, A. Thompson & S. Berko, Phys. Lett. 32A (1970)72

3.40 O. Mogensen, J. Kvajic, M. Eldrup & M. Milosevic-Kvajic, Phys. Rev. B4 (1971) 71

3.41 Y. Takakusa & T. Hyodo, J. Phys. Soc. Jpn. 45 (1978) 353

3.42 T. Hyodo & Y. Takakusa, J. Phys. Soc. Jpn. 45 (1978) 795

3.43 S. Linderoth, H. Rajainmaki, H. E. Hansen & R. M. Nieminen, J. Phys. Soc. Jpn. 55 (1986) 4504

3.44 T. Hyodo, M. Kakimoto, Y. Nagashima & K. Fujiwara, Phys. Rev. 40B (1989) 8037

3.45 H. Ikari & K. Fujiwara, J. Phys. Soc. Jpn. 46 (1979) 92

3.46 J. Kasai & K. Fujiwara, J. Phys. Soc. Jpn. 51 (1982) 3077

3.47 J. Kasai, T. Hyodo & K. Fujiwara, J. Phys. Soc. Jpn. 57 (1988) 329

3.48 Y. Toyozawa, Appl. Opt. 19 (1980) 4101

3.49 Solid State Physics, Supplement 5, Edited by R. S. Knox, p.19

3.50 J. D. Zahrd & S. H. Lin Theor. Chim. Acta 12 (1968) 256

3.51 C. H. Leung, L. Emery & K. S. Song, Phys.Rew.B28,3474(1983)

3.52 T. Hyodo & A. T. Stewart, Phys. Rew. 29B (1984) 4164

3.53 D. M. Schrader, in Positronium and Muonium Chemistry, ed. by H. J. Ache, Amenrican Chemical Society, p.203 (1979)

Remarks on the Computation

All Calculations were accomplished by using IBM mainframe computer (IBM 3090). It is a time-shared system with five classes of run time allocations. They are ranked as follows: class A (30 sec.); class B (300 sec.); class C (1800 sec.); class G (3600 sec.); class J (10000 sec.). Our programs for calculating various defect systems were coded in Fortran. For most of our jobs, the orthogonalization was limited to a sub-cluster of 300 atoms, and the lattice relaxation was restricted to about 32 atoms. Typically, a single basis job without lattice relaxation took about 15 seconds, and a single basis job with lattice relaxation cost about 400 seconds for one iteration. With the fixed lattice distortions, 16 bases were employed to calculate those well localized defect systems. This type of jobs normally took about 1100 seconds.

The calculations of a Bloch state Ps were more expensive due to the summation over all unit cells. Jobs of a single basis and a pair bases consumed about 600 seconds and 2000 seconds, repectively. The most expensive jobs were attributed to the calculations of the localized Ps with the envelop function. A single basis job and a pair bases job cost about 2000 seconds and 8000 seconds, respectively. Jobs with more than two bases would not be attempted due to their exceeding the maximum limit. In several places of the thesis, we mentioned the restriction in available computer resources. In the above, we have given some examples.